With the support of the
Erasmus+ Programme
of the European Union

University of Évora

ARCHMAT

ERASMUS MUNDUS IN ARCHaeological MATerials Science

Raman Analysis of a Maya Wall Painting

Sara Balmuth

Prof. Peter Vandenabeele, Ghent University, Supervisor

Prof. Nicola Schiavon, Universidade de Évora, Supervisor

Évora, Portugal, November 2020

With the support of the
Erasmus+ Programme
of the European Union

Universidade de Évora

ARCHMAT

ERASMUS MUNDUS IN ARCHaeological MATerials Science

Análise Raman de uma Pintura de Parede Maia

Sara Balmuth

Prof. Peter Vandenabeele, Ghent University, Supervisor

Prof. Nicola Schiavon, Universidade de Évora, Supervisor

Évora, Portugal, November 2020

Approved Jury Members

Presidente:	Cristina Barrocas Dias	Professora associada c/agregação, Universidade de Évora
Arguente:	Catarina Miguel	Investigador, Universidade de Évora
Orientador:	Nicola Schiavon	Investigador principal convidado, Universidade de Évora
Vogal:	Donatella Magri	Professora associada, Università di Roma La Sapienza

Abstract

Ek' Balam is a Maya archaeological site located in Yucatán, Mexico. Due to its considerable size, the quality of its monumental architecture, and its substantial epigraphic record, archaeologists believe that it was a powerful regional polity throughout the Late and Terminal Classic period. As part of restoration projects conducted in the early 2000s, Vandenabeele et al. (2005a) employed Raman spectroscopy using a traditional benchtop spectrometer as well as an early portable Raman spectrometer to analyze thirty-three samples of a wall painting from Room 23 of the Ek' Balam Acropolis. In the present thesis, these same samples were analyzed using two new mobile Raman spectrometers. The B&WTek i-Raman EX is a portable spectrometer that utilizes a 1064-nm excitation source and a TE-cooled InGaAs detector, while the Bruker BRAVO is a handheld spectrometer that uses a dual laser excitation source and employs a patented process known as Sequentially Shifted Excitation (SSE^{TM}) to automatically subtract fluorescence. By comparing current results to the data acquired in 2005, the performance of these two relatively new spectrometers was evaluated. The results show that the new instruments successfully captured spectra of calcite, haematite, cinnabar, Maya blue, and carbon black, all of which were reported in the original study. In addition, the new data indicates the presence of limewash putty or slaked lime, as well as the possible presence of oxalates. Although the new instruments showed some disadvantages with regard to spot size, focusing capabilities, spectral resolution, and signal-to-noise ratio when compared to benchtop instrumentation, the results indicate that the new mobile spectrometers show a great deal of promise for future cultural heritage studies, especially in cases where sampling cannot occur or can only occur sparingly.

Keywords: Handheld Raman spectroscopy, Maya painting, fluorescence

Resumo

Ek’ Balam é um sítio arqueológico Maya localizado em Yucatán, no México. Devido ao seu tamanho, a qualidade de sua arquitetura monumental e seu registro epigráfico substancial, os arqueólogos acreditam o sitio Ek' Balam como evidencia duma política regional poderosa durante todo o período clássico final e terminal. No âmbito de projetos de restauração conduzidos no início de 2000, Vandenabeele et al (2005a) utlizou espectroscopia Raman usando um modelo de bancada tradicional, bem como um espectrômetro Raman portátil antigo para analisar 33 amostras de uma pintura de parede da Sala 23 da Acrópole Ek' Balam. Na presente tese, as mesmas amostras foram analisadas usando dois espectrômetros Raman portáteis relativamente inovativos. O sistema B & WTek i-Raman é um espectrômetro portátil que utiliza uma fonte de excitação de 1064 nm e detector InGaAs, enquanto o Bruker BRAVO é um espectrômetro portátil que usa um sistema de laser duplo e emprega um processo patenteado conhecido como Sequentially Shifted Excitation (SSETM) para subtrair automaticamente a fluorescência. Ao comparar os resultados atuais com os dados mais antigos adquiridos em 2005, o desempenho desses dois espectrômetros relativamente novos foi avaliado. Os resultados mostram que os novos instrumentos capturaram com sucesso os espectros de calcita, hematita, cinábrio, azul Maya e carbono, todos relatados no estudo original. Além disso, os novos dados indicam a presença de massa de cal ou cal apagada, bem como a possível presença de oxalatos, que não puderam ser detectados em 2005. Embora os novos instrumentos apresentem algumas desvantagens em comparação com a instrumentação de bancada, incluindo o tamanho do ponto, capacidades de foco, resolução espectral e relação sinal-ruído, os resultados indicam que os novos espectrômetros portáteis mostram uma grande promessa para futuros estudos de patrimônio cultural, especialmente em casos onde a amostragem não pode ocorrer ou pode ocorrer apenas com moderação.

Palavras-chave: espectroscopia Raman portátil, pintura maia, fluorescência

Acknowledgements

The completion of a master's thesis is always a difficult endeavor. Writing this thesis in the year 2020 in the midst of a global pandemic, however, presented exceptional challenges and could not have been achieved without the support of some truly exceptional individuals.

First, I owe a considerable debt to my supervisors, Professor Peter Vandenabeele at Ghent University, and Professor Nicola Schiavon of the Universidade de Évora. Professor Vandenabeele not only welcomed me as a thesis student, but also allowed me to conduct handheld Raman spectroscopy from home in the midst of the COVID-19 lockdown restrictions. Professor Schiavon, too, was always available to assist me when I expressed concerns about the project, despite the many challenges he faced this year as coordinator of the ARCHMAT program. I would also like to thank the Ghent University Raman Spectroscopy Research Group, especially Sylvia Lycke, who taught me to use the spectrometers and software, and Anastasia Rousaki, who assisted me with interpretation of the results and had faith in my ability to complete this thesis, even when I myself experienced doubts. To Eleonora Odelli and Emma Paolin, I express my heartfelt thanks for your moral support and perpetually positive attitudes.

I would also like to thank the ARCHMAT program for affording me the incredible opportunity to learn from a vast, international, multidisciplinary team. I owe a debt of gratitude to my fellow students who became my family, and especially to Shivani Rajwade, Shraddha Khaire, Katie McClure, Anne-Di Berdin, and Faxriyya Huseynli, who helped me to be brave.

And finally, to my family: Robert, Mary Anne, Jeremy, Matthew, Rachel, and Morgan Balmuth, who cheered me on from the opposite side of the world.

Contents

List of Figures

List of Tables

List of Abbreviations

CCD detector	Charge coupled device detector
DBR	Distributed Bragg reflector
FTIR spectroscopy	Fourier Transform infrared spectroscopy
FT-Raman spectroscopy	Fourier Transform Raman spectroscopy
GCMS	Gas chromatography mass spectrometry
HPLC	High pressure liquid chromatography
InGaAs detector	Indium Gallium Arsenide detector
NIR	Near infrared
NMR spectroscopy	Nuclear magnetic resonance spectroscopy
OM	Optical microscopy
PIXE	Particle-induced X-ray emission
RR spectroscopy	Resonance Raman spectroscopy
SEM-EDS	Scanning electron microscopy and energy dispersive spectroscopy
SERDS	Shifted excitation Raman difference spectroscopy
SERS	Surface enhanced Raman spectroscopy
SSE^{TM}	Sequentially shifted excitation
SSRS	Sequentially shifted Raman spectroscopy
TE-cooled	Thermoelectric cooled
UV-Vis spectroscopy	Ultraviolet-visible spectroscopy
VMP	Voltammetry of microparticles
XRD	X-ray diffractometry
XRF spectroscopy	X-ray fluorescence spectroscopy

Introduction

In 2005, the Raman Spectroscopy Research Group at Ghent University published a Raman spectroscopy study in which thirty-three samples of a wall painting from the Maya archaeological site of Ek' Balam, Mexico, were analyzed (Vandenabeele *et al.*, 2005a). This work used a benchtop spectrometer—the RenishawSystem-1000—and an early mobile instrument—the Mobile Art Analyser (MArtA) (Vandenabeele *et al.*, 2004). This work was part of a larger conservation study in which the same samples were tested with several archaeometric methodologies, including Raman spectroscopy, optical microscopy (OM), scanning electron microscopy and energy dispersive spectroscopy (SEM-EDS), X-ray fluorescence (XRF), X-ray diffractometry (XRD), and Fourier Transform infrared spectroscopy (FTIR) (Alonso Olvera *et al.*, 2005). The original work provided important information about the materials and manufacture of wall paintings at the site.

In the intervening fifteen years, there have been many innovations in Raman spectroscopy, especially in the development of portable and handheld instruments. These improvements have allowed Raman analysis to be applied to many different types of cultural heritage objects, some of which are too fragile or valuable to be sampled or transported to a laboratory setting. However, because portability requires miniaturization, simplification, and streamlining of the instruments, mobile spectrometers have certain drawbacks and are usually outperformed by their benchtop counterparts in terms of spectral resolution, control of parameters, focusing capabilities, and signal-to-noise ratio. This raises an important question: can mobile spectrometers yield results that are comparable to their benchtop counterparts and thus eliminate the need for sampling? Or, conversely, is mobile instrumentation so hindered by difficulties such as fluorescence, background noise, poor spectral resolution, and optical focusing that it fails to measure up to the standards of the traditional methodologies?

The aim of the present thesis is to add to the growing corpus of literature on mobile spectroscopy and its application to archaeometry. To achieve this goal, the same thirty-three samples examined in 2005 were measured using two new mobile spectrometers: the i-Raman EX, a portable spectrometer manufactured by B&WTek; and the BRAVO spectrometer, a handheld spectrometer manufactured by Bruker Optics. Besides their mobility, these two instruments were of interest due to their fluorescence-limiting features. These features will be discussed in detail below, but briefly consist of a 1064-nm laser excitation source and an automated fluorescence subtraction process, respectively. Fluorescence represents a particularly important challenge in applying Raman spectroscopy to cultural heritage due to the fact that artifacts are not composed of pure substances, the complex substrates or matrices that can overwhelm the relatively weak Raman effect of the analyte, and the frequent

presence of organic substances or other materials with fluorescent properties (Vandenabeele, Edwards and Jehlička, 2014; Casadio, Daher and Bellot-Gurlet, 2016; Vandenabeele and Donais, 2016).

Current results were compared to those published in 2005 in order to answer the following questions: 1) Can the new mobile instrumentation be used to identify the same materials as the benchtop and the older mobile spectrometers? 2) How effective are the new spectrometers at eliminating fluorescence? And 3) what benefits and drawbacks does each new instrument present, and in general, are they viable alternatives to the earlier methodologies?

The following thesis is divided into five chapters. Chapter 1 provides a brief explanation of Raman spectroscopy as a technique and describes it applications to cultural heritage. Chapter 2 describes the archaeological context, including an overview of the geography and history of Ek' Balam. A summary of previous archaeometric research at this location is provided, and information regarding the manufacture of Maya mural paintings in general is briefly explored.

Chapter 3 describes the samples and methodologies used in this report. A brief description of the thirty-three samples is included, and the specifications of the spectrometers are described. Chapter 4 describes the analytical results. The new data is presented and compared with the results reported in 2005. The two new spectrometers are then evaluated.

Chapter 5 provides a conclusion to the work, explaining the significance of the results and answering the research questions posed in this introduction and at the end of Chapter 1.

Chapter 1: Raman Spectroscopy in Cultural Heritage

1.1 Raman Spectroscopy: Technique and Cultural Heritage Applications

Raman spectroscopy is a vibrational spectroscopy technique in which a laser of monochromatic light, usually at a visible wavelength, is directed at an analyte. When the light makes contact, the molecules within the analyte are briefly excited to a virtual energy state and then rapidly decay back down to a lower energy state, emitting photons in the process. The majority of this light scattering occurs at the same energy as the excitation source; this is called Rayleigh or elastic scattering. However, a small amount of the light is scattered at an energy different from the excitation source; this inelastic scattering is called Raman scattering, and can occur at either a lower energy than the laser (Stokes scattering) or at a higher energy than the laser (anti-Stokes scattering). Stokes scattering occurs because some vibrational modes in the molecule absorb energy from the laser and scatter the remainder as photons; anti-Stokes scattering occurs when a vibrational mode is excited prior to application of the laser, and thus emits more energy than the excitation source as it returns to ground state. Stokes scattering is more intense than anti-Stokes scattering. This relates to Boltzmann distribution, which describes the distribution of different energy levels; because the vibrational modes of molecules are more likely to be at ground state than in an excited vibrational state prior to application of the laser, Stokes scattering tends to be more intense than anti-Stokes scattering. For this reason, most Raman spectroscopy studies focus solely on Stokes lines, although a comparison of Stokes and anti-Stokes lines can be useful in specialized applications, such as determining the temperature of the sample (Vandenabeele, 2013, pp. 4–6, 14, 28–33; Siesler, 2016, pp. 4–5).

For a given vibrational mode to produce Raman scattering, the application of the excitation source must cause a change in polarizability (Ferraro, Nakamoto and Brown, 2003, p. 22). When Raman scattering occurs, the Raman shift (the difference in wavenumber between the laser and the scattering) depends upon the type of vibration, the type of chemical bond, and the reduced mass of the atoms in the molecule. Intensity depends upon both experimental parameters (e.g., intensity of the laser, volume of the sample, and various instrumental parameters) and the nature of the sample itself (Vandenabeele, 2013, pp. 13–19). Thus, the ability to measure Raman scattering provides a means of identifying unknown substances and of studying the structure and vibrational characteristics of molecules.

Raman spectroscopy has been applied to diverse fields of study including materials science, structural and analytical chemistry, biochemistry, medicine, forensics, pharmacology, and environmental and industrial studies (Ferraro, Nakamoto and Brown, 2003). In a particularly fascinating case, Raman

spectroscopy will be employed in a NASA mission to Mars in order to test for the presence of biomolecules, thus exploring the possibility of extraterrestrial life (Vandenabeele, 2013, pp. 139–141).

The application of Raman spectroscopy to archaeometry is fairly recent. Some of the earliest studies occurred shortly after the first couplings of Raman spectrometers to microscopes in the 1970s. These early applications were primarily pigment analyses, especially of illuminated manuscripts (Clark, 1995; Bell, Clark and Gibbs, 1997; Vandenabeele, Edwards and Moens, 2007, p. 675; Rousaki, Moens and Vandenabeele, 2018, p. 2). One of the most important publications was a database of fifty-six historic pigments by Bell et al. (1997) which provided a comprehensive resource enabling Raman spectroscopy to be applied to further cultural heritage studies of historic manuscripts and paintings; this database has since been expanded to include more pigments as well as spectra recorded at different wavelengths (Burgio and Clark, 2001). Since the 1990s, applications of Raman spectroscopy to cultural heritage have greatly increased. This relates to improvements in technology, including the development of FT-Raman in 1986 and the increased availability of the charge coupled device (CCD) detector (Gilbert, 2016, pp. 607–608) as well as the introduction of mobile instruments in the early 2000s (Vandenabeele, Verpoort and Moens, 2001).

With improvements in technology, the corpus of literature has grown considerably, and now includes studies of such diverse cultural heritage objects as oil paintings, ceramics, stones, minerals, gems, pigments, organic dyes, biomolecules, glass, lithics, corrosion products on metals, organic residues, ivory, textiles, human bone, wood, and waterlogged paper, in addition to continuing studies of illuminated manuscripts. Raman has been applied to important art and archaeological lines of inquiry, including questions regarding technique, raw materials, provenance, degradation, preservation, and authenticity (Smith and Clark, 2004; Bellot-Gurlet, Pages-Camagna and Coupry, 2006; De Gelder *et al.*, 2007; Vandenabeele, Edwards and Moens, 2007; Vandenabeele, Edwards and Jehlička, 2014; Casadio, Daher and Bellot-Gurlet, 2016; Vandenabeele and Donais, 2016).

There are many factors that make Raman spectroscopy an excellent technique for cultural heritage analysis. First, it is non-destructive and requires little or no sample preparation. Second, Raman spectroscopy is a molecular technique and can thus provide information on both inorganic and organic materials, as well as isomers and polymorphs. Finally, Raman spectroscopy can be applied rapidly, which greatly enhances its practicality (Vandenabeele, 2004; Lauwers *et al.*, 2014; Bersani *et al.*, 2016).

1.2 Mobile, Portable, and Handheld Instrumentation

Many cultural heritage objects are too valuable or fragile to be sampled or even moved, or can only be done so with extreme caution. For this reason, mobile instrumentation is enormously beneficial for

archaeometry. A major breakthrough occurred on this frontier with a 2001 publication which used optic probe heads coupled with FT-Raman spectroscopy to analyze the varnish of historically significant paintings; this laid the foundation for mobile Raman spectroscopy, allowing for the direct analysis of art and archaeology (Vandenabeele, Verpoort and Moens, 2001). Materials analyzed with mobile instrumentation now include oil paintings, glyptics, wall paintings, rock paintings, manuscripts, ceramics, glass, enamels, mosaics, and degradation products (Pérez-Alonso, Castro and Madariaga, 2006; Vandenabeele, Edwards and Jehlička, 2014; Lauwers *et al.*, 2016; Rousaki *et al.*, 2017; Vagnini *et al.*, 2017).

Vandenabeele et al. and Lauwers et al. distinguish between five types of Raman spectrometers according to their degree of mobility. Transportable instruments can be carried from site to site, but are not designed for this purpose; consequently, they may be cumbersome to move and require adjustments when transported to new places. In contrast, mobile instruments are designed to be moved, and do not require adjustments when transported. Within the category of mobile spectrometers are portable, handheld, and palm instruments. A portable instrument can be carried by a single individual, while handheld and palm instruments are even smaller spectrometers which fit within the user's hands and palm, respectively (Lauwers *et al.*, 2014, p. 295; Vandenabeele, Edwards and Jehlička, 2014, pp. 2628–2629).

Smaller instruments that require fewer user adjustments are highly desirable, in part because many archaeological sites are situated in remote locations. For example, Rousaki et al. conducted an *in situ* study of rock art at remote archaeological sites in Patagonia, which required mobile spectrometers to be carried for long distances, frequently up to high elevations (2017, 2018). For Raman spectroscopy to be employed in this way, transportable instruments would be impractical; this is partially due to their size, but also relates to issues with calibration and lack of access to a power source.

While mobile Raman potentially allows for the analysis of more cultural heritage objects than ever before, it also has some important challenges and drawbacks when compared to traditional benchtop instrumentation. Some of the issues relate to the non-laboratory environment. At an archaeological site or within a public cultural heritage setting (a church, historic building, museum, etc.) there may be background interference from ambient light or heat, which can be difficult to control. In addition, the analyte might be located in an inconvenient position, possibly requiring the use of tripods, scaffolding, or fiber optics cables (Rousaki, Moens and Vandenabeele, 2018, p. 5).

Other issues arise from limitations associated with the simplification and miniaturization of the instruments. For handheld or palm instruments, the optical head and gratings are often fixed, there is

no means of focus, and parameters associated with laser power sometimes cannot be controlled. While this makes the instrument easier to use and transport, the inability to adjust the parameters can make it difficult to acquire high quality spectra if the automatic parameters are less than optimal for a given material or in given conditions. The inability to control parameters could also create a potential danger for cultural heritage objects, as exposure to too high a laser power or for a long period of time could burn or permanently alter sensitive artifacts (Vandenabeele, Edwards and Jehlička, 2014, p. 2630).

1.3 Fluorescence: Causes and Strategies for Overcoming It

Fluorescence occurs when light from the laser excitation source is absorbed, causing the molecular bonds to become excited to higher electronic states. Initially, energy is emitted by radiationless transitions until the molecule reaches a lower energy level. Following this, light is emitted as the molecule further decays to ground state. Because Raman scattering is a weak effect, it can easily be overwhelmed by fluorescence, making it difficult or even impossible to identify Raman signal (Culka and Jehlička, 2018, p. 527). Fluorescence is a common problem for many types of studies, but is especially difficult in cultural heritage, as artifacts typically contain impurities or organic materials that tend to fluoresce. Archaeological samples are also frequently contaminated by the soils surrounding the buried artifacts (Coupry, 2000, p. 39). There are three basic strategies for overcoming fluorescence effects: 1) prevention or lessening of fluorescence itself; 2) enhancement of the Raman signal in order to improve the signal to noise ratio; and 3) removal of fluorescence during data processing.

The fluorescence phenomenon can be curbed by using lasers with long wavelengths, typically at the upper limit of the visible spectrum or in the near infrared region; these are usually below the threshold of energy necessary to cause fluorescence. The disadvantage to this method is that Raman intensity is inversely proportional to the excitation wavelength on the order of approximately λ^{-4}. Thus, Raman intensity is greatly reduced with long wavelengths (Ferraro, Nakamoto and Brown, 2003, pp. 109–110). Another method to curb fluorescence is photobleaching, in which the sample is irradiated with the laser for a prolonged period of time before recording a spectrum. Although fluorescence is reduced by this method, photobleaching has the potential to damage artifacts, making it undesirable for analysis of fragile cultural heritage objects (Macdonald and Wyeth, 2006).

Another approach is to enhance the Raman signal rather than decrease fluorescence. In Resonance Raman (RR) spectroscopy, the laser frequency is selected so that it matches the frequency of an allowed electronic transition in the studied molecule, causing Raman intensity to be greatly increased. According to Vandenabeele, the major disadvantage of this is that “the analyst is focused on a specific

molecule, and the weaker scatterers in the mixture are not easily detected" (2013, p. 48). In Surface Enhanced Raman Spectroscopy (SERS), Raman signal is enhanced by adsorbing the studied molecules on nanoparticles of noble metals. This creates a resonance effect that intensifies Raman signal, in some cases by a factor as great as 10^6 (Vandenabeele, 2013, p. 48). Major disadvantages to this method are first, the expense of the nanoparticles, and second, the lack of non-invasive or minimally invasive applications (Casadio, Daher and Bellot-Gurlet, 2016, pp. 14–15).

Finally, data treatments can be used to subtract fluorescence from the spectra. In sequentially shifted Raman spectroscopy (SSRS), two spectra are recorded by significantly shifting the grating (Casadio, Daher and Bellot-Gurlet, 2016, p. 16). Shifted excitation Raman difference spectroscopy (SERDS) is a similar method in which two spectra are recorded at slightly shifted laser frequencies (Osticioli, Zoppi and Castellucci, 2006, p. 975). The theoretical basis for these two techniques is that only the Raman signal is affected by shifts in grating and laser frequency, while fluorescence remains constant; thus, all constant data recorded in the two spectra is subtracted, in theory leaving only the Raman signal (Casadio, Daher and Bellot-Gurlet, 2016, pp. 15–16).

1.4 Conclusion and Relevance to the Present Work

As more mobile instruments become commercially available and are applied to archaeometry, there is a question of cost and benefit: can mobile instrumentation yield results that are comparable to their benchtop counterparts and thus eliminate the need for sampling? Or, conversely, is mobile instrumentation so hindered by difficulties such as fluorescence, background noise, poor spectral resolution, and optical focusing that it fails to measure up to the standards of the traditional methodologies? At its heart, this is a question of the risk of damage vs. information gained (Vandenabeele and Donais, 2016, pp. 27–28). While mobile Raman spectroscopy eliminates the need for sampling or transportation of the object, it nonetheless requires cultural heritage objects to be exposed to a high-powered laser. Conversely, benchtop instrumentation requires sampling or transporting the object to a laboratory setting, but can be performed on extremely small samples and has the potential to provide more information. Given the value of the items analysed in cultural heritage, it is essential for the archaeometrist to understand the risks and benefits of each methodology before deciding which analytical techniques should be applied. Important literature on this matter has been produced by Lauwers et al. (2014, 2016), Vandenabeele et al. (2007; 2014), and Rousaki et al. (2018; 2019).

The aim of the present thesis is to add to the growing corpus of literature on mobile spectroscopy and its application to archaeometry. In this study, thirty-three samples collected from a Maya wall painting

were analysed with two new mobile instruments, one of which has been commercially available only since 2015. Results are compared to a previous publication (Vandenabeele *et al.*, 2005a) in which the same samples were analysed with a traditional benchtop instrument and an older portable instrument. Of particular interest is the new spectrometers' ability to limit fluorescence, as both spectrometers have built-in mechanisms for this purpose. One spectrometer takes the approach of limiting the fluorescence phenomenon by using a 1064-nm excitation source, while the other uses a subtraction process to eliminate fluorescence from the final spectra.

The research questions posed were as follows:

1) Can the new mobile instrumentation be used to identify the same materials as the benchtop and the older portable spectrometers?

2) How effective are the new spectrometers at eliminating fluorescence?

3) What benefits and drawbacks does each new instrument present, and in general, are they viable alternatives to the earlier methodologies?

Chapter 2: Archaeological Context

2.1 Geographic Setting

The samples analyzed in this thesis were collected at the Maya archeological site of Ek' Balam, located on the Yucatán Peninsula in southern Mexico. In modern terms, the site is 150 km east of Mérida and 30 km north of Valladolid.

In the context of the Maya cultural area, Ek' Balam is located approximately equidistant (50-60 km) from the major archaeological sites of Chichén Itzá, Kuluba, Yaxuna, and Cóba, and lies within the Northern Lowlands region (Vargas de la Pena and Castillo Borges, 2001, p. 403). As the name implies, this region is exceptionally flat, with landforms rarely exceeding 50 m above sea level (Morley, Brainer and Sharer, 1983, p. 42; Coe, 2000, p. 16). Soil consists primarily of marine calcium carbonate formed during the late Cretaceous and early Quaternary period, which comprises a layer of sediment as thick as 2500 m. Surface rocks are mainly limestone, dolomite, and evaporite (Houck, 2004, p. 62). The region surrounding Ek' Balam is characterized by large bedrock outcrops, soils of 0.5-1.5 m in depth, and karstic sinks (Lesser and Weidie, 1988, pp. 237–239). Karstic sinks—also called *cenotes*—provide rare access to water, as there are few rivers and lakes and as annual rainfall is low (Houck, 2004, pp. 91–94). While the scarcity of water and the shallow, poor soil limit agricultural potential, other economic activities including salt, honey, and textile production as well as trade networks compensated for this during the Postclassic period. The area is also rich in faunal resources including fish and shellfish, deer, peccaries, tapirs, and wild turkeys (Coe, 2000, pp. 26–30, 193–194).

Despite the economic potential cited above, the location of Ek' Balam is considered less than ideal. Most strikingly, it is not directly adjacent to a natural water source—the nearest is 1.8 km to the east—although excavated wells are present throughout the site. In addition, there is no evidence that Ek' Balam's location afforded access to any particularly important economic resources, as one would expect from a site of this magnitude and significance. The city center of Ek' Balam was sustained by a large network of smaller hinterland sites, which provided the food and resources necessary to sustain a population of elites, administrators, and craft specialists (Houck, 2004).

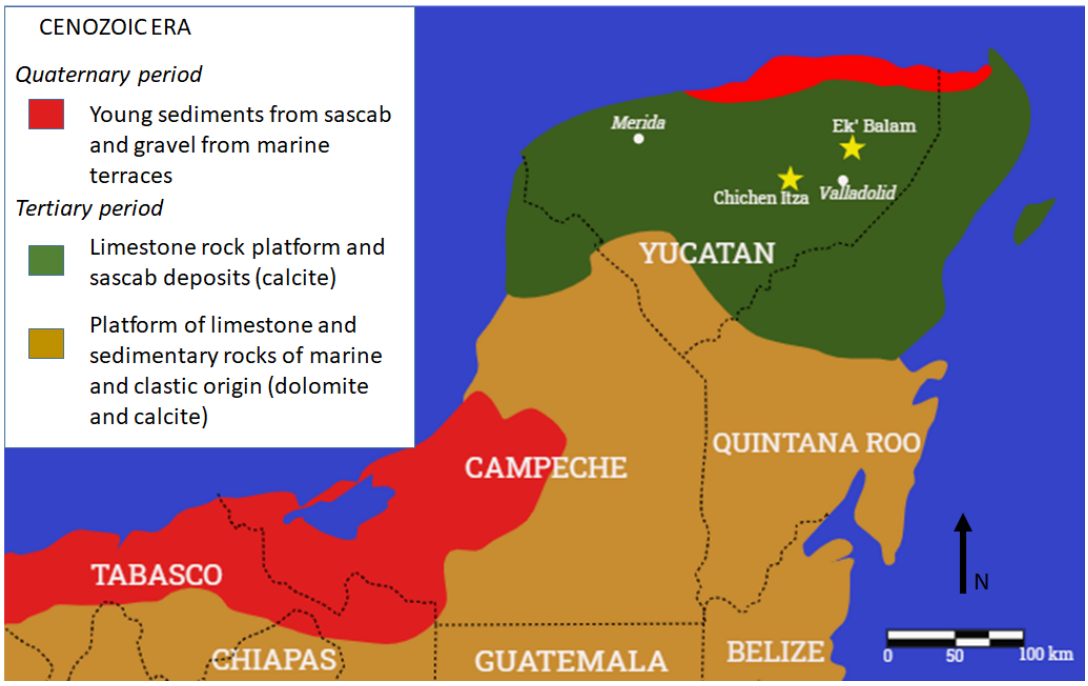

Figure 1 Geological map of the northern Yucatán peninsula. Based on Magaloni Kerpel 2001.

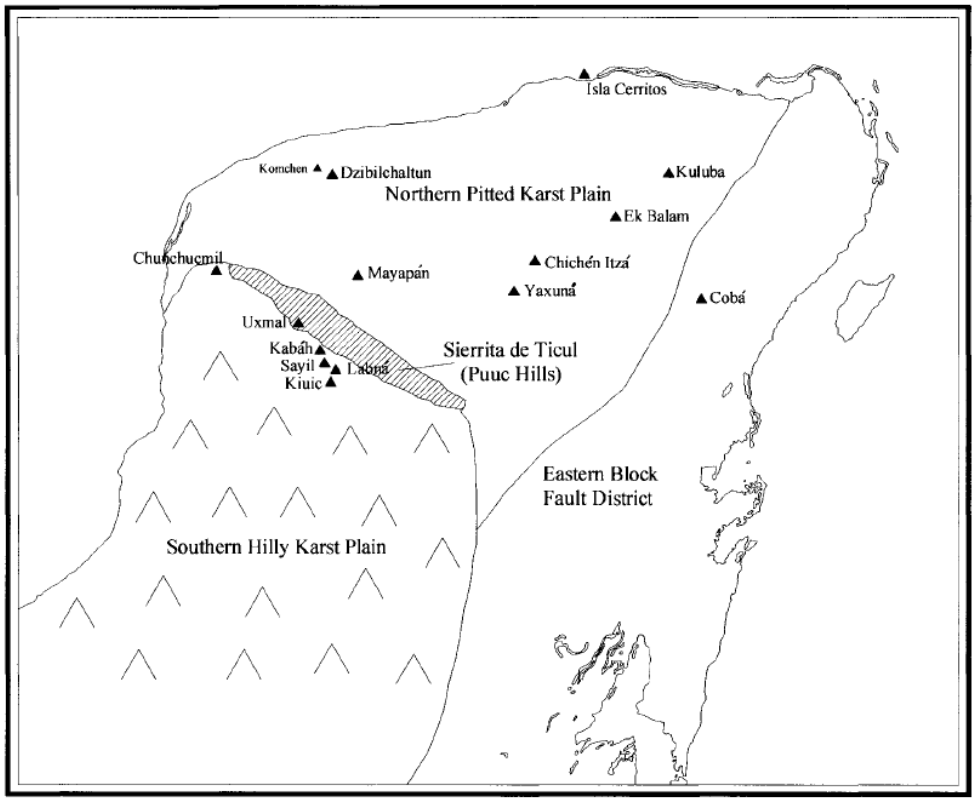

Figure 2 Map of landforms and Maya archaeological sites in the northern Yucatán. Houck 2004.

2.2 Archaeological and Historic Context

Archaeological evidence indicates that Ek' Balam was occupied continuously beginning in the Middle Preclassic period (*c.* 950-400 B.C.), and was not entirely abandoned until the seventeenth century. By

the Late Preclassic, the first monumental architecture was constructed in the central capital. Ceramic evidence implies steady population growth in the city throughout the Early Classic period, along with a decrease in population in the surrounding sites. This suggests that urbanization was fueled by depopulation of the hinterlands (Bey *et al.*, 1998, pp. 112–113; Houck, 2004, pp. 223–225).

Ek' Balam expanded throughout the Classic period, experiencing a peak in size and population during the Late Classic (*c.* A.D. 700-900). At its apex, the site occupied 12 km^2, although the majority of monumental architecture lies within a walled complex of 1.25 km^2 (Vargas de la Pena and Castillo Borges, 1999, pp. 25–28; Voß and Eberl, 1999, pp. 124–125; Lundy, 2016). During this period, many large-scale monumental structures were built or expanded within the walled complex, including the Acropolis and Structures 2 and 3 in the northern plaza and the Oval Palace, Platform of the Stelae, and Las Gemelas pyramids in the southern plaza. The main entrance to the walled site was through a vaulted archway, which was at the terminus of one of the five ceremonial "white roads" (*sacbeob*) radiating from the center (Vargas de la Pena and Castillo Borges, 1999, pp. 25–28, 2001, pp. 404–405; Lundy, 2016, pp. 16-19. 31). Despite its contemporaneity with and proximity to Chichén Itzá and with sites in the Puuc Hills, much of the architecture does not resemble styles found at these centers and seems to draw from the more distant Río Bec/Chenes style (Lundy, 2016, p. 221).

In addition to material remains, Ek' Balam contains an extensive textual record which attests to its importance as a regional polity. The city had its own emblem glyph, a rare hieroglyphic character used to identify only high status kingdoms (Marcus, 1976, pp. 46–47; Voß and Eberl, 1999, pp. 125–126). The texts themselves often refer to Ukit Kan Le'k Tok', who arrived at Ek' Balam in A.D. 770 and founded a powerful dynasty. Lundy (2016) argues that this individual was likely from the Río Bec/Chenes region based on the architectural styles of some of the buildings. Whatever his precise origins, Ukit Kan Le'k Tok' is the most-identified personage in the textual record at Ek' Balam (Lacadena Garcia-Gallo, 2004, pp. 98–101).

Under Ukit Kan Le'k Tok' and his descendants, Ek' Balam exerted considerable influence throughout the region (Sharer and Traxler, 2006, pp. 556–558). Ukit Kan Le'k Tok's name appears at the site of Ichmul de Morley, where he is identified as a ballplayer, and the emblem glyph of Ek' Balam can be found at Ikit, some 60 km away (Grube and Krochock, 2007, p. 209). Eighth and ninth century texts also indicate that Ek' Balam elites played key roles in religious rituals at Chichén Itzá and perhaps even resided there (Voß and Eberl, 1999, pp. 126–129). Based on this evidence, Grube and Krochock have argued that "prior to the ascendancy of Chichén Itzá, Ek Balam clearly dominated the political interactions in the Northern Plains" (2007, p. 209).

By the end of the Terminal Classic period, Ek' Balam's power began to decline, and monumental structures ceased to be built after *c.*1050 A.D. While there is no clear evidence for its cause, the decline occurred at roughly the same time as the rise of Chichén Itzá. Grube and Krochok have suggested that Chichén Itzá defeated Ek' Balam in battle, based on murals at Chichén Itzá that depict warriors attacking a walled city. However, there is no correlating evidence at Ek' Balam or elsewhere to confirm this theory (2007, p. 219). An alternative explanation is that Ek' Balam never experienced direct military defeat, but simply lost its political or economic influence to Chichén Itzá, perhaps by being cut off from previous allies or trade networks (Sharer and Traxler, 2006, p. 569).

Despite its decline, a substantial population remained in the northern portion of Ek' Balam. Ethnohistorical accounts described Postclassic Ek' Balam as a *cuchcabal*, a community that exacted tribute from other towns or villages (Defrance and Hanson, 2008, p. 303). In 1545, Ek' Balam became part of a Spanish *encomienda*, and a Franciscan chapel was built east of the site. Following the closure of this chapel in 1606, the site was abandoned (Voß and Eberl, 1999, p. 124; Defrance and Hanson, 2008, p. 303).

2.3 Archaeological Investigations

The first mention of Ek' Balam in the historic record is the 1579 *Relación de Tiquibolon*, in which Juan Gutiérrez de Picón described the location, history, and native population of the new *encomienda* under his charge. Gutiérrez de Picón described five large, abandoned structures made of hewn stone, with particular attention to the Acropolis: "The building is more than 400 paces in circumference: it can be mounted only with difficulty because the stairs by which it was ascended have collapsed and because it is so high, and from the top one can make out all that can be seen…" (Lundy, 2016, p. 21).

Following its abandonment after 1606, Ek' Balam remained forgotten until its rediscovery by Desiré Charnay, who partially cleared, photographed, and excavated small portions of the walled city in 1886 (Charnay, 1888). In the 1920s, archaeologist and epigrapher Sylvanus Morley visited the site in order to examine its hieroglyphic inscriptions. Morley reported to the Carnegie Institute that the city had crude architecture and "grotesque" sculptures, issuing the verdict: "Ekbalam was obviously a late provincial center, and its architecture and sculpture are such as might be expected in a Maya site of the last degenerate period in the northeastern corner of Yucatán" (1928, p. 318).

No further archaeological work was done until 1984-1996, when William Ringle and George Bey III led the Proyecto Ek Balam. This project consisted of archaeological survey and limited excavation within the site itself, survey of the hinterlands, intersite survey between Chichén Itzá and Ek' Balam, and excavation of the Spanish colonial portion of the site. Results of the project revealed that Ek'

Balam was not merely a small provincial settlement, but a powerful and largely independent regional polity (Houck, 2004, pp. 27–32).

Beginning in 1994, Leticia Vargas de la Peña led the Proyecto Arqueológico Ek' Balam. Excavations of the Acropolis done during this project uncovered impressive murals, stucco decorations, sculptures, and reliefs. These findings necessitated a conservation program, for which the samples investigated by this thesis were collected (Vandenabeele *et al*., 2005a, p. 2351). Further conservation efforts continued into the 2000s and 2010s (Alonso Olvera, 2013; Alonso *et al.*, 2014), and today Ek' Balam is a significant tourist destination. In March 2020, the *Yucatan Times* reported that there had been approximately 32,000 visitors to Ek' Balam throughout January and February of 2020 alone, making it the sixteenth most popular archaeotourism destination in Mexico (*Yucatan Times*, 2020).

PRECLASSIC PERIOD	**1000 B.C. – A.D. 250**
Middle Preclassic	Beginnings of a continuous population
Late Preclassic	Monumental architecture is first built, including the first Acropolis
CLASSIC PERIOD	**A.D. 250-950**
Early Classic	Ek' Balam increases in population size, while surrounding hinterlands experience depopulation
Late Classic	Ek' Balam experiences a peak in population and site size at 12 km^2
c.A.D. 770-900	The most powerful dynasty, founded by Ukit Kan Lek' Tok', rules the city, exerting influence over surrounding sites
	Increase in monumental architecture, including expansion of the Acropolis
Terminal Classic	The city begins to decline in importance as Chichen Itza's power increases
POSTCLASSIC PERIOD	**A.D. 950-1539**
c.A.D. 1050	Monumental architecture ceases to be constructed
	Ek' Balam remains a cuchcabal, exacting tribute from its neighbors, but is no longer a powerful kingdom
COLONIAL/CONTACT PERIOD	**A.D. 1539-1627**
1545	Ek' Balam becomes part of an encomienda
1579	*Relacion de Tiquibalon* is written – first historical record of Ek' Balam
1606	The colonial church at Ek' Balam closes, and the site is abandoned

Figure 3 Timeline of major events at Ek' Balam

Figure 4 Satellite map showing the location of the walled ceremonial center of Ek' Balam. Google Maps.

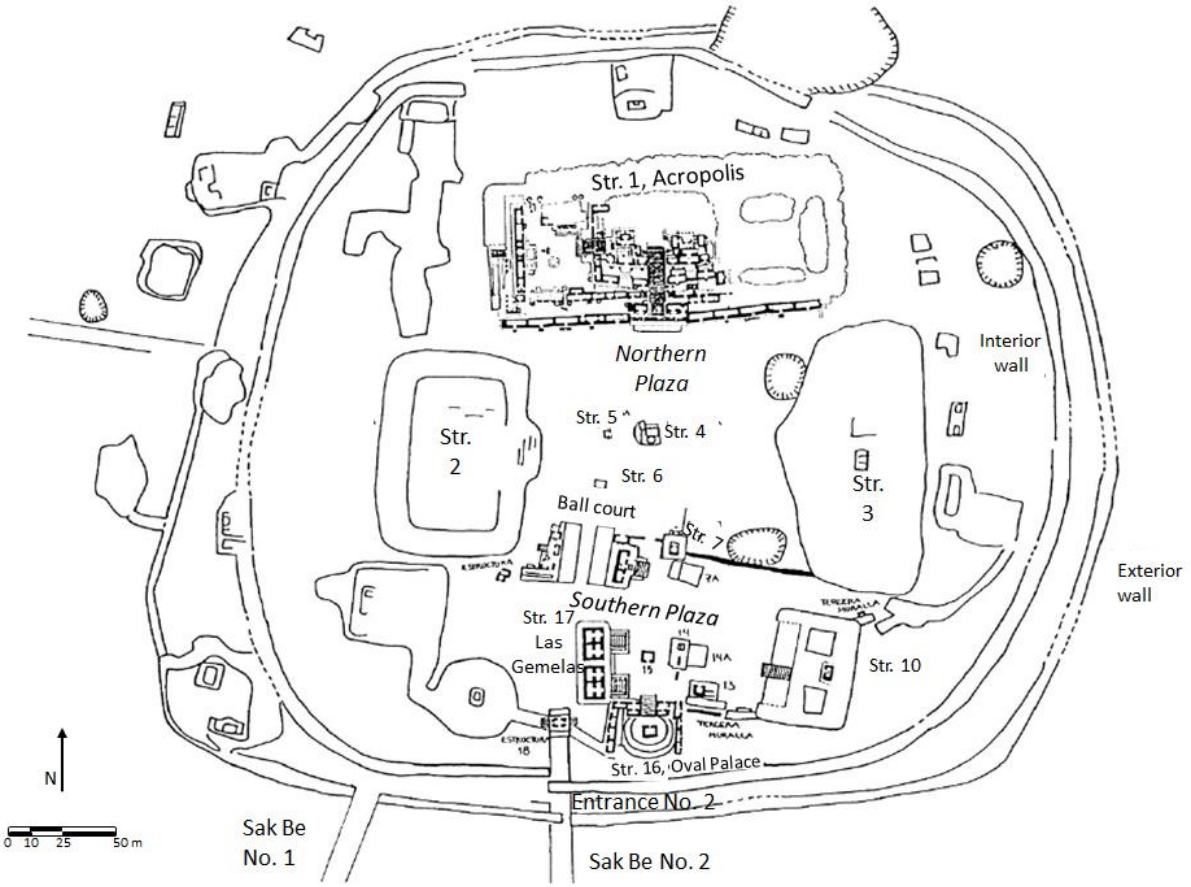

Figure 5 Sketch map of the walled ceremonial complex. Vargas de la Pena and Castillo Borges 2001.

2.4 The Acropolis of Ek' Balam

The Acropolis—also referred to as Structure 1, GT-1, and El Torre—is the largest and most elaborate building at Ek' Balam. It was first described by Gutiérrez de Picón as being more than 400 paces in length. Archaeological investigations have confirmed the massive scale of this building, and the pyramid is now known to measure approximately 160 m x 70 m and a maximum of 31 m tall (Vargas de la Pena and Castillo Borges, 1999, p. 27).

The Acropolis and Structures 2 and 3 comprise a "temple assemblage," a grouping of three pyramids delineating a rectangular, central plaza; this arrangement is duplicated on smaller scales at several sites in the Ek' Balam hinterland (Houck, 2004, pp. 29–30). Structures 1, 2, and 3 also match the designation of "acropolis group," defined as a group of three buildings that display a combination of temple and palatial structures (Lundy, 2016, pp. 113–114). Acropolises are situated on a series of tiered platforms, with access to the upper tiers carefully controlled. These structures were modified and expanded over time, reflecting changes in sociopolitical organization (Andrews, 1975, pp. 67–71).

In support of this view, excavations have shown that the Acropolis was originally a smaller structure built during the Preclassic Period, estimated to be about half as tall and only two thirds as wide as the current building (Lundy, 2016, p. 75). As Ek' Balam became more powerful during the Late Classic period, the Acropolis was greatly expanded. The present incarnation includes six well-defined tiers, with a massive staircase in the center leading to the apex. This staircase contains one of the most famous features of Ek' Balam—a pair of inscribed balustrades in the shape of stylized serpents, with open mouths and forked tongues. These have identical hieroglyphic inscriptions which identify the name Ukit Kan Le'k Tok' and the emblem glyph of the site (Lacadena Garcia-Gallo, 2004, pp. 12–18). Ukit Kan Le'k Tok's tomb is located in Room 49, and is marked by a zoomorphic stucco façade in the Chenes style. The tomb contained exotic grave goods, including jade, pyrite, pearls, and gemstones (Lundy, 2016, p. 19).

The Acropolis also contains many elaborate wall paintings with hieroglyphic inscriptions. In contrast to most Maya sites, painted glyphs outnumber carved inscriptions and have contributed significantly to data regarding the history of the site and the region as a whole (Lacadena Garcia-Gallo, 2004, p. 5). Indeed, Grube and Krochock note that, "Ek Balam has a larger corpus of hieroglyphic inscriptions than any other archaeological site in the northern Yucatan peninsula" (2007, p. 207). Many of the wall paintings are not merely decorative, but illustrate the history of the site and its rulers. For example, the Mural of the 96 Glyphs contains a large inscription detailing the arrival of Ukit Kan Le'k Tok' , while another mural in Room 22 contains information regarding Ukit Kan Le'k Tok's parentage (Lacadena Garcia-Gallo, 2004, pp. 98–101).

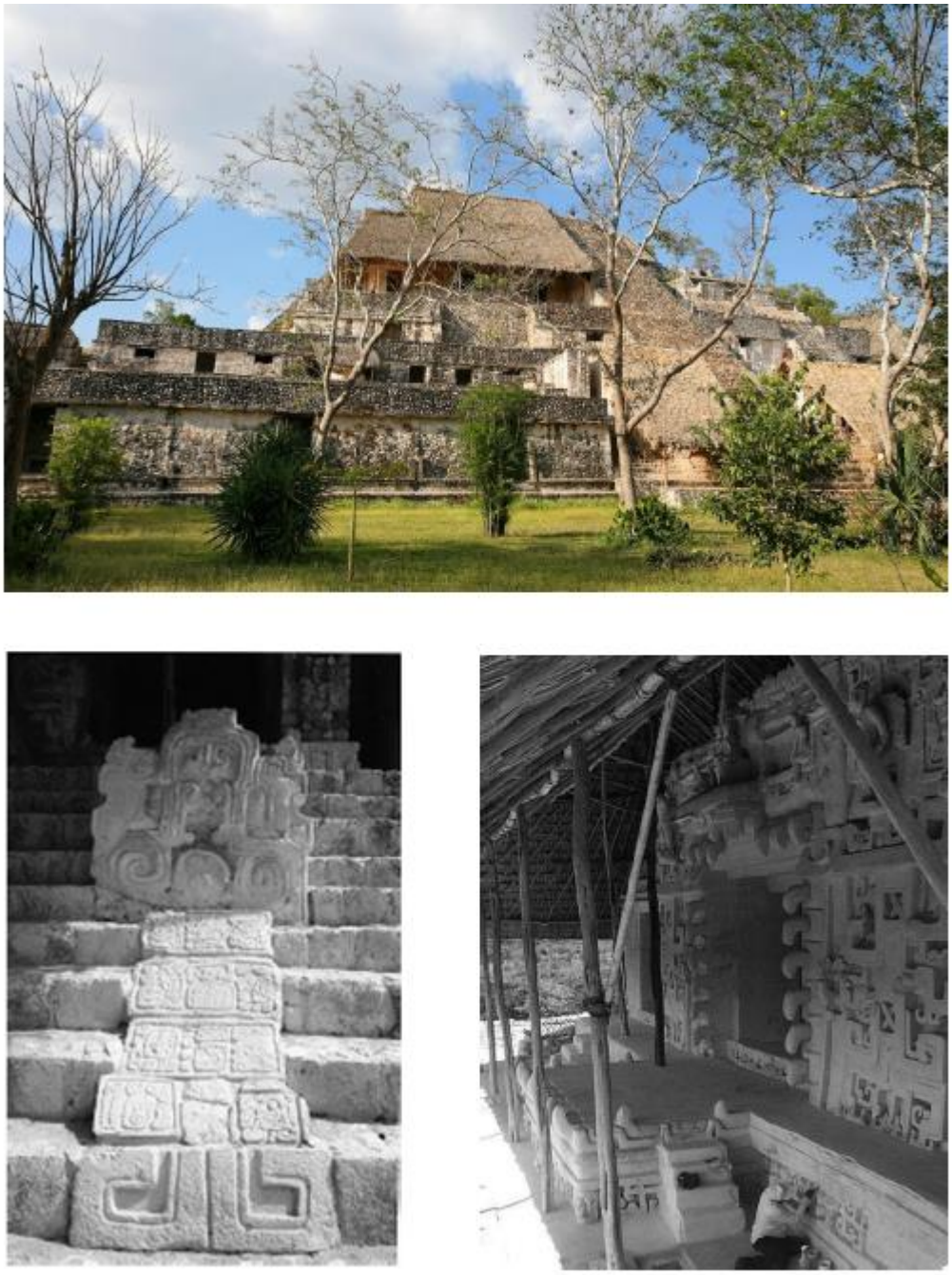

Figure 6 Top: Acropolis building. Photograph from Lundy 2016. Bottom left: Hieroglyphic Serpent balustrade; Bottom right: zoomorphic facade from Room 35. Lower photographs from Vargas de la Pena and Castillo Borges 2006.

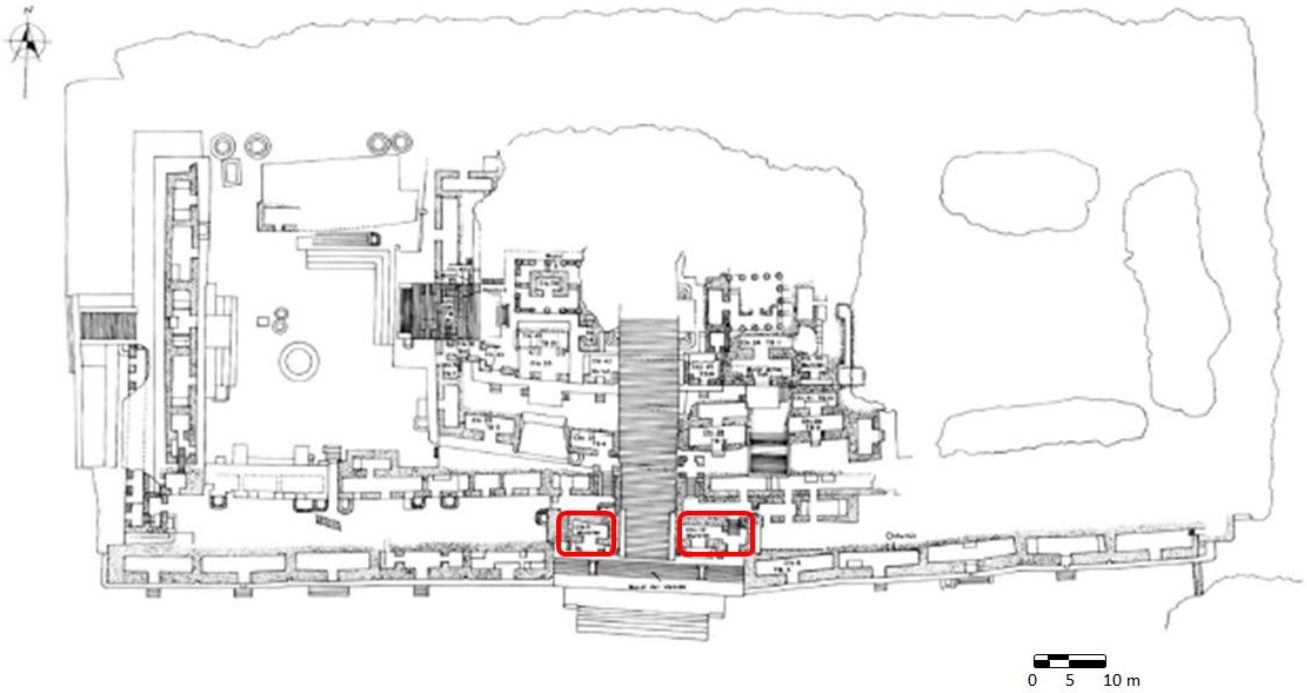

Figure 7 Diagram of the Acropolis with Rooms 11 and 12 marked in red. Room 23 was located below these, and was deliberately destroyed in ancient times. Alonso Olvera et al. 2005.

2.5 Previous Pigment Studies at Ek' Balam

2.5.1 Previous Studies of Room 23

During 1990s excavations of Rooms 11 and 12 of the Acropolis, large quantities of broken, painted plaster were found, indicating that there had formerly been a room with a large polychromatic wall painting located below. Archaeologists named this "Room 23." As part of the expansion of the Acropolis that took place throughout the Late Classic period, Room 23 was partially destroyed and filled in with rocks and sediment to improve the stability of the level above it. As a result, the painted plaster became detached from the walls (Alonso Olvera *et al.*, 2005, p. 95; Vandenabeele *et al*., 2005a, p. 2351).

As part of conservation efforts in the early 2000s, thirty-three samples were collected from Room 23 of the Acropolis. These were examined using Raman spectroscopy, X-ray fluorescence, scanning electron microscopy, Fourier Transform infrared spectroscopy, and X-ray diffractometry. The Raman spectroscopy results were published in Vandenabeele et al. (2005a), while a summary of all results was published in Alonso Olvera et al. (2005).

Raman spectroscopy was conducted by the Ghent University Raman Spectroscopy Research Group using one benchtop Raman spectrometer—the RenishawSystem-1000—and one mobile instrument—the Mobile Art Analyser (MArtA). Results were typically best with the benchtop instrument, although the mobile instrument was used to obtain spectra more quickly at a higher laser power, albeit with a lower spectral resolution (Vandenabeele *et al*., 2005a, p. 2350).

Raman spectroscopy indicated that the plaster was made of calcite ($CaCO_3$). In some cases, black spots were observed, as well as "black fibrous materials, obviously plant remains," which Vandenabeele et al. interpreted either as a deliberate additive to improve mechanical strength of the plaster, or as post-depositional contamination from the surrounding soil (2005, p. 2352). No gypsum ($CaSO_4$) was observed, meaning that the plaster was not degraded by sulfates (Vandenabeele *et al.*, 2005a, pp. 2351–2352). The results of other archaeometric methodologies indicated that along with calcite, clay particles were present within the substrate, as well as an amorphous substance that was inferred to be an organic additive. Optical microscopy showed that most samples did not have distinct strata of plaster, although a small number contained a fine layer directly beneath the paint as compared to a coarser layer below this (Alonso Olvera *et al.*, 2005, p. 102).

In all cases, calcite was also detected in the pigmented layers. Vandenabeele et al. proposed three possible interpretations for this: 1. the "shining" of the calcite substrate through the thin paint layer; 2. the mixture of calcite with other pigments to modify the color; and 3. the use of the fresco technique (2005a, p. 2352). While the results reported in Alonso Olvera et al. were consistent with these findings, optical microscopy indicated that in most cases the pigment layer did not appear to penetrate the support layer and that certain strategies for color modification had been employed, including layering of paints and mixtures of colorants. Based upon these observations, especially the superposition of layers, the authors concluded that the fresco technique was unlikely to have been employed, except perhaps on the lowest paint layers (2005, p. 88).

In addition to calcite, four pigments were identified: Maya blue, haematite (Fe_2O_3), carbon black (C), and cinnabar (HgS). Cinnabar was a surprising find, both because it is rarely identified in Maya wall painting, and because the closest known raw sources of this mineral are located in Chiapas, Guatemala, Honduras, and El Salvador, all of which are a considerable distance from Ek' Balam (Quintana *et al.*, 2015, p. 1046). While other examples of cinnabar have been found in wall paintings at Bonampak and La Blanca, the pigment was rarely used outside of funerary contexts (Magaloni Kerpel 2001, 173; Vázquez de Ágredos Pascual, Lorenzo, and Cosme 2014).

Vandenabeele et al.'s identification of Maya blue spectral features in samples of green and yellow paint was also significant. This was consistent with earlier experimental research, which hypothesized

that the components of Maya blue—indigo and palygorskite clay—could be combined in different ratios and/or heated to different temperatures to produce different shades of pigments (Reinen, Köhl and Müller, 2004). Identification of Maya blue was also possible with other archaeometric techniques. In particular, SEM and XRD were used to identify palygorskite within the blue paint. This was significant because the clay component of Maya blue typically cannot be identified by Raman spectroscopy, and variants of the Maya blue pigment made with sepiolite and potentially other types of clay are possible (see 2.6.2.1 Maya Blue below). The composition of the green colorants was less clear, as blue and green paints showed different particle sizes under microscopy, and FTIR spectra of blue and green pigments were similar but not identical. Thus, in addition to the possibility of Maya green made by modifying the ratio of indigo to palygorskite, Alonso Olvera et al. proposed that the pigment could have been created by precipitating a different yellow dye onto a clay and mixing this with Maya blue. Attempts to recreate this process were inconclusive, however (Alonso Olvera *et al.*, 2005, pp. 112–115).

Some of the pigments could not be identified by any of the methodologies. In Raman spectroscopy, many of the red paints showed large amounts of fluorescence, possibly implying the use of organic dyes. In order to decrease fluorescence, the laser beam was focused on small areas of the paint for several hours; following this, however, only the Raman bands of calcite could be observed with no evidence of the red chromophore (Vandenabeele *et al.*, 2005a, p. 2353). The yellow paint showed similarly high fluorescence with no evidence of a chromophore. This seemed either to denote the use of organic dyes or perhaps goethite (α-FeO(OH)), which exhibits only weak Raman signals with the 785-nm excitation wavelength used by both spectrometers (Vandenabeele et al., 2005a, p. 2355). Results of other analyses were also unsuccessful at characterizing the pigments, supporting the hypothesis that the colorants were organic (Alonso Olvera *et al.*, 2005, pp. 109, 117–118).

2.5.2 Other Pigment Analysis Studies at Ek' Balam

Doménech et al (2009) included a sample from Room 64 of the Acropolis in a study of Maya Blue pigments from different Maya sites. The authors found that all samples were made of indigo and clay, that different shades of Maya blue seemed to be caused by the presence of multiple indigo derivatives, and that there were slight correlations between the recipes used to create Maya blue and the chronological and geographic context. Unlike most other samples, the sample from Ek' Balam appeared to contain kaolinite rather than palygorskite based on the elemental ratios measured with SEM-EDS.

Vázquez de Agredos-Pascual (2010, cited in Alonso et al. 2014) used a variety of techniques to further study the pigments in Room 64 of the Acropolis. It was determined that some of the red pigments

were haematite and ilmenite ($FeTiO_3$), blue was composed of Maya blue, and orange pigments were made of goethite. Mural paintings from Room 64 of the Acropolis were also included in a 2010 study of red, orange, and yellow paints potentially made from annatto (*Bixa orellana*) lake pigments. This was part of a larger study of twenty-five Maya mural paintings from the Lowlands region, as well as a survey of ethnographic and ethnohistoric accounts of dye usage. The authors concluded that annatto was a strong possibility, but could not definitively confirm its presence (Vázquez de Agredos Pascual, Batista dos Santos and Yusa Marco, 2010).

Finally, Alonso et al. (2014) used Raman spectroscopy, optical microscopy, XRD, XRF, FTIR, and particle-induced X-ray emission (PIXE) to analyze wall paintings from rooms 12 and 50 of the Acropolis. Haematite, cinnabar, Maya blue, and carbon black were identified. Some inorganic yellow pigments—goethite and limonite ($FeO(OH)\cdot nH_2O$)—were also identified, while the remaining yellows were tentatively identified as organic dyes. The authors suggested that this might be "Maya yellow," a yellow pigment produced with the same components as Maya blue. Alonso et al. also noted that many of the samples exhibited overpainting, which was apparently used to modify the appearance of some colors. In addition to the colorants, the minerals in the plaster were identified through XRD and PIXE as "…calcite and potassium alumino-silicate and some samples is a mixture of calcite and dolomite [$MgCO_3$], but the dolomite was in very small concentration [*sic*]" (Alonso *et al.*, 2014, p. 66).

Identification				
Color	Room 23	Room 64	Room 12	Room 50
Red	Hematite, cinnabar	Hematite, ilmenite	Hematite, cinnabar	Hematite, cinnabar
Blue	Maya blue	Maya blue	Maya blue	Maya blue
Green	Maya green	-	Earth pigments, organic dye similar to indigo	Maya blue mixed with ochre, Maya blue on top of ochre
Yellow	Organic dye, limonite, goethite	-	Ochre, organic dye	Ochre
Orange	Hematite	Goethite	Illite, goethite	
Purple	Maya blue combined with hematite	-	Maya blue on top of hematite	Maya blue on top of hematite
Black	Carbon	-	Carbon	Carbon

Figure 8 Summary of previous pigment identification studies. Alonso et al. 2014

2.6 Maya Mural Painting: Materials and Significance

Extensive archaeometric studies of Maya mural paintings are a recent phenomenon, with large-scale and interdisciplinary approaches beginning during the 1990s and 2000s. Prior to this, archaeometric studies were conducted only sporadically, mostly used X-ray spectroscopy and light microscopy, and were usually concerned with large-scale mural paintings. Since the 1990s, several multisite and multi-technique archaeometric studies have been conducted. These include the Project on Prehispanic Mural Painting in Mexico, notable for its focus on smaller-scale murals rather than exclusively large-scale wall paintings, as well as its methodologies which include infrared photography, spectroscopy, and chromatography. The ANDREAH project and the Materials and Techniques of Prehistoric Painting have also produced significant results using similar approaches (Vazquez de Ágredos-Pascual and Munoz Cosme, 2014, pp. 168–169). Other comprehensive archaeometric studies were conducted by Magaloni Kerpel in the 1990s and early 2000s, in which OM, SEM-EDS, XRD, gas chromatography mass spectrometry (GCMS), and high pressure liquid chromatography (HPLC) were employed to analyze thirty-seven mural paintings from twenty-three sites located throughout the Maya area. Results provided information on the materials themselves as well as geographical and temporal differences in technology (Magaloni Kerpel, 2001).

In addition to these large-scale comparative enterprises, numerous archaeometric analyses have been undertaken at individual Maya sites. Besides the aforementioned studies at Ek' Balam, there have been many studies of the wall paintings at Chichén Itzá, Palenque, Copán, La Blanca, and Calakmul (Goodall, 2007; Garcia Moreno, Strivay and Gilbert, 2008; Goodall *et al.*, 2008; Arnold *et al.*, 2012; Vázquez de Ágredos Pascual, Lorenzo and Cosme, 2014).

2.6.1 Plaster Substrate

All plaster and stucco were made primarily of lime, which was obtained from natural limestone. While limestone is found throughout the Maya area, its exact mineral composition varies by location, with limestones from the northern Yucatán peninsula containing primarily calcite, and those from the southern Yucatán containing dolomite and magnesite; in coastal areas, aragonite ($CaCO_3$) may also be present (Magaloni Kerpel, 2001, pp. 158, 161–165).

In order to make plaster, limestone was first burned, reducing $CaCO_3$ to CaO (quicklime) with carbon dioxide as a byproduct; this process is called calcination (Vandenabeele *et al.*, 2005a, p. 2351). Water was then added to drive off the heat from burning and to cause a chemical reaction between the lime and water, creating slaked lime [$Ca(OH)_2$]. From here, aggregates such as sand or small particles of stone or clay were added to provide structure and resistance to the mixture. The composition of aggregates varied depending on the desired texture of the plaster, as well as the local geology of the

region (Magaloni Kerpel, 2001, pp. 161–165). Ethnographic accounts indicate that the Northern Lowlands Maya often used aggregates made of *sascab*, a chalky, friable material composed of weathered limestone and small amounts of quartz and clays (Houck, 2004, p. 64). Restorations at Ek' Balam have recreated the process of collecting and refining aggregates by excavating, washing, drying, and grinding *sascab* with a stone into smaller pieces of varying fineness (Alonso Olvera, 2013, p. 87). According to optical microscopy studies by Magaloni Kerpel (2001), the substrates of Late Classic Maya wall paintings usually consist of two layers. The lower stratum contains coarser aggregates, while the upper stratum beneath the paint is a more homogeneous mixture in which the aggregates are nearly indistinguishable. In other cases, however, there are no distinct strata beneath the paint; this is true of most plaster at Ek' Balam (Alonso Olvera *et al.*, 2005).

In addition to aggregates, plaster was also mixed with saps and vegetal substrates, including "those from the chucum tree (*Havardia albicans*), the *holol* (*Heliocarpus spp.*), the *ha 'bin* (*Piscidia piscipula*), or the *chaka'* (*Bursera simaruba L.*)…" This allowed for slower drying of the plasters, enabling the use of the fresco technique (Vazquez de Ágredos-Pascual and Munoz Cosme, 2014, pp. 166–167). Experimental recreations have also shown that adding gums to the slaked lime mixture increases the solubility of lime in water, while slightly heating the mixture creates a plaster with improved plasticity, high density, and good setting properties (Magaloni Kerpel, 2001, p. 161).

After the creation of slaked lime and the addition of aggregates and organic materials, the wet mixture was applied in the desired areas. As the slaked lime dried, the mixture was exposed to carbon dioxide. This caused another chemical reaction called carbonation, in which slaked lime transformed into calcite, with water as a byproduct (Vandenabeele *et al.*, 2005a, p. 2351). Raman spectroscopy studies of wall paintings have revealed that this transformation is not always uniform. For example, in Raman spectra recorded on an eighteenth-century wall painting, Fernandes et al. noted the presence of limewash, meaning that even centuries after its application, some of the slaked lime never underwent the transformation into calcite (2017, pp. 5–6).

The Maya sometimes applied the fresco technique in which the wall painting was created while the plaster was wet, allowing the slaked lime to act as a binding agent and to form a protective calcite covering upon drying. In other cases, the *secco* method was employed in which paint was applied only after the plaster dried; this latter technique necessitated the use of a binding agent such as egg, animal or plant fat, gum, or resin. GCMS and HPLC studies by Magaloni Kerpel found that the six monosaccharides present in the painted layers and their ratios seemed to correspond best to a mixture of sap from the bark of the *jonote* or *holol* (*Heliocarpus spp.*) tree and gum from the

pseudobulbs of local orchids, meaning that these were most likely the binding agents used; these results were consistent with ethnohistoric accounts (2001, pp. 192–195).

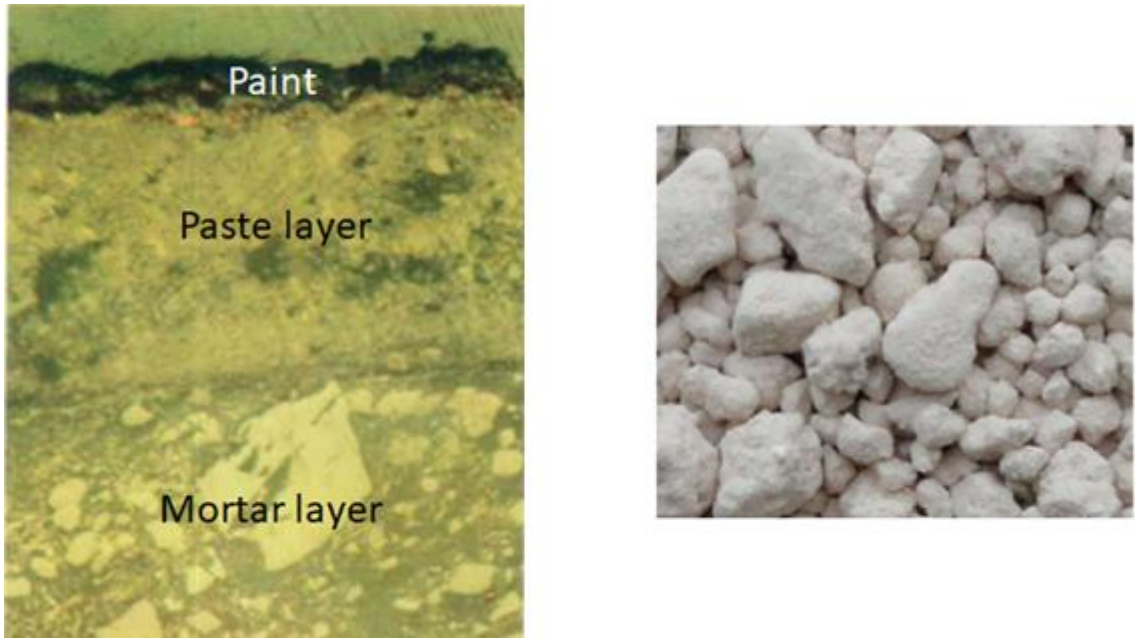

Figure 9 Left: optical microscopy photograph of plaster, showing mortar and paste layers. Magaloni Kerpel 2001. Right: sascab, a material composed primarily of deteriorated limestone. Alonso Olvera 2013

2.6.2 Colorants

Archaeological studies have found that the Maya color palette changed over time, with red, black, and white heavily favored during the Preclassic period. In part, this was due to availability, as haematite or red ochre, carbon black, and white limestone were ubiquitous (Houston *et al.*, 2009, p. 69). In the Late Preclassic and throughout the Classic period, technology to make new colorants arose, including yellow, orange, brown, and most importantly, Maya blue. Additional lake pigments were probably also used (Houston *et al.*, 2009, p. 62). The highest variety of colorants existed during the Late Classic period, with Magaloni Kerpel identifying more than thirty distinct paints used during this time. The most common of these were Maya blue, iron oxides, calcite, and carbon black. More rarely-used pigments included wollastonite ($CaSiO_3$), green earth, malachite [$Cu_2CO_3(OH)_2$], azurite [$Cu_3(CO_3)_2(OH)_2$], and cinnabar. Organic pigments were also thought to have been used, although they could not be identified (2001, p. 172).

Houston et al. suggested that the increase in colorants during the Classic period as well as the growing power of Maya elites encouraged a new “Naturalistic” style of painting, chiefly concerned with the realistic depiction of historic scenes that glorified Maya royalty. Naturalistic painting included the development of techniques such as overlaying different colorants, employing transparent color washes, varying the thickness of paint layers, and using gradations of saturation to create three dimensional effects. According to the same authors, Ek’ Balam is a counterexample of this, as it seems

to have resisted innovation and generally "adhered to Classic Maya color traditions", with a color palette that remained largely based upon red, white, black, yellow, and blue/green (Houston *et al.*, 2009, pp. 84–85, 92). While this is broadly true, Alonso Olvera et al. (2005) and Alonso et al. (2014) noted that several complex techniques such as the overlaying of paint layers to produce new shades were employed at Ek' Balam, perhaps allowing for some of the same effects used in the Naturalistic style.

During the Postclassic period, color use became more limited and seems to have been produced through standardized recipes, likely indicating that Maya blue, yellow ochre (made of a mixture of lepidocrocite [γ-FeO(OH)] and montmorillonite clay), haematite, and carbonized resins were mass produced and traded to various localities (Magaloni Kerpel, 2001, p. 172). By the Spanish colonial period, five colors associated with the cardinal directions and a fifth "central" direction predominated Maya aesthetics. Red (*chak'*) was associated with the east, black (*ek'*) with the west, yellow (*k'an*) with the south, and white (*sak'*) with the north, while green and blue (*yax*) were associated with centrality (Houston *et al.*, 2009, p. 13). Colors were also associated with tangible objects, and with broader concepts related to these objects. For example, yellow was affiliated with ripeness and fertility, likely because it is the color of ripe maize and dried, harvested plants. In contrast, green/blue (*yax*) was associated with fresh or unripe plants, as well as with water and rain (Houston *et al.*, 2009, pp. 16–42). *Yax* was also associated with sacrifice, as sacrifices at Chichén Itzá—both humans and objects—were painted blue (Tozzer, 1941, p. 321; Arnold *et al.*, 2012, pp. 2253–2254).

2.6.2.1 Maya Blue

Initially, the composition of Maya blue was puzzling to scientists. The pigment was first described in 1931 (Merwin, 1931), although the term "Maya blue" was not coined until 1946 (Gettens and Stout, 1946). Laboratory analyses revealed that "…the blue color is not discharged by boiling nitric acid and is not affected by heat much below redness. When ignited on a platinum spoon to glowing, the pigment turns to grayish white, but sometimes with a dull reddish tone" (Gettens, 1962, p. 558). X-ray diffraction showed only a white clay mineral called attapulgite (now called palygorskite)—a magnesium aluminum phyllosilicate with the ideal formula $(Mg, Al)_4\ Si_8\ (O, OH, H_2O)_{24} \bullet nH_2O$ (Brindley, 1957)—while elemental analyses detected only calcium, magnesium, aluminum, and iron, all of which are components of the same white clay (Gettens, 1962, p. 558). This data led to two opposite interpretations: the first was that Maya blue was a natural blue clay related to palygorskite (Gettens, 1962); the second was that it was composed of an organic dye precipitated onto clay (Shepard and Gottlieb, 1962). In 1966, Van Olphen demonstrated the viability of the latter interpretation by preparing the Maya blue pigment from indigo and clay, which were mixed, soaked in water, and heated to moderate temperatures. Although blue colorants could be produced with

several kinds of clays, only palygorskite and sepiolite—which have tunnel or channel structures—produced acid-resistant colorants (van Olphen, 1966). Kleber et al. (1967) detected indigo in archaeological samples of Maya blue using infrared absorption spectroscopy, confirming the identity of Maya blue. Further studies undertaken on archaeological samples have shown that palygorskite was the most commonly used clay component for the Maya blue, although variations of the Maya blue made with sepiolite [$Mg_8Si_{12}O_{30}(OH)_4(OH_2)_4 \bullet nH_2O$] are also known (Giustetto *et al.*, 2011, p. 42).

There have since been numerous studies to understand the properties of the pigment, including its precise chemical structure and crystallinity, color values, and archaeological use (Sánchez Del Río *et al.*, 2011). Domenech et al. have undertaken a large variety of analyses, using techniques such as UV-Vis spectroscopy, SEM-EDS, voltammetry of microparticles (VMP), FTIR, XRD, nuclear magnetic resonance spectroscopy (NMR), and OM. Results of these studies found that different shades of Maya blue, including green and yellow, could be achieved with different compounds present in indigo (2006; 2011; 2012). Reinen et al. have also shown through optical spectroscopy that indigo is the only chromophore present in Maya blue, and that when indigo attaches to palygorskite, there is a chromatic shift toward turquoise and green (2004).

Raman spectroscopy studies have found that the spectrum of Maya blue is similar but not identical to that of indigo. Vandenabeele et al. reported the presence of several bands visible in the spectra of Maya blue which appeared to have no direct counterparts in the spectra of indigo reported in earlier publications; other bands were related to those seen in indigo and could be assigned the same vibrational modes, but were shifted, sometimes by 10 cm^{-1} or more (2005a, p. 2354). While it would be logical to infer that the clay component of Maya blue is directly responsible for these differences, clay is not usually identifiable in Raman spectroscopy due to high levels of fluorescence, and thus cannot account for this phenomenon; furthermore, Raman spectroscopy of Maya blue made with clays other than palygorskite have produced spectra that are essentially identical to those made with palygorskite (Sánchez del Río *et al.*, 2006). This has led to two primary hypotheses: the first is that the differences in spectra between indigo and Maya blue are due to changes in the planarity of the indigo molecule when it attaches to the clay (Witke, Brzezinka and Lamprecht, 2003); the second is that indigo derivatives such as dehydroindigo are present along with indigo and contribute to the spectra (Doménech, Doménech-Carbó and Edwards, 2011, pp. 91–93). Sánchez del Río et al. used simulations to test whether the loss of planarity could account for the differences and concluded that "a single loss of planarity (a few degrees rotation of half molecule around the C=C axis) is not sufficient to explain the changes observed in indigo–clay mixtures" (2011, p. 1052). Based on the same data, it has been hypothesized that in addition to the loss of planarity and possible presence of dehydroindigo, different "topological isomers" could potentially form when indigo and/or dehydroindigo become

incorporated within the clay lattice structure, and that the sum of all of these factors could account for the differences observed (Doménech, Doménech-Carbó and Edwards, 2011, p. 95).

Although the term "Maya blue" is now ubiquitous, in reality the pigment was neither exclusively used by the Maya, nor exclusively blue. Maya blue was used by many cultures throughout the region; one of the most surprising examples of this occurred in Cuba, where a variant of the pigment was imported from the Yucatán peninsula (Tagle *et al.*, 1990). Vazquez de Agredos-Pascual et al. (2019) recently identified the oldest known use of Maya blue, which occurred at sites in western Mexico associated with the Chupicuaro culture, dating approximately 600-1000 B.C., although the colorant did not come into popular use until the Late Preclassic/Early Classic period (Houston *et al.*, 2009, p. 69).

The same components of Maya blue also can create green and yellow pigments. Smaller ratios of indigo to palygorskite can yield greener colorants; this can be accomplished either by applying only small amounts of *Indigofera* sp. or by soaking the clay for only a brief length of time (Vandenabeele *et al.*, 2005a, p. 2354-2355). Some scholars have also argued that yellow can be produced. Vandenabeele et al. observed that yellow paint crystals from the Ek' Balam samples exhibited the same spectra as those of the blue and green pigments, leading them to suggest that, "in these cases the aeration of the indigo/clay mixture was incomplete and…the indigo molecule is trapped in the reduced form (leuko-indigo) into the crystal lattice" (2005, p. 2355). This is supported by Doménech et al. (2011), in which VMP was employed to test archaeological examples of yellow paint against a variety of yellow colorants thought to have been used by the Maya. The spectra of the archaeological samples best matched isatin found in indigo. According to the authors, "The preparation of such 'Maya yellow' pigments could be carried out as an intermediate step during the preparation of indigo and Maya Blue…leaves and twigs of the *Indigofera* plants would be soaked overnight in a suspension of slaked lime in water. Then, the coarse material could be removed by filtration and a portion of the yellow suspension separated to add palygorskite and prepare the 'Maya Yellow' pigment" (Doménech, Doménech-Carbõ and Vázquez De Agredos-Pascual, 2011, p. 5743).

From an archaeological standpoint, Maya blue was a highly significant development. Symbolically, the color blue was associated with deities, agricultural fertility, and sacrificial rituals (Arnold *et al.*, 2012, p. 2253). The technology to produce Maya blue was also important in an art historical sense, as the few natural blue and green pigments in Mesoamerica are exceptionally rare (Houston *et al.*, 2009, p. 65; Vázquez de Ágredos Pascual, Lorenzo and Cosme, 2014, pp. 49–50); in most cases, Maya blue thus afforded the use of a completely new color, which greatly impacted artistic styles throughout the Classic period (Houston *et al.*, 2009, p. 69). Geological studies indicate that palygorskite could be obtained from several deposits on the Yucatán Peninsula including Sacalum,

Yo' Sah Kab, and several localities near the Maya city of Uxmal (Sánchez Del Río *et al.*, 2011, pp. 471–472). Ethnographic studies have shown that palygorskite remains important to modern Maya populations in these regions, who use it both as a temper in pottery manufacture and as a medicine (Arnold *et al.*, 2012, p. 2253). Despite its clear significance, however, no written record exists describing how Maya blue was manufactured, necessitating archaeometric studies to answer questions of provenance and technique (Doménech, Doménech-Carbó and Edwards, 2011, p. 86).

2.6.2.2 Other Organic Colorants

Several studies of Maya mural paintings have found colorants that could not be fully characterized by traditional archaeometric techniques; authors usually infer that these contained organic dyes, and were possibly lake pigments similar to Maya blue (Vázquez de Agredos Pascual, Batista dos Santos and Yusa Marco, 2010). This is supported by ethnographic and ethnohistoric accounts, which have noted the use of at least three other lake pigments in more recent times. First, in Lacandon Maya pottery a yellow lake pigment is made from the roots of the *kante* (*Gliricidia sepium*) plant (Houston et al. 2009, 62). Second, a red lake pigment made from *chucum* (*Pithecollobium albicans*) or *jabin* (*Piscidia communis, Piscidia piscipula*, or *Ichthyomethia communis*) tree bark was likely used to make red buff plaster (Littmann 1960, 593, 596). And finally, anthropologist Thompson reported that, "following the tradition of the ancients, annatto [*Bixa orellana*] continued to this day to be used to colour stucco and as preparation base for these works [wall paintings]" (Vázquez de Agredos Pascual, Batista dos Santos and Yusa Marco, 2010).

Many additional lake pigments are also possible in theory, as the Maya had access to a large number of dyes. In the Yucatán, a rich cotton textile tradition had developed by the Postclassic period, which gave the Northern Lowlands Maya a sophisticated knowledge of dyes (Coe, 2000, p. 193). Red dyes besides those listed above include the well-known cochineal (*Dactylopius coccus*), logwood (*Haematoxylum campechianum*), and brazilwood (*Haematoxylum brasiletto, Caesalpinia* sp.), while yellow organic colorants may have included *Chlorophora tinctoria*, *Cosmos sulphureus*, *Cuscuta* sp., *Gliricidia sepium*, and *Maclura tinctoria*. Houston et al. have compiled an extensive list of possible colorants throughout the Maya region based upon ethnohistoric and ethnographic accounts; however, it is unknown whether they were used in antiquity, whether the Maya made them into lake pigments, or whether they were employed in mural paintings or were only used for other purposes such as cloth dyes, body paint, or pigments for codices (Houston et al. 2009, 60–61).

Chapter 3: Experimental

3.1 Samples

Thirty-three samples of broken, painted plaster were collected in the early 2000s from Room 23 of the Acropolis in Ek' Balam. These were selected from an assemblage of over 1000 fragments, with the goal of representing the full color palette used at Ek' Balam (Alonso Olvera *et al.*, 2005, p. 95). Samples were previously examined using a variety of techniques, including OM, SEM-EDS, XRF, XRD, FTIR, and Raman spectroscopy; results of all of these analyses are reported in Alonso Olvera et al. (2005), while Raman spectroscopy results are reported in detail in Vandenabeele et al. (2005a). The goal of the current work was to reexamine all thirty-three of these samples with new mobile Raman spectrometers (a portable and a handheld model), and to compare this data to the results reported in Vandenabeele et al. (2005a) in order to evaluate the new technology.

The samples are approximately 0.5-4 cm in length and width, and about 0.5-1 cm in thickness. The unpainted plaster is white to pale yellowish brown in color, and texture is very fine to medium grained. Visible inclusions are primarily small, light brown pebbles and dark spots that appear to be charred fibrous plant fragments and flecks of charcoal. Paint colors include red, blue, green, black, gray, purple, and yellow. Red varies in shade from strong scarlet to orange and very light pink. Green comprises bluish green, grayish green, and dark olive green, while blue is either a bright teal or has a washed out, grayish appearance. Three samples appear purple, one of which could also be considered a very dark red, one of which is grayish, and the last of which is pale and contains patches of reddish purple and light grayish blue. Only one sample is entirely brownish yellow. One blue sample has a small stripe of a brighter yellow, while a bluish gray sample contains a yellowish brown stripe. Many of the samples were painted with multiple colors, and examples can be seen of overlaid paint, stripes, dots, and mottling of several colors to produce various aesthetic effects.

Because of the nature of Raman spectroscopy, no sample preparation was necessary. Raman spectra were collected on each sample with each instrument at two to four different locations, depending on the size of the sample and the different visible colors. In addition to measurements recorded on the painted surface, several measurements were also taken on the unpainted plaster. Samples and

locations for the plaster were primarily chosen at random, although measurements were also recorded where inclusions were observed.

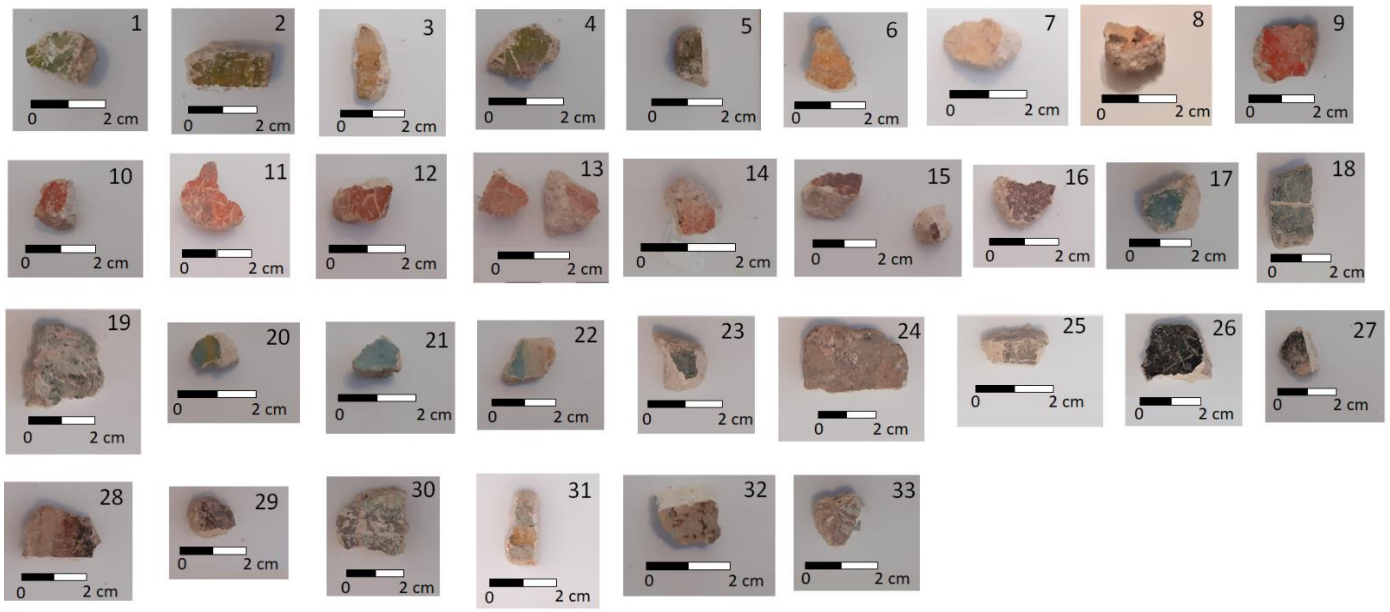

Figure 10 Samples tested in this study.

Figure 11 Left: i-Raman EX spectrometer. Photo © Metrohm SG, www.metrohm.com. Right: i-Raman set up, using a microscope stage for positioning.

Figure 12 BRAVO spectrometer.

3.2 Instrumentation

3.2.1 i-Raman EX (B&WTek) Portable Spectrometer

The i-Raman EX spectrometer, manufactured by B&WTek, is a portable system with an NIR laser excitation wavelength of 1064 nm. Laser power is adjustable, and can be increased to a maximum of 499 mW. The system is equipped with a TE-cooled InGaAs detector. Spectral range is 2500-100 cm^{-1}, with a spectral resolution of less than 10 cm^{-1}. The laser contains a fiber optics probe 1.5 m in length.

The i-Raman spectrometer is a portable system, as it is "a mobile instrument that can be carried and brought at the field by a single person" (Lauwers *et al.*, 2014, p. 295). In total, the device weighs 3.4 kg and measures 17 × 34 × 28 cm. The system is not battery operated and is controlled through connection with a laptop.

Measurements were collected with this instrument in a laboratory setting. To decrease ambient light, spectra were recorded in a windowless room with all lights turned off. The fiber optic probe was raised and lowered with an adjustable microscope stand, while the sample was placed below on the stage, on top of a circular glass plate. The continuous capture feature was used to obtain the correct focus for each sample, and then the time, accumulations and laser power were set accordingly to allow for a longer, single capture. Laser power was only applied up to 15% in order to avoid damaging the samples. Exposure times were typically set as low as 10 seconds and as high as 30 seconds. Accumulations were set between 5 and 10. At longer times and accumulations, the detector would usually flood, recording a flat, entirely unusable spectrum. Unfortunately, spectra recorded with this

instrument were generally poor. Potential reasons for this will be discussed below, but are likely due to short acquisition times and difficulties in obtaining focus.

3.2.2 BRAVO Handheld Spectrometer (Bruker Optics)

The BRAVO handheld Raman spectrometer, manufactured by Bruker Optics, became commercially available in 2015. The spectrometer has two temperature-controlled diode lasers (DuoLaser™) at excitation wavelengths of 785 nm and 852 nm, respectively. One laser collects data from the fingerprint region while the other collects data from the CH stretching region. Laser power is controlled automatically, but does not exceed 100 mW for either laser. The instrument uses a patented process known as Sequentially Shifted Excitation (SSE™) to eliminate fluorescence from the final spectra. In this process, each laser records three spectra at different wavelength excitations; the different wavelengths are achieved by changing the temperature of the laser. This concept is explained by Conti et al. as follows: "A typical measurement consists of collecting Raman spectra at DBR [distributed Bragg reflector] laser temperatures of 20, 23, 26, and 29° C...This yields excitation wavelengths of 784.630, 784.852, 785.074, and 785.296 nm, respectively and gives a constant excitation shift of 0.222 nm. When converted to wavenumbers (cm^{-1}), this gives a separation of substantially 3.60 cm^{-1} between the different excitations" (2016, p. 4600). The software then compares the spectra, eliminates the portions that are static and therefore fluorescence-caused, and compiles a single, fluorescence-free spectrum. The end result is a spectrum with a spectral range of 3200-300 cm^{-1}. Spectral resolution is 10-12 cm^{-1} (Saelens, 2018, p. 28; Rousaki *et al.*, 2019, pp. 5–6).

The BRAVO is a handheld instrument because it "can be operated while held in one hand of the operator" and is battery-powered (Lauwers *et al.*, 2014, p. 295). The instrument weighs 1.5 kg (not including the docking station) and measures 27 x 15.6 x 6.2 cm. Calibration is integrated. The device is operated by a touchscreen, and the laser emanates from a fixed optical head, exiting the instrument through a measuring tip (the device comes with a standard tip with a small circular opening, as well as a tip designed specifically for vials) (Saelens, 2018, pp. 28, 77; Rousaki *et al.*, 2019, p. 5).

Because it is extremely new, the spectrometer has been applied to only a handful of studies and material types, including modern and historic art materials (Vagnini *et al.*, 2017; Pozzi *et al.*, 2019), minerals (Jehlička *et al.*, 2017; Culka and Jehlička, 2018), archaeological wall paintings from Pompeii (Germinario *et al.*, 2018), and mosaic tesserae (Saelens, 2018; Rousaki *et al.*, 2019).

In the course of this work, the BRAVO spectrometer was used in a non-laboratory setting. This was by necessity, as the COVID-19 pandemic forced the closure of the Ghent University chemistry laboratory. Therefore, spectra were recorded in my apartment. To avoid contamination from ambient light, window curtains were kept closed and all lights were shut off. The instrument was placed on a table,

and the samples were carefully positioned so that the aperture of the measuring tip covered the desired measuring location. In most cases, automatic settings were applied. In cases where the automatic settings failed to capture high-quality spectra, manual parameters were applied by connecting the instrument to the docking station and laptop. By this methodology, acquisition time and number of scans could be changed; however the BRAVO's laser power cannot be adjusted by the operator and thus remained automated. Times were selected between 200 and 500 ms; number of scans was left at the default five scans. In most cases, the manual parameters did not greatly improve the results, although at longer exposure times, some of the spectra showed a slightly improved signal to noise ratio.

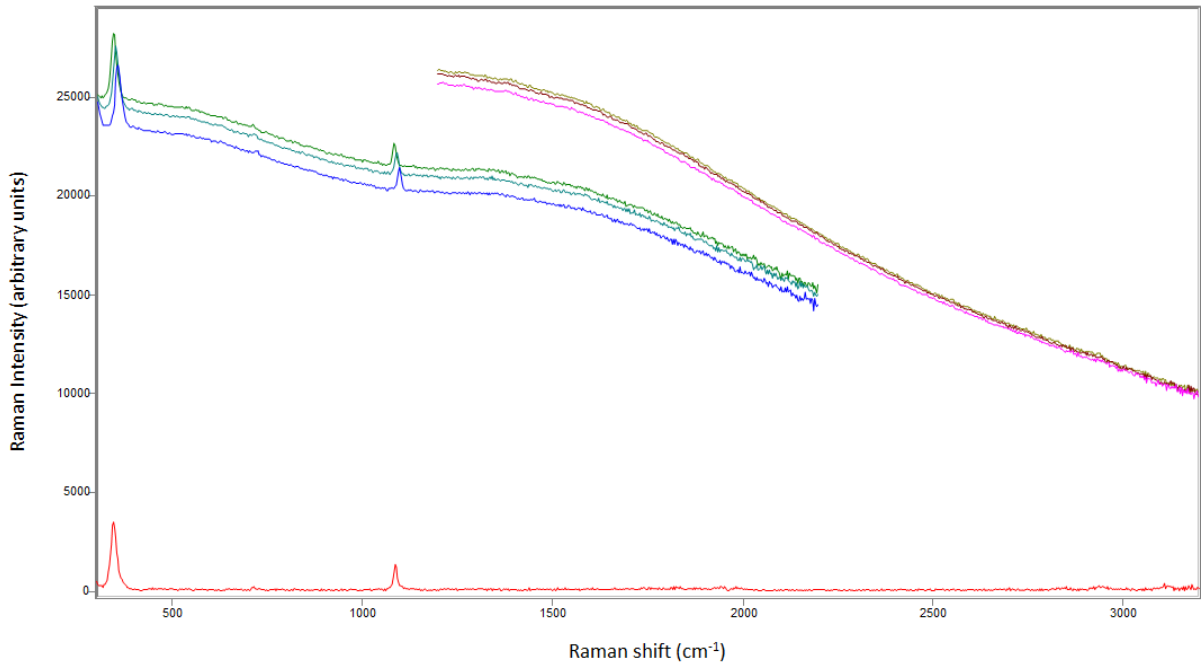

Figure 13 Example of BRAVO data-collection on a sample containing cinnabar and calcite. Six spectra (top) are collected in total (three with each laser) at different excitation wavelengths. The software automatically subtracts fluorescence and produces a single composite spectrum (bottom).

Chapter 4: Results and Discussion

4.1 Materials Identifications

4.1.1 Ground Layer

As in the original publication, spectra recorded on the unpainted plaster substrate show primarily calcite ($CaCO_3$). In the BRAVO spectra, this is observable by two peaks: the strongest band at 1086 cm^{-1} and a less intense band at 712 cm^{-1}, corresponding to the symmetric stretching vibration and the symmetric deformation of CO_3, respectively. In some cases, a third band is visible at 1436 cm^{-1}, although this is often difficult to recognize due to noise; this is attributable to the asymmetric stretching vibration of CO_3. The i-Raman data show the same peaks at 1085 and 711 cm^{-1}, as well as two lattice vibrations occurring at lower wavenumbers: 155 and 280 cm^{-1} (Edwards *et al.*, 2005; Gunasekaran, Anbalagan and Pandi, 2006). These are absent in spectra recorded with the BRAVO due to the instrument's spectral range, which does not extend below 300 cm^{-1}.

As reported in 2005, calcite was also visible in all spectra recorded on the painted surfaces. Vandenabeele et al. proposed several possible interpretations of this, including use of the fresco technique, the mixing of calcite with other colorants to modify color saturation, and the "shining" of the plaster substrate through the thin layers of paint (Vandenabeele et al., 2005a, p. 2352). The data produced here could similarly be used to support all of these assertions. However, based upon optical microscopy, Alonso Olvera et al. suggested that the fresco technique was unlikely, given that there are several instances of overpainting observable in these samples; while the bottom layers of paint could have been applied as a fresco, the thin upper layers logically would have been applied after the plaster had dried (2005, pp. 85–86). No organic binder could be observed in the Raman spectra recorded here or in the 2005 publication, although this is not proof of its absence. Binding agents are typically amorphous organic compounds that are weak Raman scatterers, and Raman spectroscopy often does not have adequate sensitivity to detect them (Vandenabeele *et al.*, 2005b, p. 708).

While the fresco technique may be unlikely given the data acquired with microscopy, the use of calcite as a colorant or additive to the paint seems probable, given the very pale hues of some of the pigments in this assemblage. The Aztecs were known to have used calcium carbonate as a white colorant called *tetiçatl*, which may have been used by other pre-Hispanic cultures as well (Haude, 1998, p. 252); in addition, Magaloni Kerpel reports a white pigment composed of calcite or aragonite at four Maya sites, as well as calcite mixed in with red colorants at twelve locations (2001, p. 173). The probable use of calcite as a pigment or additive does not exclude the other two possibilities—that calcite from the plaster substrate is "shining" through the thin paint layers, or that the fresco technique was used.

The original publication used a microscope objective lens to focus the laser on small areas, including tiny black spots and fibrous plant remains within the plaster. However, this was not possible here. The spot sizes of handheld spectrometers—typically estimated at 0.3-1 mm in diameter—are considerably larger than those of benchtop instruments (Vandenabeele, Edwards and Jehlička, 2014, p. 2641). Thus, the spot size of the BRAVO spectrometer was too large to focus on submillimeter areas. Although the spot size of the i-Raman is smaller than that of the BRAVO, the fact that the laser is invisible as well as the requirement that it be positioned at least 6 mm above the sample without the use of an objective lens made it difficult to be certain that the laser was positioned in the correct spot, particularly when the target area was a millimeter or less in diameter. In spite of these limitations, one measurement recorded on black fibrous materials suspended in the plaster did yield a possible spectrum for carbon, as is consistent with the original publication. However, this was visible only in the BRAVO spectra with no subtraction applied; as will be discussed below, this is part of a greater interpretive problem with the BRAVO instrument. Other spectra recorded on larger inclusions—pebbles, a large reddish inclusion, and a white crust-like material—produced only the spectra of calcite. This is consistent with ethnohistoric and ethnographic data that indicate that the Maya of the Northern Lowlands region used *sascab*—a chalky material composed primarily of deteriorated limestone—as aggregates added to the wet plaster (Houck, 2004, p. 64; Alonso Olvera, 2013, p. 87).

The i-Raman spectra recorded on two samples (samples 18 and 32) show a broad, intense band centered at approximately 772 cm^{-1} which partially overlaps the calcite band at 711 cm^{-1}. A similar feature, centered this time at 790 cm^{-1}, is present in a spectrum recorded on a third sample (sample 13). The literature indicates that features in these locations are common in the Raman spectra of calcium minerals at 1064 nm, but are not visible at shorter wavelengths (Aminzadeh, 1997; Edwards and Farwell, 2008; Chiriu *et al.*, 2014); this is consistent with results seen here, as the BRAVO spectra show no indication of these features. The features were also not observed in the 2005 study, presumably because both spectrometers used an excitation source of 785 nm. Aminzadeh notes that in FT-Raman, some calcium minerals show fluorescence emissions bands in this region; these include hydroxyapatite [$Ca_{10}(PO_4)_6$ $(OH)_2$], which shows a doublet at 704 and 771 cm^{-1} and calcium hydroxide (slaked lime, $Ca(OH)_2$), which shows fluorescence features at 776 cm^{-1} and 920 cm^{-1} (1997). In studies of historical wall paintings, broad bands centered at approximately 780-790 cm^{-1} are typically identified as limewash putty (Edwards and Farwell, 2008; Fernandes *et al.*, 2017). A study of pottery from Pompeii using the i-Raman instrument similarly reported a broad feature centered at approximately 780 cm^{-1}; this was likewise interpreted to be slaked lime which had been used as a binder for the pigment (Chiriu *et al.*, 2014).

The precise cause of these peaks is debated; some authors have argued that trace quantities of rare-earth metals are responsible, while others believe that they are related to the process of calcination (the burning of limestone to produce lime) which affects the crystal lattice structure of the material (Kaszowska *et al.*, 2016, p. 14). In European fresco painting, the term "limewash" often refers to a particular technique in which calcinated limestone (quicklime, CaO) was partially slaked and applied as a mortar. In some cases, the manufacture of this was highly specialized, as in the preparation of *Bianco di San Giovanni* in which moist lime was stored for several days and ground into a paste with a fine texture distinct from that of plain "slaked lime" (Edwards and Farwell, 2008, pp. 985–986). The Maya may have used $Ca(OH)_2$ in a similar manner, as optical microscopy has indicated that the support layer directly beneath most Late Classic Maya wall paintings was made of a finer paste with fewer inclusions than the lower mortar layers (Magaloni Kerpel, 2001, pp. 158, 161–165). The spectrum of slaked lime has also been reported in FT-Raman spectroscopic studies of stuccowork found at the Maya site of Copán, producing a broad feature at 770 cm^{-1}; the authors attribute this to the incomplete reaction of the slaked lime in the mortar with carbon dioxide (Goodall *et al.*, 2007, p. 670). Based on this evidence, the features observed in the i-Raman can be identified as slaked lime, or "limewash putty." It is perhaps worth mentioning that all three of these features occur on the painted surface of the samples rather than on the unpainted surface. This may support Magaloni Kerpel's observation that the layer immediately below the paint is often composed almost solely of lime with few or no inclusions (2001, pp. 158, 161–165). Optical microscopy conducted by Alonso Olvera et al. demonstrated that while many of the samples do not show distinct stratigraphy, some do contain evidence of an extremely thin preparation layer just below the pigmented layer (2005, p. 107).

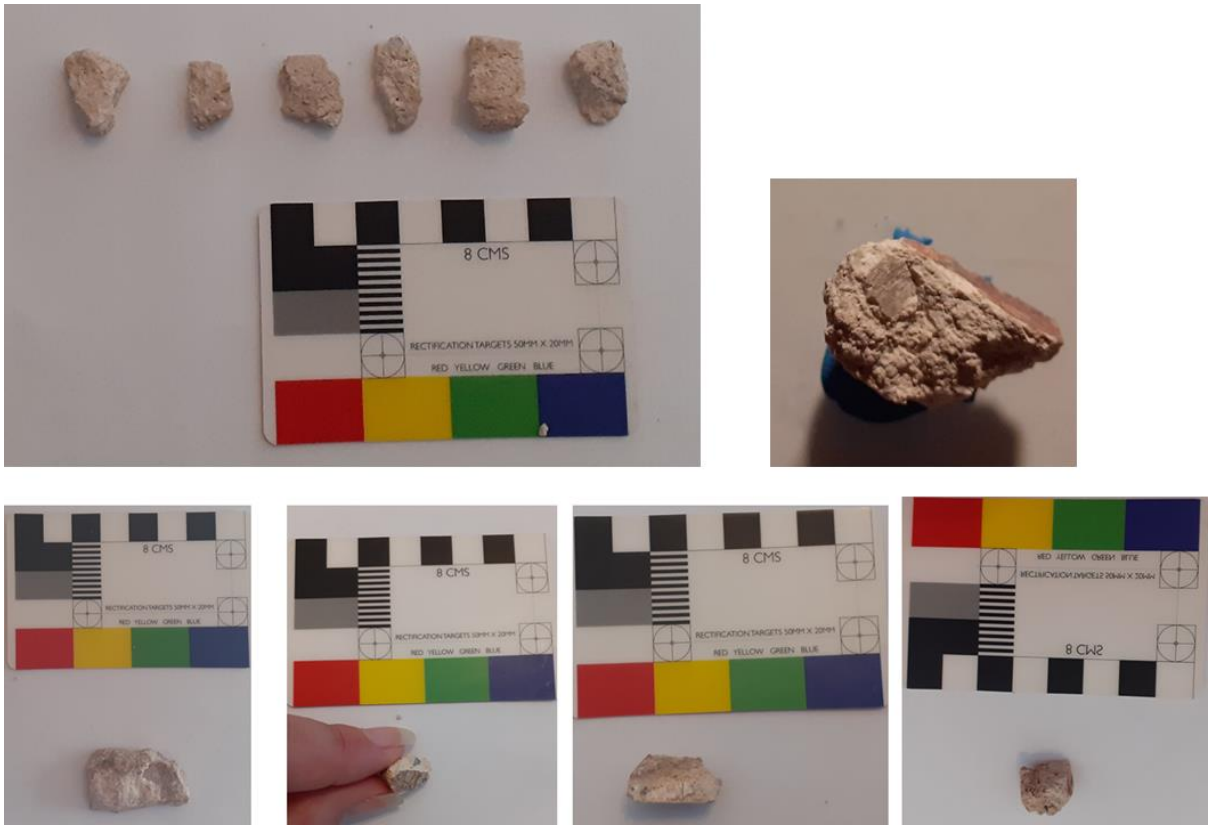

Figure 14 Photographs of unpainted plaster. Pebbles, flecks of charcoal, and dark fibrous matter were typical inclusions. A single sample (bottom far left) contains a smooth reddish inclusion and a white incrustation.

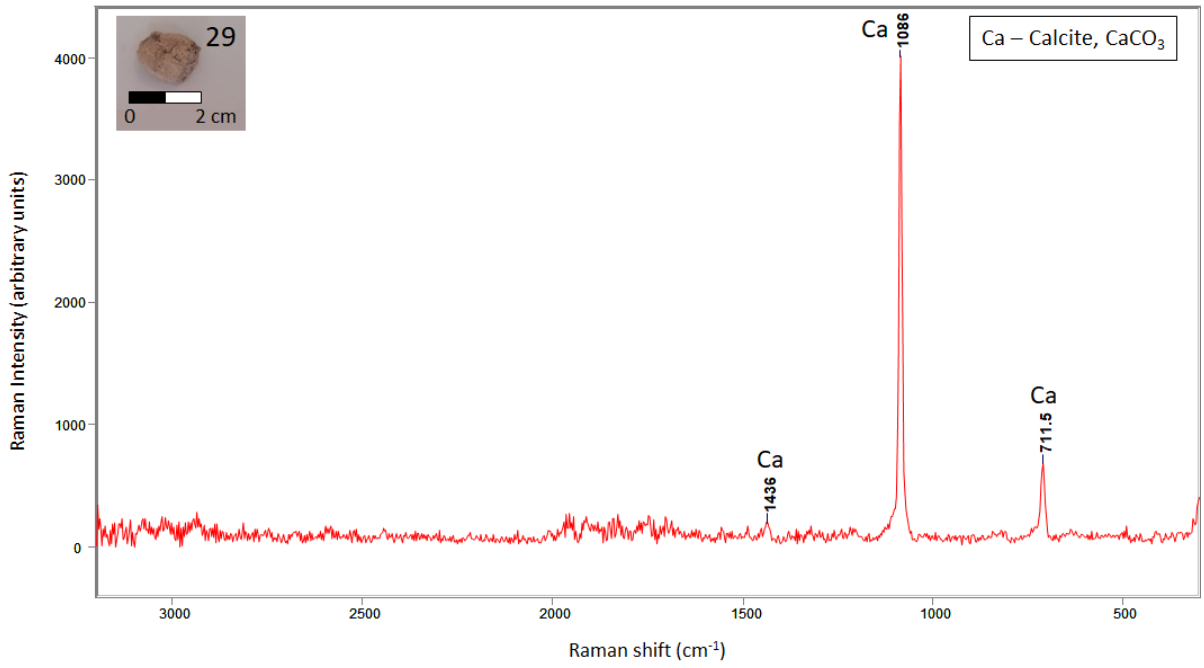

Figure 15 BRAVO spectrum recorded on unpainted plaster. Calcite is visible by the strongest band at 1086 cm^{-1} and the smaller band at 712 cm^{-1}. In this case, a third very weak band of calcite is also visible at 1436 cm^{-1}.

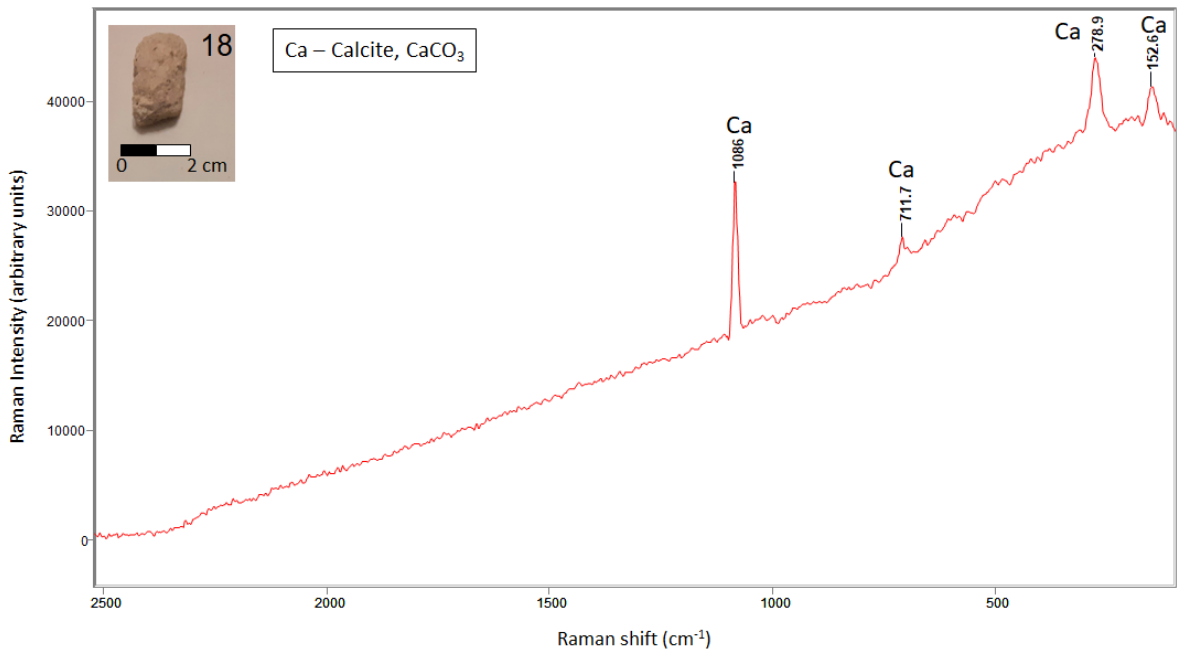

Figure 16 i-Raman spectrum recorded on unpainted plaster. Features for calcite are visible at 153, 279, 712, and 1086 cm^{-1}.

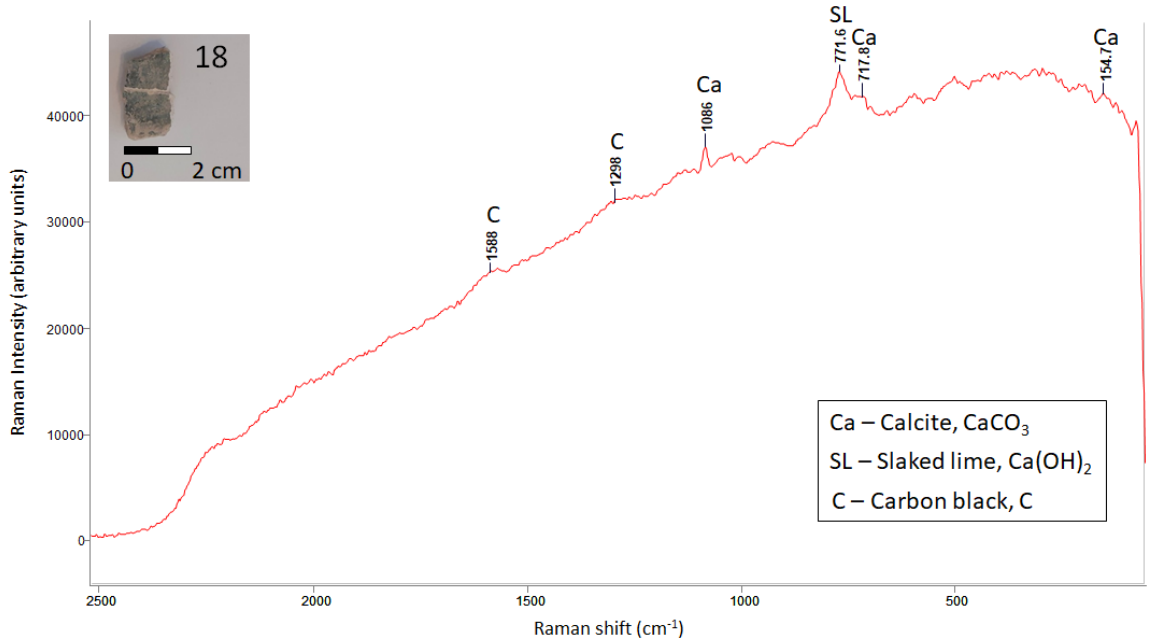

Figure 17 i-Raman spectrum recorded on sample 18, showing a feature for slaked lime at 772 cm^{-1}. Features for calcite are present at 1086, 712, and 155 cm^{-1}. The small, broad features at 1588 and 1298 cm^{-1} are characteristic of carbon black.

4.1.2 Paint Layers

Cinnabar

Cinnabar (HgS) was identified in three of the samples—Samples 9, 10, and 14. In the i-Raman spectra, this is easily recognizable by three peaks, with the strongest at 254 cm^{-1}, a weaker band at 282 cm^{-1} that is poorly resolved with the first and overlaps with one of the peaks for calcite, and a third medium

intensity band at 344 cm^{-1}. This is consistent with Raman spectra reported for cinnabar in the literature (Scheuermann and Ritter, 1969; Frost, Martens and Kloprogge, 2002).

The BRAVO has a spectral range of 3200-300 cm^{-1} and therefore the two bands at the lowest wavenumbers are not visible. For samples 9 and 10, this does not present an obstacle in identification, as the band at 344 cm^{-1} is extremely intense. However, in sample 14, there is only a very weak band at this wavenumber. The i-Raman spectra recorded on the same sample confirm that this is cinnabar due to the presence of peaks at lower wavenumbers; however, whereas the cinnabar band at 254 cm^{-1} in samples 9 and 10 was considerably more intense than the calcite band at 280 cm^{-1} (overlapping with the 282 cm^{-1} band of cinnabar), the bands are of nearly equal intensity in the spectrum of sample 14. This sample is a much lighter red color than samples 9 and 10 and has an overall faded or washed-out appearance. It is uncertain whether this represents an intentional lightening of the shade, perhaps by mixing small amounts of cinnabar with calcite, or is a sign of degradation of the paint over time.

In addition to its faded appearance, sample 14 contains several very small black spots. Spectra recorded in these areas showed only cinnabar. Cinnabar is known to darken with exposure to light and humidity; the precise mechanisms of this discoloration are not entirely understood, and at least four mechanisms of degradation have been proposed: 1) the transformation of cinnabar into its cubic polymorph metacinnabar; 2) chemical reactions that occur directly between cinnabar and chlorine and produce photo-sensitive compounds such as calomel and corderite; 3) the breakdown of cinnabar into metallic mercury and sulfur, catalyzed by the presence of chlorine; and 4) a chemical reaction between cinnabar and calcite which produces gypsum (Keune and Boon, 2005; Cotte *et al.*, 2006; Radepont *et al.*, 2011; Neiman, Balonis and Kakoulli, 2015). Given that gypsum was not detected on this sample, the fourth mechanism is unlikely in this instance, although the other three processes are possible. Raman spectroscopy studies have found that black and red cinnabar produce essentially identical Raman spectra, although blackened cinnabar typically shows lower Raman intensity than red cinnabar (Vandenabeele, Lambert, *et al.*, 2005, p. 711; Baraldi *et al.*, 2007, p. 423; Chiriu, Ricci and Cappellini, 2017, pp. 74–75). While the results of the current work are thus consistent with cinnabar degradation, this interpretation must be treated with caution given the small size of the black spots. As previously discussed, the large spot size of the BRAVO spectrometer and the lack of precision in positioning the i-Raman laser make it difficult to identify the materials present in very small areas.

The presence of cinnabar is considered highly significant, as it is extremely unusual in Maya wall paintings (Vandenabeele *et al.*, 2005a, p. 2353). At present, this pigment has been reported in Maya wall paintings at only two additional sites—La Blanca and Bonampak, both of which are located near cinnabar sources (Magaloni Kerpel 2001, 173; Vázquez de Ágredos Pascual, Lorenzo, and Cosme 2014).

The few sources of cinnabar known throughout the Maya area are located in Chiapas, Guatemala, Honduras, and El Salvador, all of which are far from Ek' Balam (Houston *et al.*, 2009, p. 65; Quintana *et al.*, 2015, p. 1046). Despite its scarcity, it was commonly used in Maya funerary contexts, and was applied to human remains as well as grave goods and the walls and floors of tombs. Spectroscopic studies of red funerary pigments from several Maya sites have indicated that cinnabar was used primarily in elite funerary contexts, while the more easily obtained haematite was often used in burials of commoners as a less expensive substitute, underscoring the cost and value of the rare material (Quintana *et al.*, 2015). While the reason cinnabar was used at Ek' Balam is unknown, the use of this pigment certainly indicates the exceptional wealth attained by the kingdom, which could afford to import the mineral from a considerable distance. Since 2005, cinnabar has been discovered in additional wall paintings of the Acropolis, including room 12, described as a battle scene with red walls, and in room 50, a mural that included personages identified by hieroglyphic characters (Alonso Olvera *et al.*, 2005, pp. 93–94; Alonso *et al.*, 2014, p. 69).

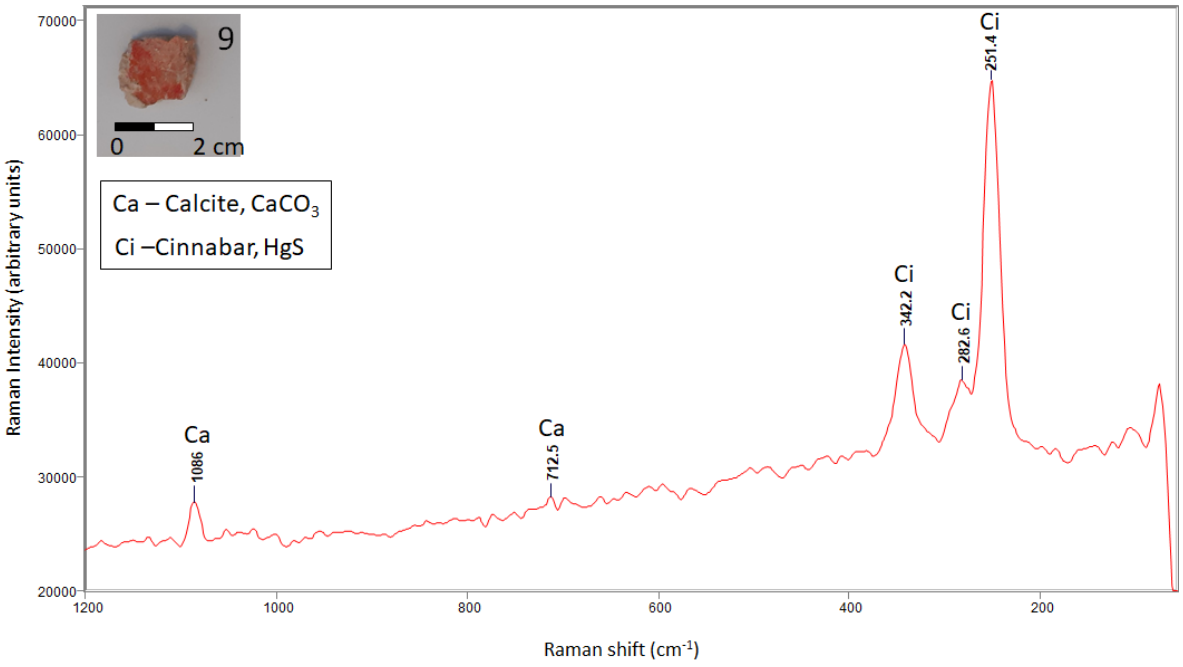

Figure 18 i-Raman spectrum recorded on sample 9 showing the presence of cinnabar at 251, 283, and 342 cm^{-1}. All other features are characteristic of calcite. Spectral range of 1200-100 cm^{-1} is shown.

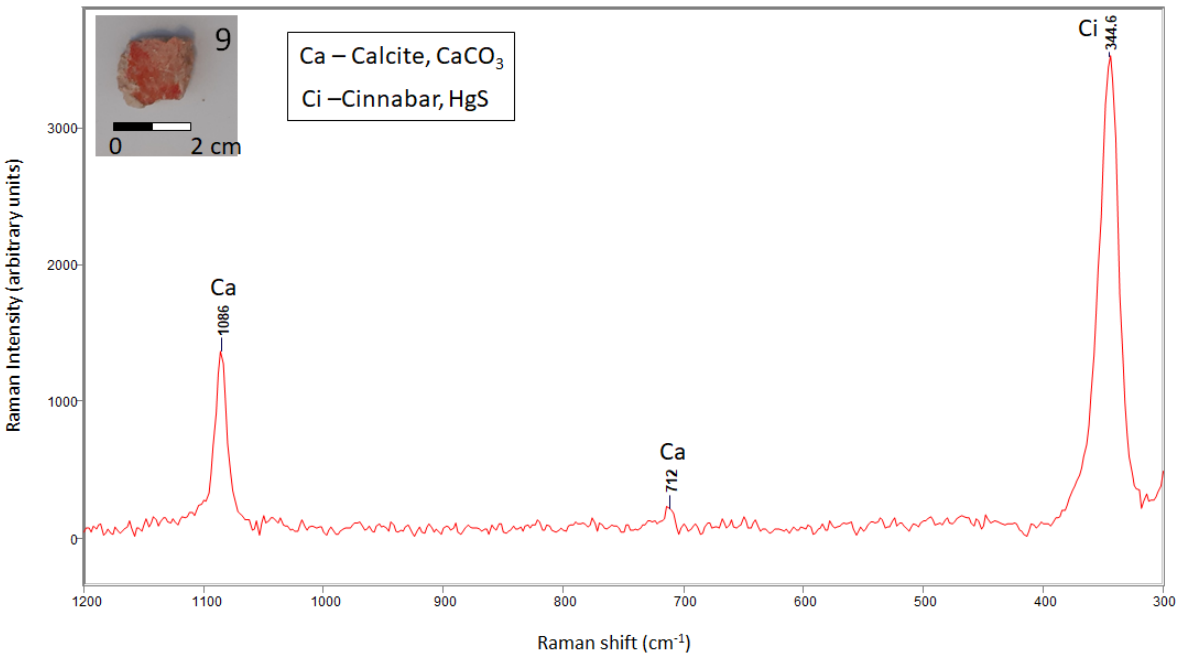

Figure 19 BRAVO spectrum recorded on sample 9. Because of the BRAVO's spectral range, only a single band of cinnabar is visible (345 cm^{-1}). Spectral range of 1200-300 cm^{-1} is shown.

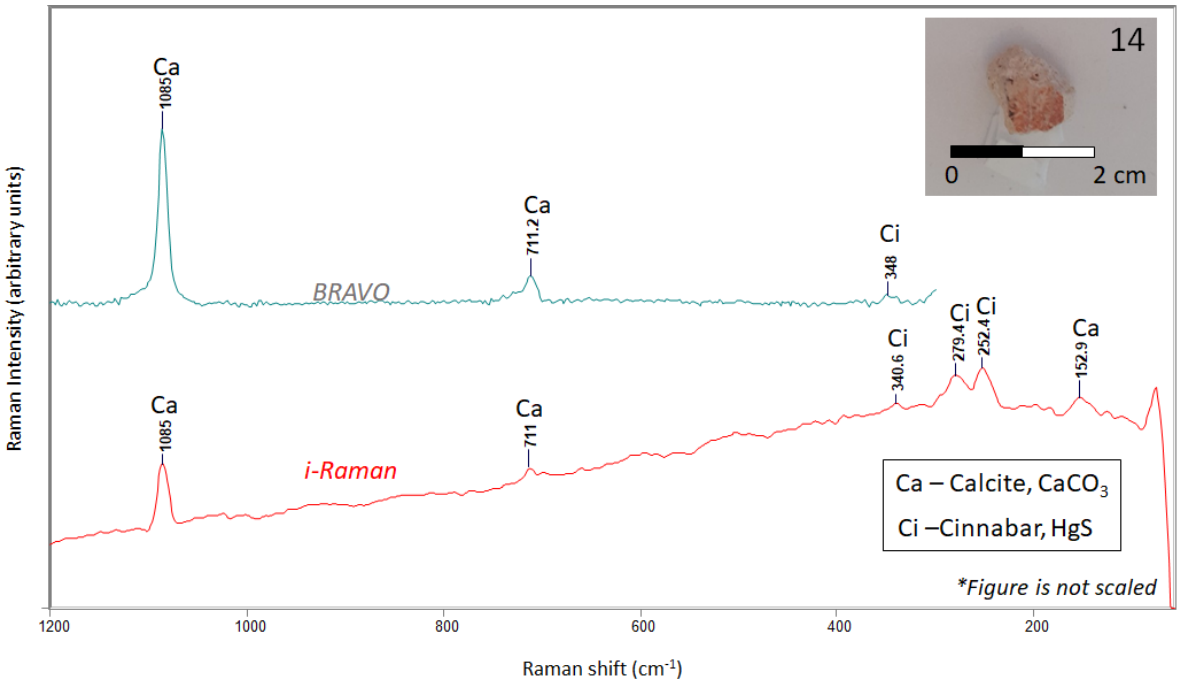

Figure 20 Spectra recorded on sample 14 with the BRAVO (blue) and the i-Raman (red), at spectral range 1200-100 cm^{-1}. The features of cinnabar are of low intensity. This makes identification of cinnabar with the BRAVO instrument difficult, because only a single band is present at 348 cm^{-1} is visible within its spectral range.

Figure 21 Close-up of sample 14. The red paint is pale, and small black spots are visible along the margins.

Haematite

Four samples—sample 12, 15, 30, and 33—showed the characteristic spectra of haematite (Fe_2O_3). While haematite could be detected by both spectrometers, identification was more straightforward with the i-Raman than the BRAVO spectrometer due to the spectral range of the instruments. As noted by Rousaki et al., the BRAVO's spectral cutoff at 300 cm^{-1} can be especially disadvantageous in identifying pigments such as oxides and sulfides, which produce peaks at lower wavenumbers (2019, p. 6). As with cinnabar, the strongest feature of haematite occurs below 300 cm^{-1}, at approximately 293 cm^{-1}, along with a second band of medium intensity at approximately 225 cm^{-1} (Košařová *et al.*, 2013, p. 1575). The spectral range of the i-Raman, 2500-100 cm^{-1}, includes these features; however, the band at 293 cm^{-1} overlaps with one of the features for calcite, centered at 288 cm^{-1}. While the spectral resolution for this instrument is reported at less than 10 cm^{-1} (Rousaki *et al.*, 2019, p. 5), it is apparently inadequate for separating these peaks, and they appear as a single, intense band, centered roughly at 290 cm^{-1}. The band at 225 cm^{-1} is visible between the two lattice vibrations for calcite (155 cm^{-1} and 288 cm^{-1}); other visible bands of haematite are a strong feature at 409 cm^{-1} and a medium intensity feature at 609 cm^{-1}. A weak feature at approximately 495-500 cm^{-1} is often reported as well (Jubb and Allen, 2010; Košařová *et al.*, 2013). Here, a band at approximately 503 cm^{-1} likely corresponds to this peak.

Haematite is identifiable in the BRAVO spectra by a sharp, medium-intensity band centered at 409 cm^{-1}. In some cases, a second, weaker band is observable at approximately 611 cm^{-1} but this is often indistinct. The weak band at 495 cm^{-1} is seldom visible due to noise or fluorescence. Therefore, identification of haematite with the BRAVO instrument typically relies on the presence of a single distinct band that is frequently of only medium or low intensity. In one case, this led to a "false positive" identification: a spectrum recorded on the dark red stripe of sample 13 appeared to show a small peak centered at 409 cm^{-1} which was originally believed to be haematite. However, the i-Raman spectrum was unable to confirm this result. A closer inspection of the unsubtracted BRAVO spectra revealed that there was no distinct peak at this wavenumber, but that the subtraction algorithm had misleadingly resolved noise in this region into a peak. This shows both the occasional disadvantages of the BRAVO's automated fluorescence subtraction, and also the disadvantage of the reduced fingerprint region; had the spectral range extended into lower wavenumbers, the absence of the other haematite features would have been observable, preventing the misidentification.

Haematite is a commonly studied pigment in Raman spectroscopy. The literature indicates that the precise wavenumber positions as well as the relative intensities and broadness of the bands observed in haematite spectra depend on a variety of factors including experimental parameters such as laser excitation wavelength and laser power, as well as crystallinity, the presence or absence of different types of clays, and substitutions by aluminum, yttrium, or indium (De Faria, Venâncio Silva and De Oliveira, 1997, pp. 874–875; Froment, Tournié and Colomban, 2008, pp. 563–565; Bersani and Lottici, 2016, p. 500). Additional variations can arise because different iron oxides are frequently found together, and can also undergo reactions when heated. For example, it is known that some prehistoric peoples produced haematite by roasting hydrated iron oxides, usually goethite. In many Raman studies, the presence of a band at 660-670 cm^{-1} has been noted, which can either be interpreted as magnetite (Fe_3O_4) present alongside haematite, or as disordered haematite (Bersani and Lottici, 2016, p. 500). While magnetite can occur naturally in ochres, it can also be produced as a byproduct when other iron oxides are heated to manufacture haematite (Froment, Tournié and Colomban, 2008, p. 561). Although the methodologies used in the present work are not precise enough to make determinations regarding complex factors such as crystallinity or elemental substitutions, it can be noted that there is no evidence of a feature at 670-660 cm^{-1}, implying that magnetite is absent. There is equally no evidence of other substances besides haematite and those typically seen in the plaster substrate.

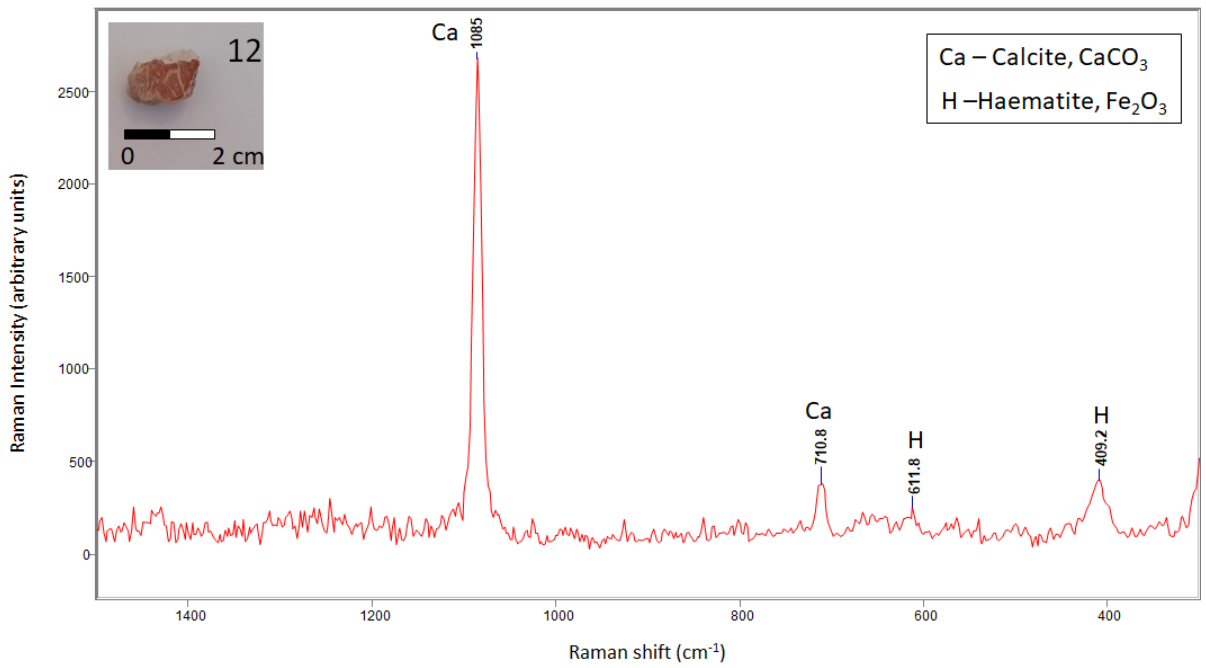

Figure 22 BRAVO spectrum of haematite (409 and 612 cm^{-1}) and calcite recorded on sample 12. Spectral range of 1500-300 cm^{-1} is shown.

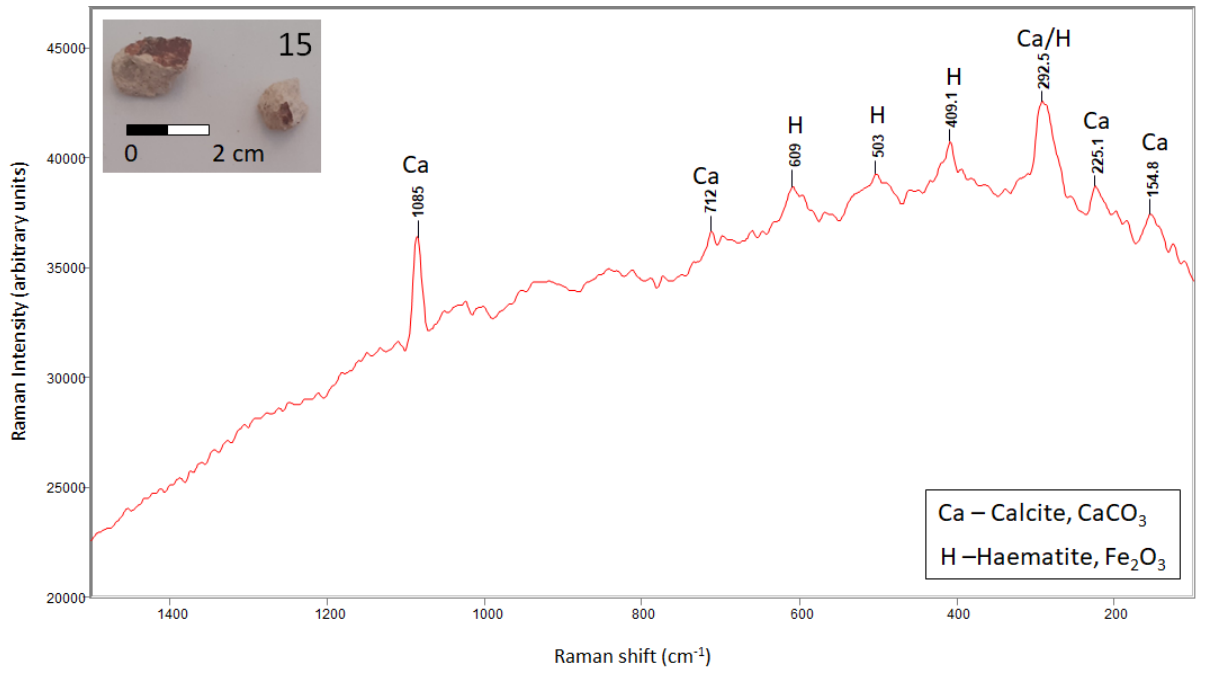

Figure 23 i-Raman spectrum recorded on sample 15 showing haematite at 225, 293 (overlapping with one of the features of calcite), 409, 503, and 609 cm^{-1}. Spectral range is shown from 1500-100 cm^{-1}.

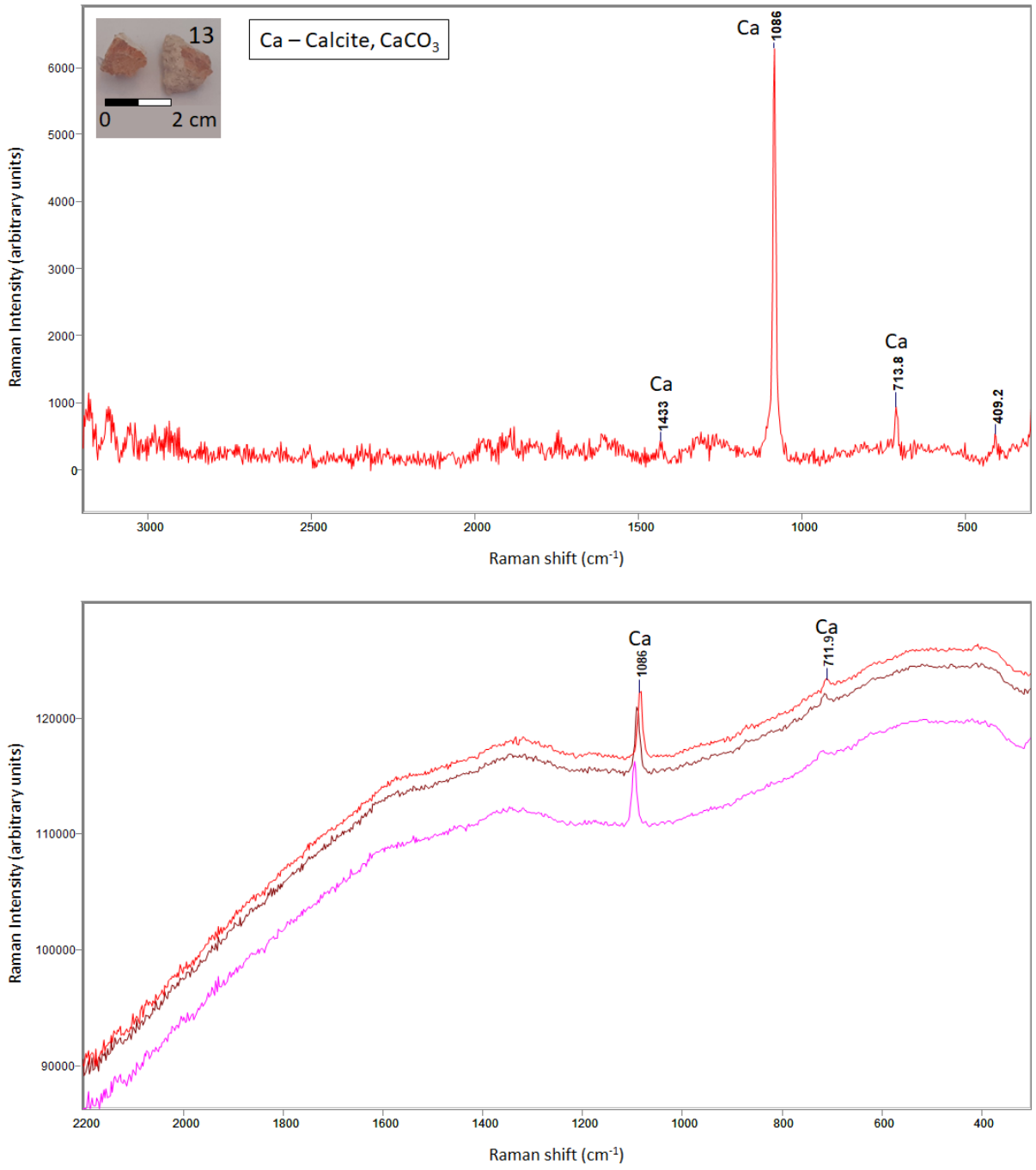

Figure 24 BRAVO spectra recorded on sample 13. The subtracted spectrum (top) appears to show a feature at 409 cm^{-1}, usually indicative of haematite. However, the unsubtracted spectra (bottom) show noise and fluorescence at this location rather than a distinct feature, illustrating the sometimes-misleading nature of the automated subtraction process. This result was confirmed by the i-Raman spectra (not shown), which showed no evidence of haematite.

Maya Blue

The BRAVO instrument enabled unambiguous identification of Maya blue for all five of the bright blue samples—samples 17, 20, 21, and 22. In the 2005 publication, up to twenty-five features of Maya blue were identified in the spectra, with the most prominent bands occurring at 555 cm^{-1} (assigned as the δ(C=C-CO-C) bending vibration) and 1573 cm^{-1} (the ν(CC), ν(C=C), and ν(C=O) stretching vibrations)

(Vandenabeele *et al.*, 2005a, p. 2353-2354). In the spectra collected with the BRAVO, both of these features were readily observable, although the band at 555 cm^{-1} often occurred at a lower intensity than reported by Vandenabeele et al. This difference in intensity likely relates to the excitation wavelength. In Raman spectra recorded of indigo using a 785 nm wavelength, resonance enhancement of certain features has been reported; these include the band at 544 cm^{-1}. In the spectrum of Maya blue, the same band is slightly shifted, occurring at 555 cm^{-1} (Vandenabeele and Moens, 2003, p. 187; Vandenabeele *et al.*, 2005a, p. 2354). Both spectrometers used in the 2005 study had an excitation source of 785 cm^{-1}. The BRAVO spectrometer uses two lasers at excitation wavelengths of 785 nm and 852 nm, respectively. While the first of these is at the correct wavelength to cause resonance, the second is at too high a wavenumber to produce this effect, and the sequentially shifted excitation process entails the shifting of both wavelengths by raising the laser temperature (see 3.2.2 BRAVO Handheld Spectrometer above). Thus, the BRAVO evidently did not yield the same resonance effect observed with the benchtop instrument.

In the BRAVO data, the band at 1573 cm^{-1} was therefore the most intense feature, and a third band at approximately 1317 cm^{-1} was also often visible; this latter feature corresponds to the ν(CC) stretching vibration (Vandenabeele *et al.*, 2005a, p. 2354). Other features reported by Vandenabeele et al. were sometimes also visible, but were rarely distinct from noise or fluorescence. In some cases, the features were easier to identify in the unsubtracted spectra, which frequently showed bands at 1255, 1632, and 1687 cm^{-1} as well (Vandenabeele *et al.*, 2005a, p. 2354). As discussed above (see 2.6.2.1 Maya Blue), the clay component of Maya blue is rarely observable in Raman spectroscopy; all of these features are thus caused by the vibrational modes of indigo and possibly dehydroindigo molecules. Raman spectroscopy alone cannot confirm that the clay component of Maya blue is palygorskite, as indigo mixed with clays such as sepiolite or montmorillonite produce nearly identical spectra (Sánchez del Río *et al.*, 2006). However, SEM and XRD have confirmed that palygorskite is indeed present within the Maya blue paint of these samples (Alonso Olvera *et al.*, 2005, pp. 112–115).

The presence of multiple features made Maya blue a fairly straightforward identification for the BRAVO spectrometer. Identification is made even easier by the fact that the Maya employed few other blue colorants, and those that were used—primarily azurite, but also occasionally veszelyite $[(Cu,Zn)_2ZnPO_4(OH)_3•2(H_2O)]$ and wollastonite ($CaSiO_3$)—have distinct spectra from those of Maya blue (Garcia Moreno *et al.*, 2008; Buzatu and Buzgar, 2010; Marucci *et al.*, 2018).

While readily identifiable with the BRAVO instrument, Maya blue could not be identified in the i-Raman data. The only evidence of the Maya blue spectrum is a very slight rise at approximately 1571 cm^{-1}. This poor result is inconsistent with the literature. In theory NIR excitation should be optimal for

producing a spectrum of indigo, given that indigo has a broad absorption band in the visible range of light (Marucci *et al.*, 2018, p. 1225). FT-Raman spectroscopy has successfully recorded the spectrum of synthetic Maya blue at 1064 nm excitation, which seems to indicate that the excitation wavelength itself is not to blame (Manciu *et al.*, 2007, p. 1194). However, in a Raman spectroscopy study conducted on artifacts containing Maya blue, Wiedemann et al. were able to obtain recognizable spectra using a visible excitation wavelength (512.5 nm) but in some cases failed to obtain spectra of Maya blue when using NIR excitation. The authors attributed this to low concentrations of indigo and a strong background arising from the palygorskite clay or from the substrate (2007, pp. 60–1). Similar factors may be at work here, although it is also possible that different parameters set with the i-Raman could yield better results in different circumstances. Unfortunately, the detector of the i-Raman spectrometer frequently flooded when exposure times, number of accumulations, or laser powers were set to even moderate levels, producing entirely unreadable spectra. Therefore, both of these parameters were kept low to avoid this outcome. This was a constant problem with this spectrometer that was not exclusive to Maya blue samples.

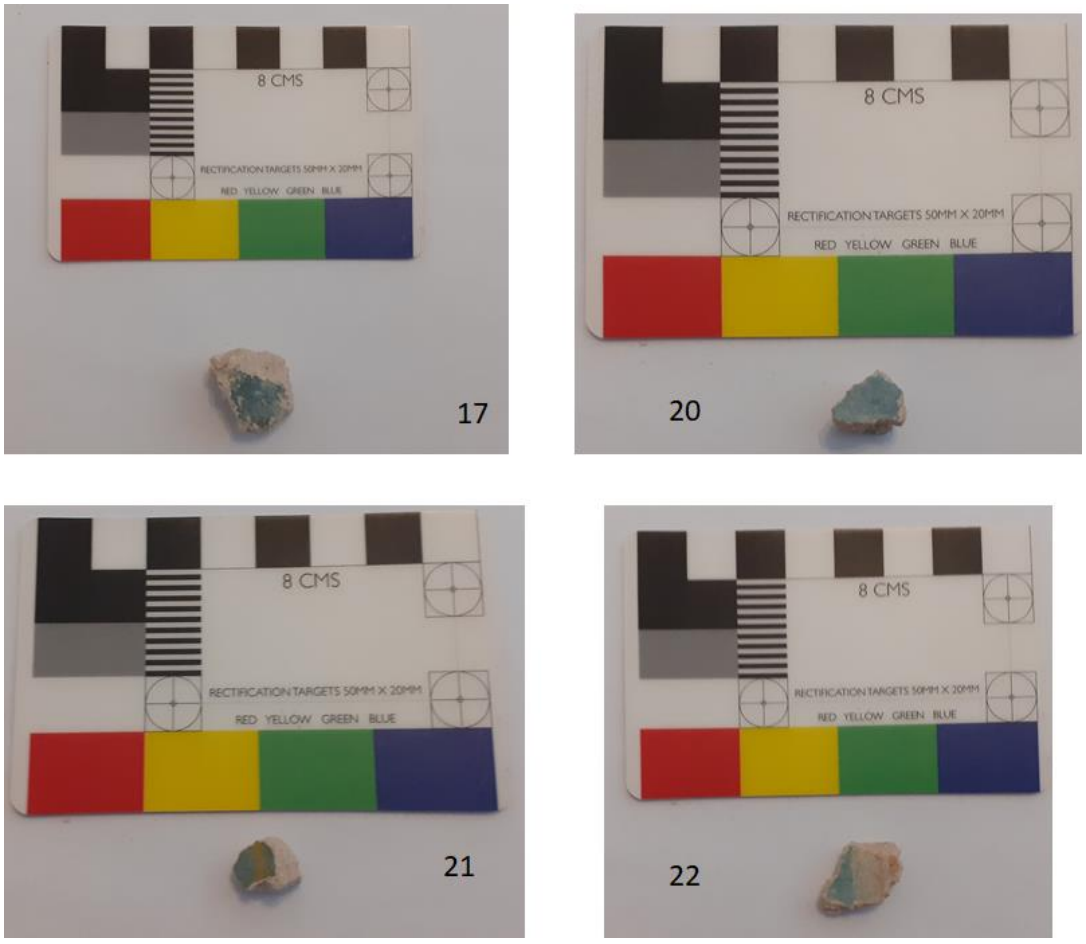

Figure 25 Maya blue samples.

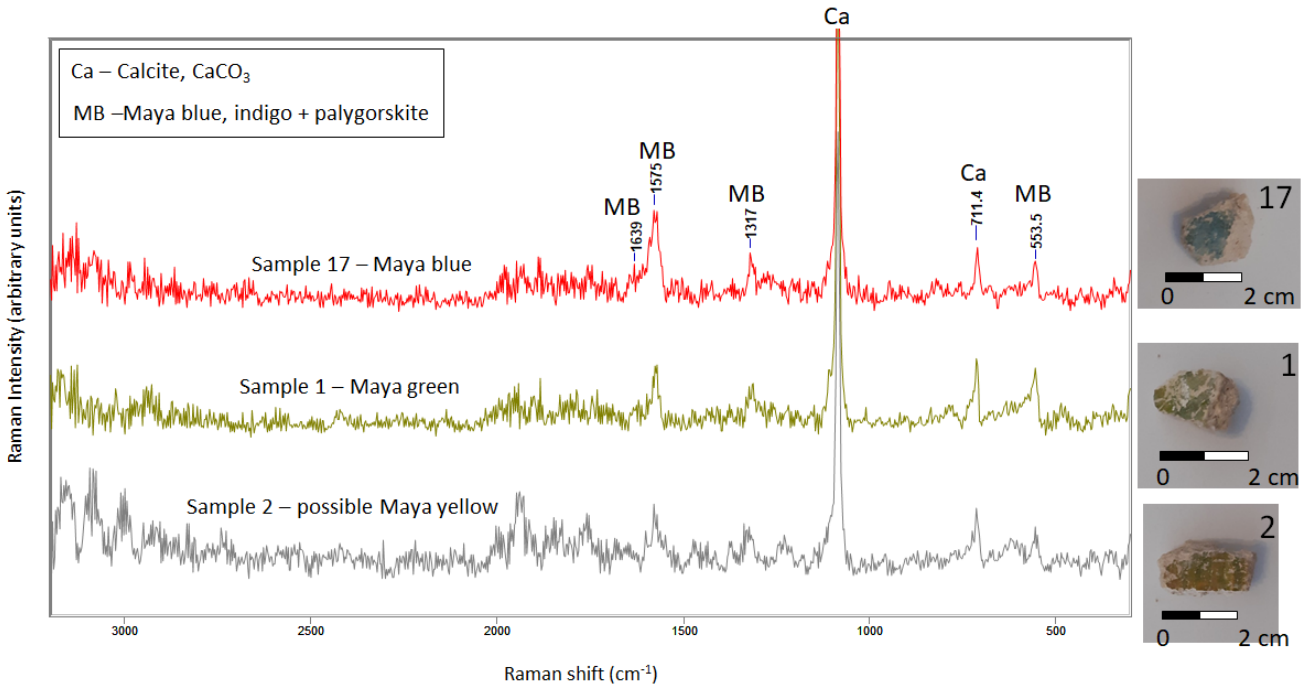

Figure 26 BRAVO spectra showing the characteristic features of Maya blue, Maya green, and possible Maya yellow.

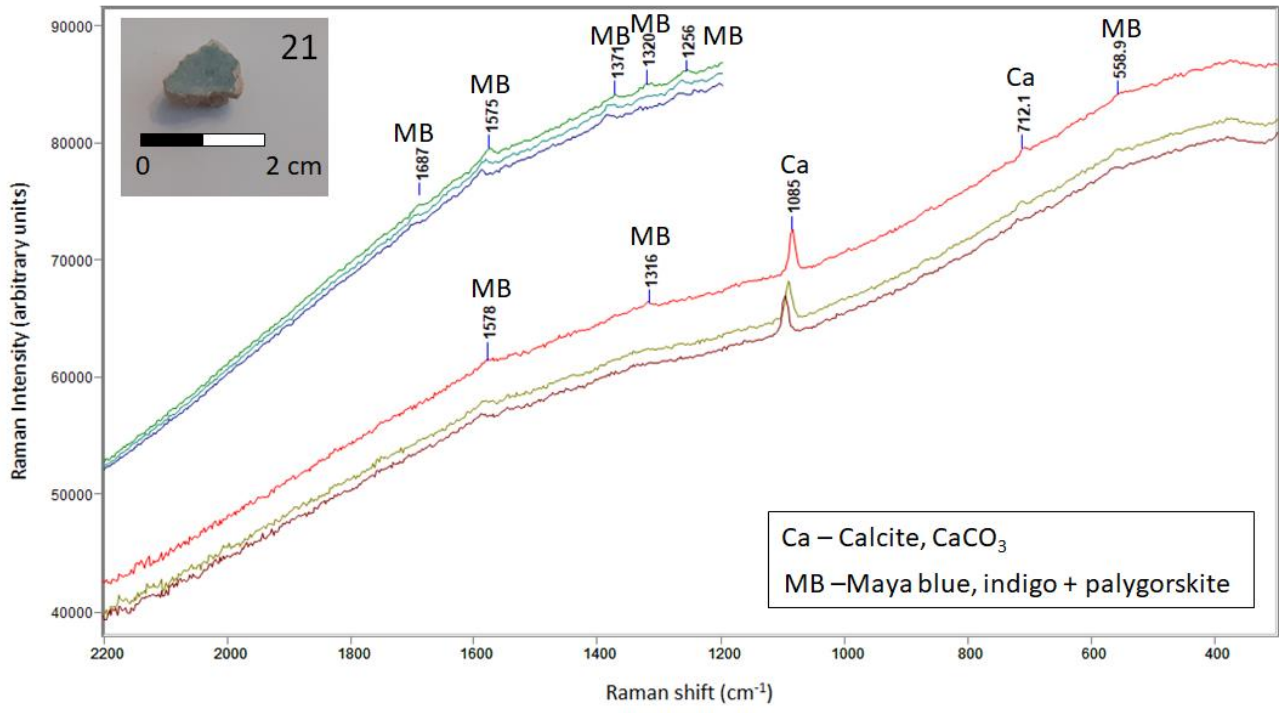

Figure 27 BRAVO unsubtracted spectra of sample 21 between 2200-300 cm^{-1} showing Maya blue and calcite.

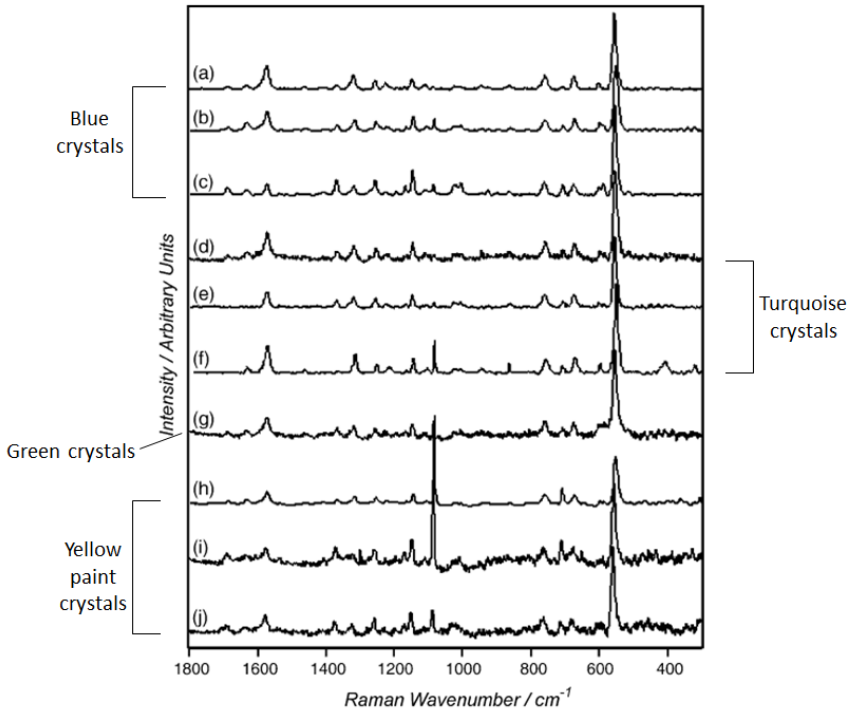

Figure 28 Spectra of Maya blue, Maya green, and Maya yellow recorded by Vandenabeele et al. 2005.

Blue samples Raman wavenumber (cm^{-1})	Blue part of a Mayan statue [21] Raman wavenumber (cm^{-1})	Indigo according to [36] Raman wavenumber (cm^{-1})	Indigo according to [21] Raman wavenumber (cm^{-1})	Assignment of the vibration
1687	1680 (+7)	1703 (−16)	1690 (−3)	ν(C═O)
1632	1631 (+1)	1628 (+4)	1635 (−3)	ν(CC), δ(CH)
		1581		
1573	1573 (0)	1573 (0)	1577 (−4)	ν(CC), ν(C═C), ν(C═O)
1483	1493 (−10)			ν(CC), δ(CH)
1463	1466 (−3)	1462 (+1)	1459 (+4)	ν(CC), δ(CH)
1411				
1368	1362 (+6)	1364 (+4)	1365 (+3)	δ(NH), δ(CH)
1318	1322 (−4)	1310 (+8)	1310 (+8)	ν(CC)
1254	1254 (0)	1250 (+4)	1252 (+2)	δ(CH), δ(C═O)
1224	1221 (+3)	1224 (0)	1219 (+5)	δ(CH), ν(CN)
1191				$\nu(CC)_{ring}$
1166				δ(CC)
1146	1146 (0)	1148 (−2)	1147 (−1)	δ(CC)
1108	1107 (+1)	1096 (+10)		δ(CC), γ(CH)
1026	1023 (+3)			γ(CH)
1017		1013 (+4)		δ(CH)
1008	1005 (+3)			δ(C─CO─C═C)
930	945 (−15)	940 (−10)	(+)	γ(CH)
862	861 (+1)			ν(CN)
811				$\gamma(CC)_{5\text{-ring}}$
758	754 (+4)	762 (−4)		δ(CH), δ(N─C─C)
673	669 (+4)	674 (−1)	(+)	δ(CC)
600	599 (+1)	599 (+1)	599 (+1)	δ(C═O), δ(CH), δ(C─NH─C)
586				γ(CH), γ(NH)
555	553 (+2)	545 (+10)	550 (+5)	δ(C═C─CO─C)

Figure 29 Wavenumbers of Maya blue Raman features recorded in Vandenabeele et al. 2005 (far left), Maya blue features recorded on a Maya statue (Smith, 2000), indigo features reported in two publications (right: Smith, 2000; left: Karapanayiotis *et al.*, 2004), and vibrational assignments. Vandenabeele et al. 2005

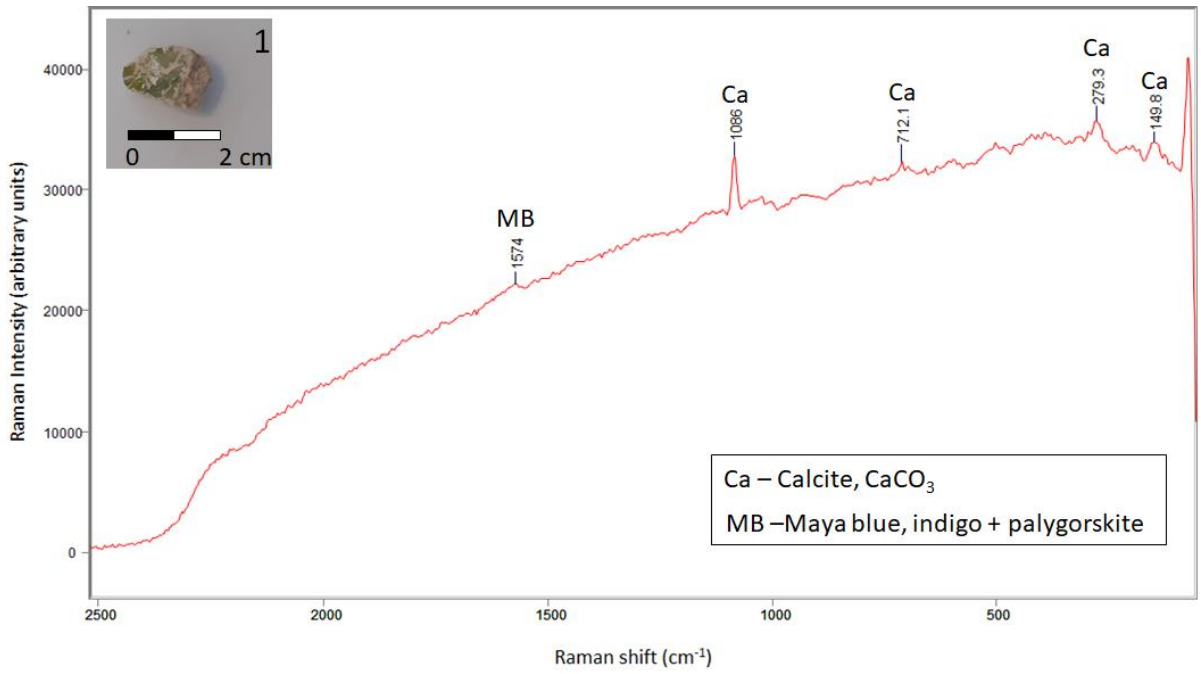

Figure 30 i-Raman spectrum of sample 1. The only indication of Maya blue/green is a small, indistinct rise at 1574 cm^{-1}, corresponding to the strongest band. All other features are of calcite.

Maya Green

As in the 2005 publication, the green pigments were found to have identical spectra to those of the blue pigments. Once again, this was observable in the BRAVO spectra only. Vandenabeele et al. interpreted this as an example of "Maya green," in which the ratio of indigo to palygorskite was altered to produce a green rather than blue colorant. Alonso Olvera et al. (2005) also proposed that some of the green pigments could have been created by first precipitating a different yellow dye onto a clay and then mixing this with Maya blue rather than by altering the ratios in the Maya blue recipe. Magaloni Kerpel has similarly reported mixtures of Maya blue and yellow colorants, typically either ochre or possibly organic yellow dyes, occurring at several Maya sites (2001, p. 173). While there is no evidence of this in the Raman data, ochre and organic dyes are known to be poor Raman scatterers and might be present in only small amounts. In addition, spectra recorded on the single entirely yellow sample in the assemblage (sample 3) showed no evidence of the colorant. Thus, results recorded here cannot determine whether the paint was created by altering the ratio of indigo to palygorskite or by mixing Maya blue with an unknown yellow colorant.

An interesting example of a potential mixture is Sample 5, which is a very dark olive green. This is peculiar for Maya green, which generally appears in brighter shades of green or turquoise. However, the spectrum for this sample contains extremely clear Maya blue features, making identification unambiguous. Magaloni Kerpel reports a dark olive paint composed of a mixture of Maya blue and yellow ochre observed in mural paintings at ten Maya sites, as well as a dark green composed of Maya blue and saponite clay [$Ca_{0.25}(Mg,Fe)_3((Si,Al)_4O_{10})(OH)_2 \cdot n(H_2O)$] (2001, p. 173). Alonso et al. also

identified a dark green pigment made from yellow ochre and Maya blue in the mural of Room 50 of the Ek' Balam Acropolis (2014, p. 69). However, there is no evidence of yellow ochre in the spectra acquired here.

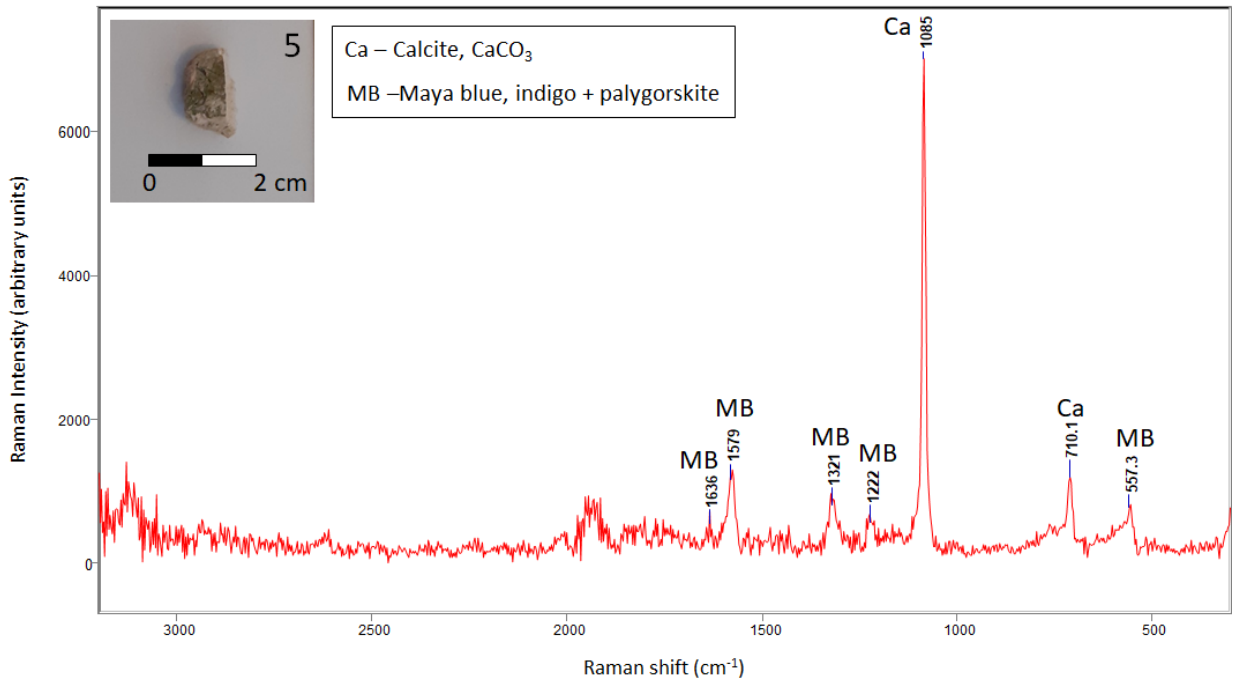

Figure 31 BRAVO spectrum of Maya blue/green and calcite, recorded on a dark olive green sample.

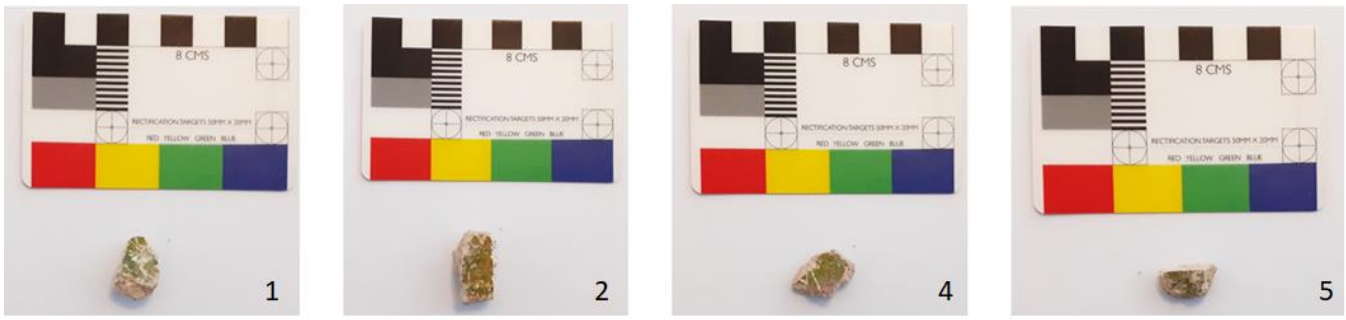

Figure 32 Green samples that produced the spectra of Maya blue.

Maya Yellow

Vandenabeele et al. observed that spectra recorded on yellow paint crystals also showed features of Maya blue. They hypothesized that this was due to incomplete aeration of the indigo, resulting in a reduced form of indigo (leuko-indigo) becoming trapped in the crystal lattices (2005, p. 2355). Due to the fixed optical head and large spot size of the BRAVO spectrometer and the inability to capture distinct spectra of Maya blue with the i-Raman spectrometer, this result could not be entirely confirmed by the present work. Sample 2, which consists of a mixture of yellow and dark green colorants, did yield spectra of Maya blue, both on the yellow and green portions of the sample. However, the colors are mottled and overlaid with each other, meaning that there are no large areas that are solidly yellow. Thus, it is impossible to determine whether the Maya blue spectra indicate the

green colorant, the yellow colorant, or both. A similar result was seen in sample 20, which consists of a thin yellow stripe against a blue background. While spectra recorded on both the blue and yellow components of the sample yielded features of Maya blue, the yellow stripe is too narrow to preclude interference from the Maya blue background. Given that the 2005 study used instruments with small spot sizes and a microscope objective lens for focusing, there is no reason to doubt their original result or interpretation. However, results of the present study would by themselves be inadequate for making this determination. This highlights a major disadvantage of the new mobile instrumentation as compared to the traditional benchtop methodology.

Fiedler et al. noted a few differences between the FT-Raman spectra of indigo and that of leuko-indigo, including, "the disappearance of the carbonyl stretching vibration *v* C=O present in indigo around 1701 cm^{-1} , [and] the appearance of a new signal around 1107 cm^{-1} due to *v* C-OH…" (2011, pp. 554–555). However, this distinction does not prove useful here, as no band at 1701 cm^{-1} was observable in any of the Maya blue or Maya green spectra recorded here, and as a band at 1107 cm^{-1} would potentially overlap with the strongest feature of calcite.

Carbon Black

Carbon black (C) was the primary chromophore for producing black, gray, and possibly grayish blue paints. This was fairly easy to observe in the i-Raman, which consistently showed the two characteristic broad features of amorphous carbon—the D (disorder) and G (graphite) bands—at approximately 1285 cm^{-1} and 1580 cm^{-1}, respectively. This is in keeping with values reported for amorphous carbon at 1064 nm excitation (Mennella *et al.*, 1995). No evidence of the phosphate stretching mode at 965 cm^{-1} was observed, which likely indicates the use of charcoal rather than bone black (Tomasini *et al.*, 2012, p. 1672). This correlates with other archaeometric research that has shown that bone black was rarely used in Maya painting (Vázquez de Ágredos Pascual, 2007, p. 57). More typically, carbonized resins were used as black pigments, often made from pine or copal trees; this may have had a religious component, as ethnohistoric sources have reported that the pigment material was often collected from the incense burned at sweat lodges (Houston *et al.*, 2009, p. 63).

In sample 18, which is dark gray or black, an intense feature at 772 cm^{-1} was observed in the i-Raman spectrum, as was discussed above. Aminzadeh notes that at 1064 nm wavelength excitations, a fluorescence feature at 771 cm^{-1} may be characteristic of hydroxyapatite; however, this is typically paired with a second band at 704 cm^{-1}, which was not observed in this case (1997). Given this, as well as the absence of the phosphate stretching mode at 965 cm^{-1}, this feature more likely corresponds with slaked lime or limewash putty.

The BRAVO results for carbon were more difficult to interpret due to the automated fluorescence subtraction. The darkest sample, sample 26, produced an extremely noisy subtracted spectrum, with two intense, broad features centered at roughly 1311 cm^{-1} and 1578 cm^{-1} corresponding to amorphous carbon. The unsubtracted spectra reveal the two features more clearly defined, centered at 1341 and 1587 cm^{-1}. This matches the values reported in Tomasini et al. for lamp black as well as those reported in Marucci et al. for several carbon black pigments including lamp black and bistre (a black pigment made from wood soot) (Tomasini *et al.*, 2012; Marucci *et al.*, 2018).

For other black or gray samples, the subtracted BRAVO spectra showed no evidence of carbon, or displayed only very slight features at the approximate locations for the D and G bands. When examining the unsubtracted spectra, however, the two broad bands diagnostic of carbon were observable. Given that black and gray are typically made with carbon and given the support of the i-Raman data, it seems clear that carbon is present in these cases. Thus, the automated subtraction process apparently had the unintended consequence of eliminating or muting the signals for carbon, which it interprets as fluorescence. Alonso Olvera et al. (2005) noted that for several samples, carbon seemed to have been applied in small concentrations and adhered to the plaster very poorly, perhaps accounting for some of these difficulties.

While the BRAVO subtracted spectra's "false negative" results for carbon can often be corrected by verifying them with the unsubtracted spectra, in some cases, the identification is not so straightforward. Some of the samples are not distinctly black or dark gray, but appear as a light bluish gray, meaning that there are several possible colorants that could have produced them. For sample 19, which is primarily bluish gray and contains darker gray mottling, the BRAVO subtracted spectrum showed no evidence of a chromophore, while the i-Raman spectrum showed two weak features in the locations for carbon. The BRAVO unsubtracted spectra appeared to confirm that the colorant is carbon, visible by the two diagnostic broad bands; however, these are of low intensity and are not nearly as distinct as in the black or dark gray samples.

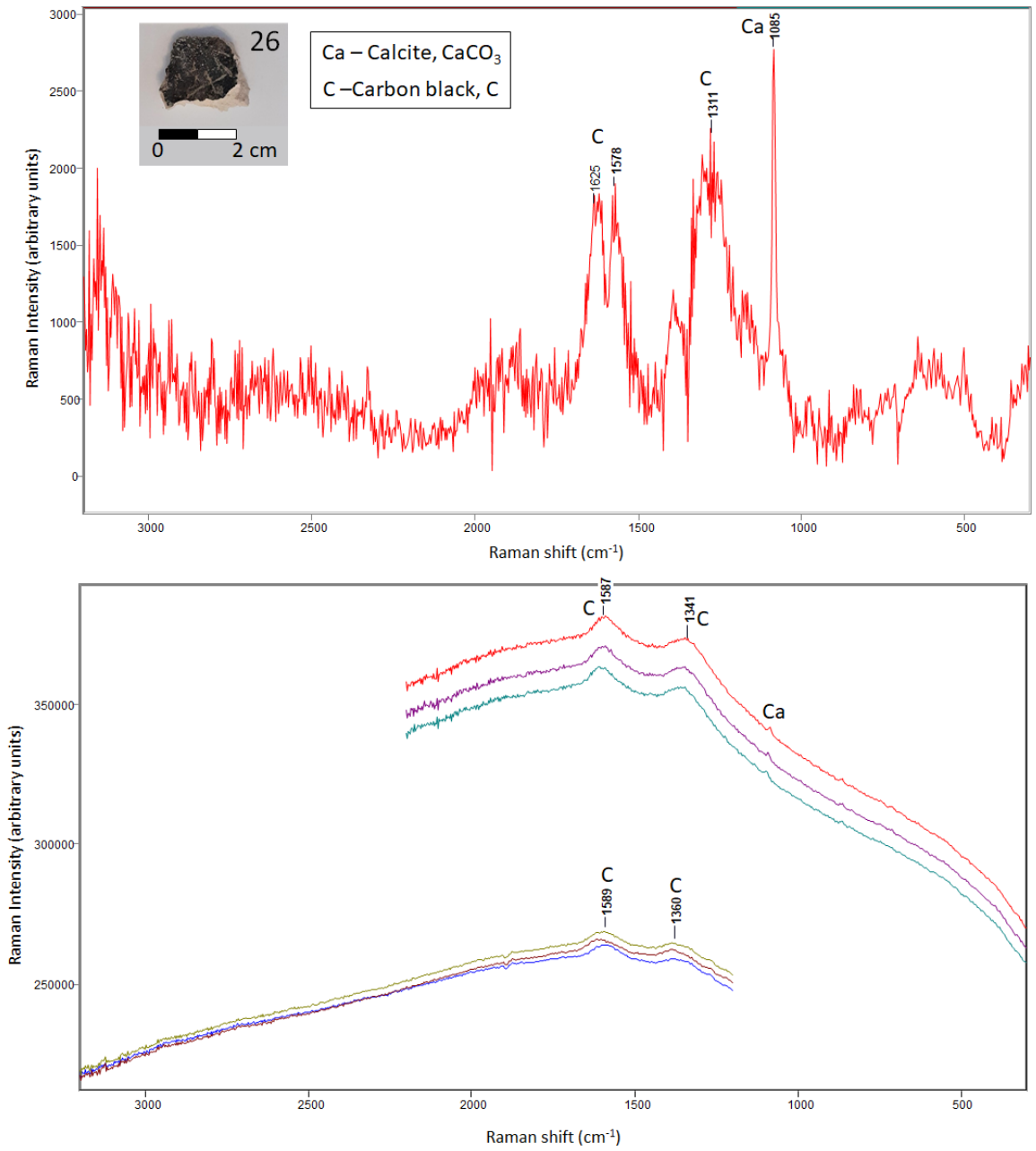

Figure 33 Subtracted (top) and unsubtracted (bottom) BRAVO spectra of sample 26, showing carbon black and calcite.

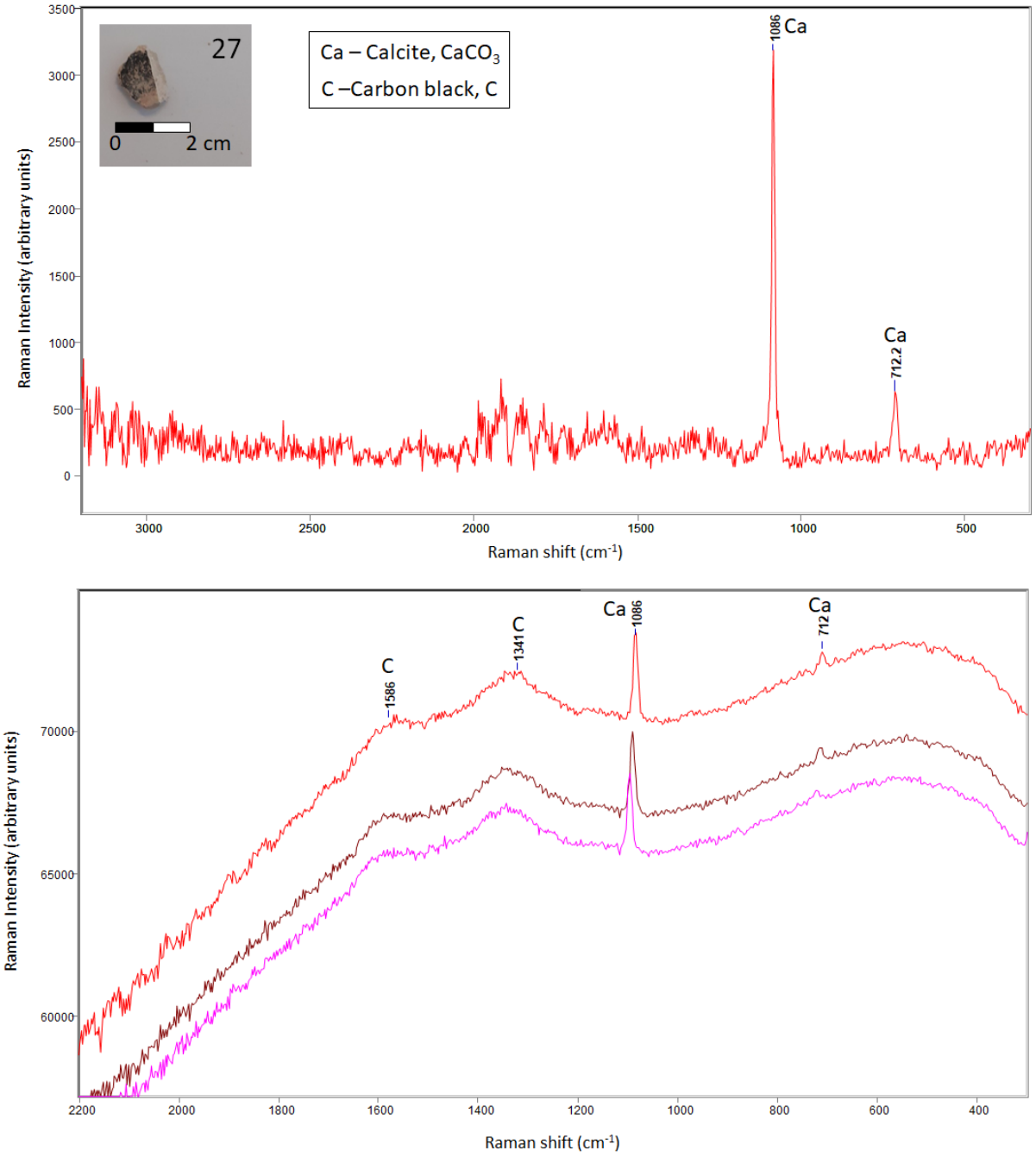

Figure 34 Subtracted (top) and unsubtracted (bottom) BRAVO spectra recorded from 2200-300 cm^{-1} of sample 27. The subtracted spectrum shows no evidence of carbon black, but the unsubtracted spectra show the characteristic broad features centered at 1586 and 1341 cm^{-1}.

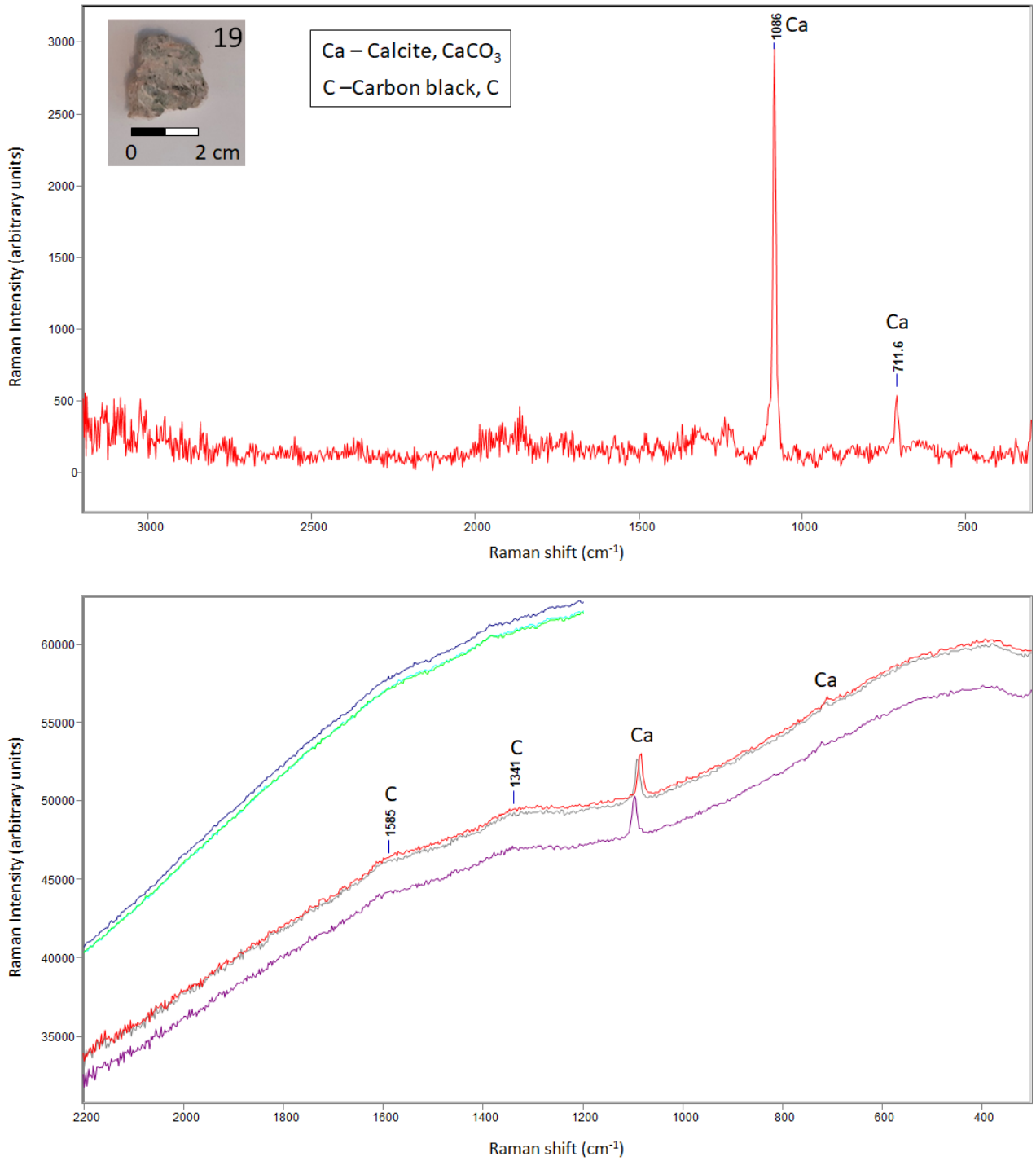

Figure 35 BRAVO subtracted (top) and unsubtracted (bottom) spectra (shown at 2200-300 cm^{-1}) of bluish-gray sample 19. No evidence of carbon black is visible in the subtracted spectrum, but two small broad features centered at 1585 and 1341 cm^{-1} may correspond to the D and G bands of amorphous carbon. This result is confirmed by the i-Raman spectra (not shown).

Purple: Maya blue + Haematite

Vandenabeele et al. noted the presence of a purple paint made by mixing haematite and Maya blue. However, they did not note which sample(s) displayed this mixture, or how many examples of this were seen (2005a, p. 2353).

The BRAVO spectra recorded on sample 30 clearly show both Maya blue and haematite, while the i-Raman spectra from this sample show bands of haematite along with the small rise at 1571 cm^{-1} that is usually seen in i-Raman spectra of Maya blue. Confusingly, however, sample 30 does not appear purple, but seems to consist of a red stripe surrounded by a pale blue colorant. In the photograph of the samples included in the original publication, this sample appears to be larger than the one analyzed here and does appear purple. I believe that some of the samples I worked with in this study were cut or broken from the original 2005 samples, accounting for the difference in size. The apparent difference in color seems to be merely the result of differing lighting conditions during photography. An optical microscopy photograph taken by Alonso Olvera et al. clarifies the matter, showing that the sample is a mixture of colors, including purple, light and dark blue, and orange (2005, p. 100). Regardless, the original result was recreated, showing a spectrum of Maya blue and haematite together, although it is unclear whether the two pigments have been mixed or were applied separately, either in mottled daubs or as thin, translucent layers.

Another purple sample—sample 24—produced very high degrees of fluorescence when analyzed with both spectrometers. Sample 16, which could be considered purple or dark red, showed only the spectrum of calcite, with no indication of the colorant.

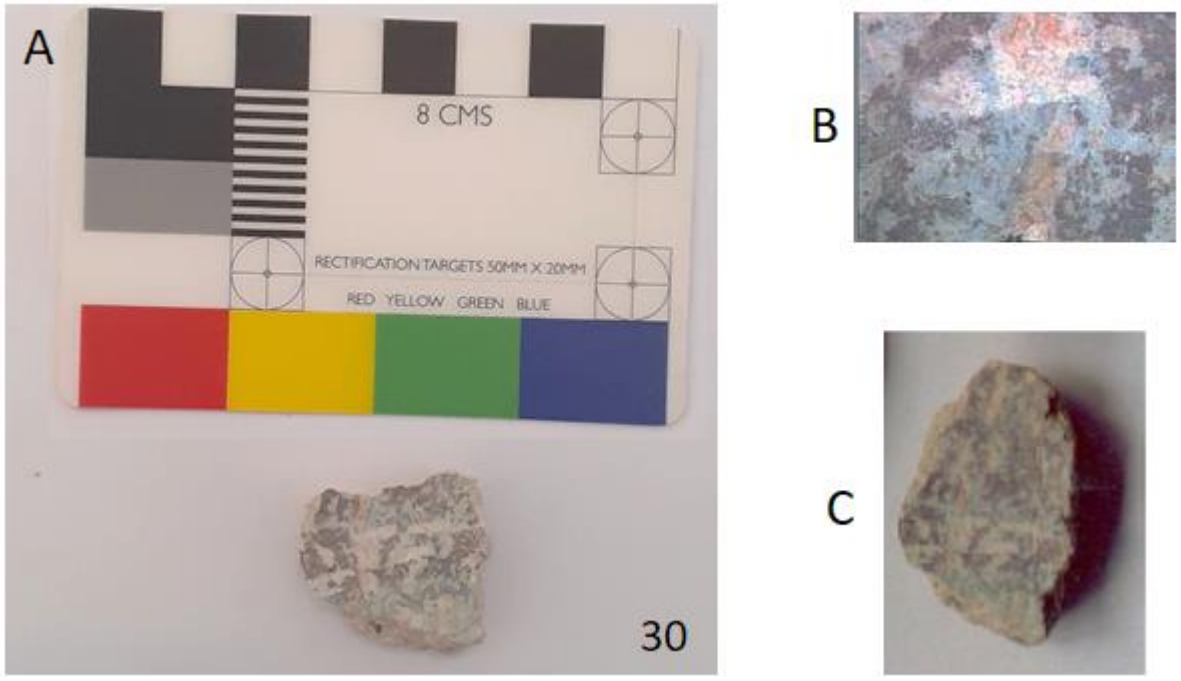

Figure 36 Sample 30. A) photograph of the sample analyzed in this work. B) Optical microscopy photograph by Alonso Olvera et al. 2005, showing a mixture of purple, pale blue, and orange paint. C) Photograph of the sample analyzed by Vandenabeele et al. 2005; the sample was apparently trimmed or broken at some point between 2005 and 2020.

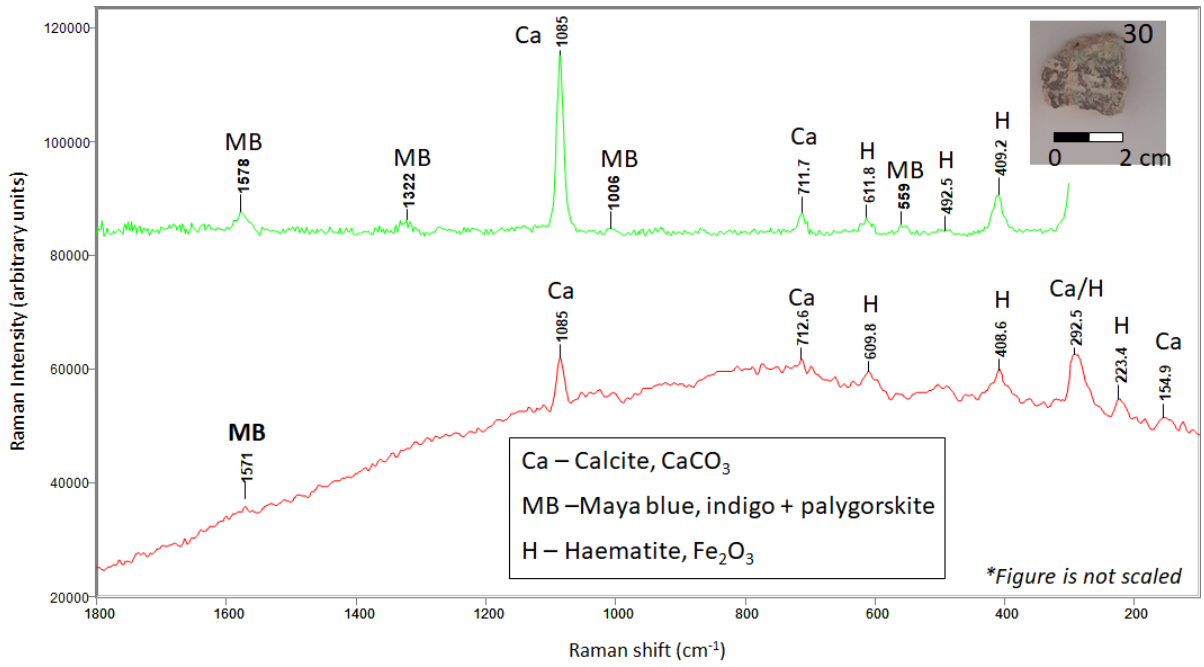

Figure 37 BRAVO (top) and i-Raman (bottom) spectra of sample 30 shown at 1800-100 cm^{-1}, showing a mixture of Maya blue (MB), calcite (Ca), and haematite (H).

Figure 38 Sample 24 also appeared purple, but produced only large amounts of fluorescence with the BRAVO and only the spectra of calcite with the i-Raman.

Unidentified Pigments

In addition to the purple and dark red samples mentioned above, several of the red and yellow colorants could not be identified. This was true of the 2005 study as well: "Red crystals were observed…but due to excessive fluorescence, no proper Raman spectrum could be obtained...When focusing the laser beam on these crystals for several hours, the amount of fluorescence background was reduced, resulting in distinguishable bands of calcite but still no evidence of a red pigment. It may be suggested that a fluorescence red dye had been precipitated on $CaCO_3$ crystals to provide a different shade" (Vandenabeele *et al.*, 2005a, p. 2353). The i-Raman and BRAVO spectrometers did

not show the excessive fluorescence described in the 2005 publication, perhaps due to their longer wavelength excitations. However, in all cases, the spectra showed only the features of calcite.

As discussed above, two of the yellow pigments showed the spectral features of Maya blue, although it is uncertain whether this accounts for the yellow colorant or merely arises from the blue and green background colorants. The other yellow paints showed no evidence of a chromophore. In the 2005 publication, the results were the same as the red colorants: "The yellow fragments…showed a high amount of fluorescence…It has been suggested that an organic dye might have been applied. Another yellow pigment that has often been used is yellow ochre, with limonite or goethite as its main mineral component. These minerals usually show a weak Raman spectrum, when working with a 785-nm laser, such that these will presumably be hidden when strong fluorescence occurs" (Vandenabeele *et al.*, 2005a, p. 2355). Once again, in the present work the spectra of the yellow pigments did not show excessive fluorescence, but also showed no evidence of a chromophore.

Unsubtracted BRAVO spectra of sample 3, the only sample that is entirely yellow, show a small feature at 1445 cm^{-1}, which is not visible in the subtracted spectrum and does not appear in the i-Raman spectra. Edwards et al. identify some features in carbonate minerals at approximately this wavenumber. Dolomite and magnesite ($MgCO_3$) show a weak feature at 1443 and 1444 cm^{-1}, respectively, while calcite shows a weak band at 1436 cm^{-1}, but not typically at 1445 cm^{-1} (2008, p. 2278). In Raman spectra of limestone and marble, Martínez-Hernández et al. identify a feature at 1445 cm^{-1} as a CO_3^{2-} vibration, but also suggest that it may include "a contribution of bands assigned to organic residues". However, an organic component is uncertain in the present work; Martinez-Hernandez et al. speak of this feature in conjunction with a second feature at 1744 cm^{-1} (ν(C=O)), which is not present in the spectrum (2018, p. 3). In the absence of other evidence, it thus seems most likely that this feature corresponds to the plaster substrate rather than a yellow colorant.

The lack of Raman signals could indicate that the chromophore used in some red and yellow paints was an organic dye or lake pigment or is an inorganic substance that is a poor Raman scatterer. According to the literature, the Maya had access to a wide array of organic colorants and were known to have used at least three lake pigments in addition to Maya blue. One of these was used in Lacandon Maya pottery and consisted of a yellow pigment made from the *kante* (*Gliricidia sepium*) plant, while another used the bark of the *chucum* (*Pithecollobium albicans*) or *jabin* (*Piscidia communis, Piscidia piscipula, Ichthyomethia communis*) tree to make reddish plasters (Littmann, 1960, pp. 593, 596; Houston *et al.*, 2009, p. 62). A third lake pigment used red, yellow, or orange dye from the annatto (*Bixa orellana*) plant and was said to have been used in wall paintings (Vázquez de Agredos Pascual, Batista dos Santos and Yusa Marco, 2010). Other red and yellow organic colorants that may have been

used include cochineal, logwood, brazilwood, and orange/sulphur cosmos (Houston *et al.*, 2009, pp. 103–109). Results of other Ek' Balam studies that have employed multiple archaeometric techniques have identified the use of yellow ochre for some of the pigments, and have also found certain pigments that could not be characterized and were thus thought to be organic dyes (Alonso *et al.*, 2014). Vazquez de Agredos Pascual et al. (2010) suggested that red, orange, and yellow colorants observed in Room 64 of the Ek' Balam Acropolis may have been made with annatto, but were unable to confirm this. In the Postclassic period, a yellow paint made of a mixture of montmorillonite and lepidocrocite was widely used (Magaloni Kerpel, 2001, pp. 172–173); as both of these mineral compounds are poor Raman scatterers, their presence is also possible. However, the other archaeometric techniques employed by Alonso Olvera et al. (2005), which included XRD, XRF, SEM-EDS, and FTIR, showed no evidence of their presence, supporting the hypothesis that organic colorants were used.

4.1.3 Degradation Products

As in the original publication, no evidence of gypsum ($CaSO_4$) was observed in the plaster. Vandenabeele et al. considered this result surprising because gypsum is a common weathering product of calcite and noted, "This could be an indication of the absence of SOx, sulphur compounds and thiobacillus in the environment in which they have been conserved in these centuries" (2005a, p. 2352). The present data support this statement.

The unsubtracted BRAVO spectra of one sample—sample 15, a red sample with several shallow cracks—may indicate the presence of calcium oxalate. This is shown by a small broad feature centered at 1471 cm^{-1}. The v(C-O) stretching vibration of oxalates occurs in the 1456-1473 cm^{-1} range (2004, pp. 208–209). Calcium oxalates are frequently observed in historic wall paintings and are usually interpreted as degradation products caused by the biological activity of lichens, bacteria, algae or fungi. An alternative explanation is that they may form due to the breakdown of organic materials, which can lead to the formation of several weak acids including oxalic acid (Pérez-Alonso, Castro and Madariaga, 2006, p. 125). This identification is considered tentative, as no comparable result was yielded in the i-Raman spectra.

With the exception of the possible presence of an oxalate on a single sample and the possible fading and darkening of the cinnabar sample mentioned above, no degradation products were observed. It seems that except for deliberate destruction of the mural during ancient times, the plaster and paint have been well preserved. Being deposited within a structure and untouched for several centuries, the mural fragments were evidently protected from weathering conditions such as ultraviolet radiation, moisture, and modern air pollution.

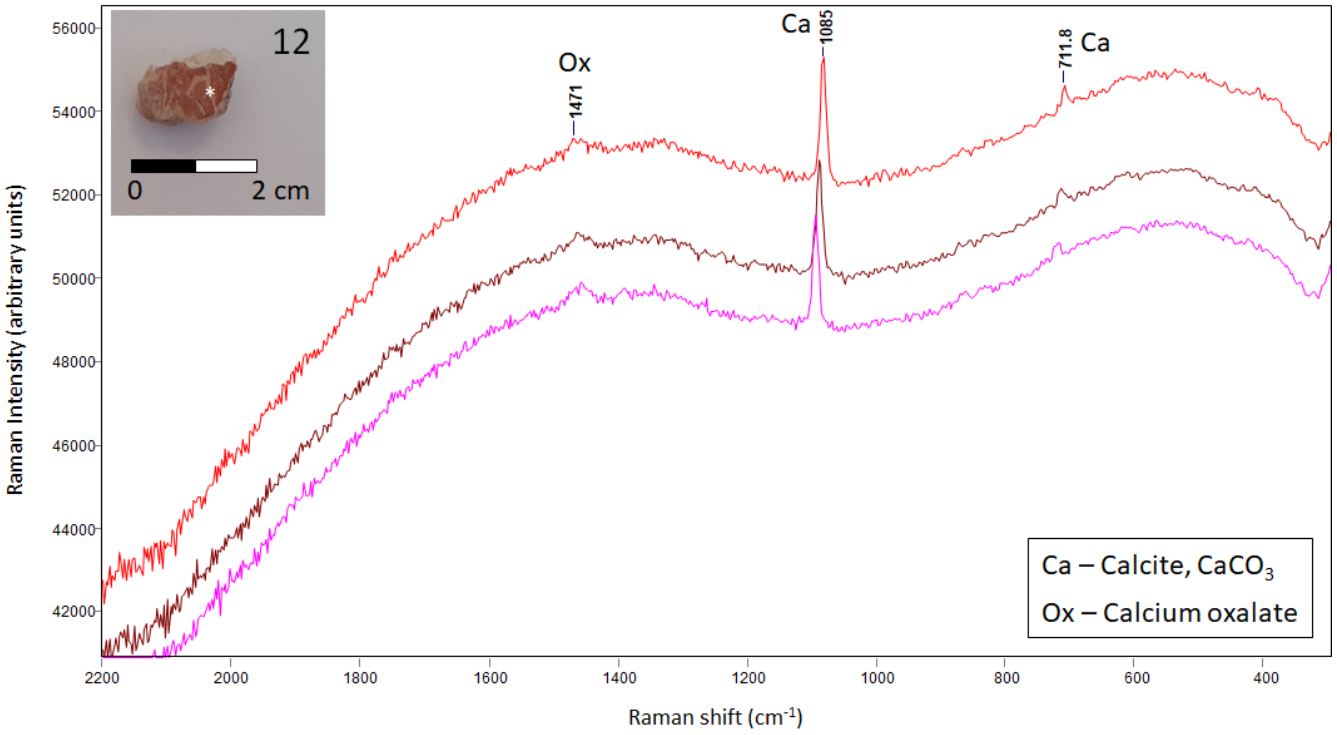

Figure 39 BRAVO unsubtracted spectra of sample 12, recorded from 2200-300 cm^{-1}. The small feature present at 1471 cm^{-1} may be evidence of calcium oxalate, although this result could not be confirmed by the i-Raman data.

4.2 Technical Comparison of Raman Spectrometers Used

4.2.1 Setup

Of the two instruments used in this thesis, the BRAVO spectrometer was the easier setup. The touchscreen interface is extremely intuitive, and the automatically-set parameters allow for rapid measurements. The operator does little except to position the sample and spectrometer appropriately so that neither object moves during measurement, and to control ambient conditions such as lighting to the degree possible. During this experiment, this was straightforward. Spectra were measured indoors, allowing for control of light and temperature. The samples were small, meaning the spectrometer could be set flat on a table while the sample was positioned over the aperture of the measuring tip. This allowed for the sample and spectrometer to be kept steady, although in a few cases, the sample moved slightly due to vibrations throughout my second-floor apartment as the tram passed on the street below. In the few instances where this occurred, it was immediately observed as a series of peculiar shapes in the spectrum, and the measurement was retaken. Acquisition time was selected automatically for most measurements and varied depending on the sample, but was typically brief, usually lasting less than two minutes. Darker samples such as the black sample 26, or very fluorescent samples like the purple sample 24, took up to several minutes to record.

As observed in this work, the largest drawbacks to the BRAVO setup were as follows: 1) the fixed optical head, which could be difficult to position over the desired area; 2) the large spot size, which did not allow for focus on small areas; and 3) the inability to control the laser power, and the ability to control exposure time and number of accumulations only when the device was fixed on the docking station and connected to a laptop. In this experiment, the first condition did not present a major obstacle. Because this was not an *in situ* measurement, it was possible to maneuver the sample and instrument to the desired positions, although it was sometimes difficult to confirm that the aperture was centered on the target area. However, *in situ* studies conducted on large cultural heritage items with this spectrometer have noted difficulties associated with manually positioning the spectrometer and holding it in place for up to several minutes as the measurement is accrued (Saelens, 2018; Rousaki *et al.*, 2019).

For this thesis, the large spot size of the instrument presented one of the greatest challenges, as the samples frequently contained small spots of colorants or inclusions in the plaster. The BRAVO was thus ill-equipped to test certain aspects of the samples, including whether small yellow spots are made of the Maya yellow pigment and whether the black spots on a cinnabar sample represent discoloration of the cinnabar or were made with carbon or another black substance.

Finally, while the automated settings were convenient and allowed for rapid acquisition of spectra, there were some cases in which the automated settings failed to capture adequate measurements. In benchtop systems, this problem could potentially be corrected by altering the experimental parameters. In the BRAVO instrument, acquisition time and number of scans can be set manually when the BRAVO is placed in the docking station and connected to a laptop. While this was possible during this study, it would not be feasible at remote archaeological sites without access to power. Even when using manual settings is possible, however, the operator has no control over the laser power, which is one of the most important parameters. Aside from making it difficult to control the quality of spectra, the inability to control laser power poses a potential risk of damage to the analyte, as lasers at high powers can burn sensitive materials, thus permanently damaging them.

The i-Raman spectrometer is slightly more difficult to set up than the BRAVO. While the system is portable, it is not battery-operated and requires connection to a power source and laptop. This condition could make the spectrometer difficult or impossible to use at remote archaeological sites. The instrument is larger than the BRAVO, but is equipped with a 1.5-m optic fiber, allowing the laser to be more easily positioned. However, while the fiber optic head was convenient and afforded more control over the spot location than the fixed optical head of the BRAVO, the laser is invisible and there is no objective lens, which made it difficult to know whether the spot was centered on the desired

location, particularly if that location was a very narrow target. To record a high quality spectrum, it was first necessary to focus the laser. The best approach to this was to use the "continuous capture" option, in which spectra were repeatedly recorded at the specified parameters; when set to low acquisition times and accumulations, the exact position of the optic fiber and sample could be adjusted until proper focus was obtained. Following this, laser power, time, and number of accumulations was set to collect higher quality spectra. The collected spectra were visible immediately on the laptop screen so that the operator (myself) could determine whether the measurement was adequate or needed to be repeated with different parameters.

In theory, the ability to manually choose parameters, especially laser power, gives the i-Raman a major advantage over the BRAVO, which may use automated settings that are not optimal for the sample. In practice, the increase in control may be difficult for users with limited experience with Raman spectroscopy, and may also be more time-consuming, as it requires trial and error to find the best settings. To make an imperfect analogy, I found that using the BRAVO was similar to taking a photograph with a simple point-and-shoot camera with automated settings, whereas the i-Raman was similar to a more complex professional grade camera. While the latter captures better pictures if the correct settings are selected, it also requires greater knowledge and skill from the photographer and may require several attempts to find the perfect settings; a point-and-shoot camera has the advantage of being simple and quick for even inexperienced users, but the disadvantage that less control over the settings may produce poor photographs, especially if ambient conditions are poor.

4.2.2 Interpretation

Although the BRAVO instrument was easier to set up, the resulting spectra were often more difficult to interpret than those produced with the i-Raman. One of the major interpretive problems observed in this work was that the software occasionally eliminated Raman features from the subtracted spectrum, apparently misinterpreting them as fluorescence. As explained above, this was frequently problematic for samples that contained carbon black. In other cases, the subtracted spectrum showed what appeared to be Raman features, but what were actually noise that the software resolved into peaks. In one instance, this caused a "false positive" identification of haematite, as the subtracted spectrum seemed to show a peak at 409 cm^{-1}, while a closer examination of the unsubtracted spectra showed only a few spikes of noise in this region. For accurate interpretations, the unsubtracted spectra thus had to be carefully examined in conjunction with the subtracted spectrum.

Another disadvantage of the BRAVO was that because the spectral range did not extend below 300 cm^{-1}, the strongest features of some materials could not be observed. In this study, this complicated the identification of cinnabar in one case, as the single feature visible in this wavenumber range was

of low intensity. As discussed above, in another case haematite was incorrectly identified because the subtracted spectrum appeared to show a small band at 409 cm^{-1}. In both of these cases, the i-Raman spectra were more straightforward, with the i-Raman clearly showing the lower wavenumber features for cinnabar in the former case, and showing no evidence of the lower wavenumber features for haematite in the latter. Despite these challenges, the BRAVO spectrometer produced clear spectra for Maya blue, and usually produced identifiable spectra of haematite and cinnabar despite the fact that their strongest features fell below spectral range.

On the whole, spectra acquired with the i-Raman were poor. When collecting measurements, the detector would frequently flood and produce unusable spectra, requiring very low exposure times, laser power, and number of accumulations to record readable results. Unfortunately, this often resulted in spectra with poor signal to noise ratios. Despite these complications, the i-Raman has the advantage of yielding straightforward results. Its spectral range is 2500-100 cm^{-1}, meaning that the strongest features of haematite and cinnabar were visible. In addition, the long excitation wavelength enabled the visibility of limewash putty (Aminzadeh, 1997; Edwards and Farwell, 2008; Chiriu *et al.*, 2014). For this particular case study, the largest disadvantage was that the i-Raman failed to record a recognizable spectrum of Maya blue. Given the ubiquity of this pigment throughout pre-Columbian Central America, this might be a severe limitation for future studies of ancient Mesoamerican art.

4.2.3 Comparison to the Original Study

Results obtained with the new spectrometers were able to identify the same substances as the 2005 publication. Given that the original publication used a more complex benchtop spectrometer that provided the user with more control over the parameters and took longer to acquire spectra, this is an impressive result that suggests a great deal of promise for the new spectrometers. Of particular importance is the BRAVO spectrometer, which is of such simple usage and of such portability that it could easily be applied at remote locations and by individuals with little prior training in Raman spectroscopy (although interpretation of the results may require more expertise). The i-Raman is more difficult to use for *in situ* archaeometric studies, but could also be applied provided that a power source was available. While the i-Raman did not allow for identification of Maya blue, it produced favorable results when recording all other types of colorants. Because Maya blue is not known to have been used in antiquity outside of Mesoamerica, this issue perhaps would not present a serious obstacle for pigment analyses in other regions.

The current work was also able to identify two substances not noted in the original publication. The i-Raman spectrometer detected slaked lime, which cannot be observed at laser excitation wavelengths below 1064 nm. The BRAVO spectrometer also indicates a possible oxalate, which was not detected

in the original study; this may relate to the longer wavelength excitation used by the BRAVO, although it is also possible that the single location where this was observed was simply not tested in 2005. In addition, fluorescence limitation in each of the spectrometers showed some success. While the 2005 publication notes that spectra recorded on several of the red and yellow colorants were overwhelmed by fluorescence, this was not observed here. Though some fluorescence was present, the spectra were still readable, with the features of calcite clearly visible. The fluorescence visible in the BRAVO unsubtracted spectra was usually entirely eliminated in the subtracted spectra, which allowed for easy identification of calcite but no other materials. The only instance of severe fluorescence instead occurred on a purple sample (sample 24); despite several attempts to adjust the parameters of both instruments, neither spectrometer produced readable spectra of this sample. The original study makes no mention of a highly fluorescent purple sample, perhaps indicating that better results were achieved with the earlier equipment in this instance.

Despite their successes in recreating most aspects of the original study and in limiting fluorescence, the new instruments have clear disadvantages when compared to the benchtop instruments. The large spot size and fixed optical head of the BRAVO spectrometer and the difficulties in positioning the i-Raman spectrometer's optical fiber are fairly large drawbacks compared to benchtop systems. In the previous study, objective lenses were used to focus on small areas and acquire spectra with little or no interference from the surrounding area. This could not be done with any reliability with the new instruments. In true *in situ* conditions, positioning the new spectrometers would likely have been even more difficult, as the BRAVO would have had to be held steadily in place against the object, while the i-Raman would have had to be positioned in a way that afforded access to a power source and laptop while spectra were collected. Finally, in terms of quality, spectra published in 2005 generally show a better signal to noise ratio than those recorded here. While fluorescence did not overwhelm Raman signals in measurements recorded on red and yellow paints as was reported in 2005, the BRAVO subtracted spectra are frequently noisy, while the i-Raman spectra show fluorescence despite the long excitation wavelength. The latter problem could be partially fixed by performing a baseline correction; this was not attempted here, as the focus of this work is primarily on the spectrometers themselves rather than on data processing. Recording spectra at longer exposure times, increased accumulations, or increased laser power would theoretically improve the signal to noise ratio, but in practice frequently caused the i-Raman detector to flood. Despite numerous attempts to adjust parameters, in most cases I was unable to acquire high quality spectra with this instrument.

Table 1 Comparison of analytical results between Vandenabeele et al. 2005 and the present work.

Material	Vandenabeele et al 2005	BRAVO spectrometer		iRaman Spectrometer
		Subtracted spectra	Unsubtracted spectra	
Calcite	X	✓✓✓	✓✓✓	✓✓✓
Maya Blue	X	✓✓✓	✓✓✓	-
Maya Green	X	✓✓✓	✓✓✓	-
Maya Yellow	X	A	A	-
Haematite	X	✓✓	✓✓	✓✓✓
Cinnabar	X	✓✓	✓✓	✓✓✓
Carbon black	X	✓	✓✓	✓✓
Haematite + Maya blue (purple)	X	✓✓✓	✓✓✓	✓*
Limewash Putty	-	-	-	✓✓✓
Calcium oxalate	-	-	✓	-

X	Identified
✓✓✓	Identification straightforward
✓✓	Identification usually possible
✓	Identification sometimes possible
✓*	One substance was identified, but not the other
-	Not observed
A	Ambiguous due to issues with spot size

Chapter 5: Conclusion

The goal of this thesis was to test the efficacy of new mobile Raman spectrometers as compared to more traditional benchtop instrumentation. To achieve this, mobile Raman spectroscopy with two new instruments—the BRAVO handheld spectrometer and the i-Raman EX portable spectrometer—was conducted on an assemblage of thirty-three fragments of a Maya wall painting, which had previously been examined using a benchtop instrument and an older portable spectrometer (Vandenabeele *et al.*, 2005a). The earlier results were used as a point of comparison to determine whether the new mobile instruments were capable of collecting data of a similar quality. The significance of this endeavor lies in its potential, as the new mobile instruments allow for increased application of Raman spectroscopy to cultural heritage objects that may be too fragile or valuable to sample, and also allow results to be obtained more quickly and more easily than with benchtop instrumentation. In part because of their extreme portability, however, both of the new instruments lack the precision of the benchtop instruments in terms of setup (i.e., the mobile instruments offer less control over major parameters and do not allow for as precise a focus as the benchtop instrumentation) and in terms of the final data, which show inferior spectral resolution and often inferior signal to noise ratio compared to benchtop instruments. This thesis explored whether the advantages of the new mobile instruments are sufficient to balance these costs.

The results showed that all of the materials identified by Vandenabeele et al. (2005a) using benchtop Raman spectroscopy could be successfully identified with the new mobile instrumentation. As in the original publication, calcite was ubiquitous, identified in layers of plaster and in the paint layers as well, although how exactly the calcite is associated with the paint—whether it was mixed with pigments to alter the saturation, is simply the substrate "shining through" the paint, or indicates application of the fresco technique for the lowest paint layers—remains undetermined. In addition to calcite, the same four pigments identified in the original study were once again observed: cinnabar, haematite, Maya blue, and carbon black. Thus, if the goal is merely to identify the primary components of the paint and plaster, the efficacy of the two new instruments is demonstrated.

However, while each of these substances was generally identifiable in the data, certain disadvantages inherent to the new instruments were highlighted as follows: 1) the spectral range of the BRAVO, which does not include wavenumbers below 300 cm^{-1} and thus excludes the strongest features of cinnabar and haematite; 2) the inability of the i-Raman to record a recognizable spectrum of Maya blue; and 3) the occasionally misleading nature of the BRAVO's subtraction process, which often muted or eliminated the D and G bands of carbon. Of these issues, the first had the least impact on this study. Although two major features of cinnabar fall below the spectral range of the BRAVO, the

single feature that is in range was usually of a high enough intensity that it was unmistakable. Likewise, haematite was usually identifiable by a distinct, medium-intensity band at 409 cm^{-1} and sometimes a weak feature at 610 cm^{-1} as well. Nevertheless, identification of a substance based on a single feature was problematic for two samples as discussed above.

The second issue—that the i-Raman failed to collect recognizable spectra of Maya blue—was more detrimental to this study. The precise reason for this failure is unknown. Manciu et al. (2007) successfully acquired spectra of synthetic Maya blue using FT-Raman, implying that the 1064-nm excitation of the i-Raman is not to blame per se. However, Wiedemann et al. (2007) studied archaeological examples of Maya blue with both NIR excitation and excitation in the visible range and reported similar results to what was observed here: the spectrum of Maya blue was successfully recorded with the shorter wavelength, but sometimes could not be recorded at 1064 nm, perhaps due to low quantities of Maya blue and background arising from palygorskite or the substrate. Alternatively, it is possible that Maya blue could potentially be recorded at higher accumulations times or laser powers; however, this could not be tested here because the detector would flood when these parameters were raised. Whatever the cause, this result was disappointing, given the large academic interest in Maya blue and intriguing questions as to whether yellow and green paints were manufactured from the same materials. In spite of this, Maya blue could perhaps be identified using solely the i-Raman data in part by the presence of a small, broad feature at 1571 cm^{-1} and in part by process of elimination: the Maya region contains very few blue and green colorants, and those that were used—primarily azurite and malachite—produce distinct Raman spectra.

Finally, the issue of the BRAVO subtraction potentially eliminating the features of carbon also presented a challenge. While this could usually be rectified by examining the unsubtracted spectra, the results could occasionally be ambiguous, especially when the color of the sample was a pale gray or grayish blue rather than black or dark gray. Results recorded with the i-Raman were generally more straightforward in this matter, consistently producing two broad features in the characteristic locations for the D and G bands of carbon.

In addition to producing recognizable spectra of the same materials identified in 2005, the i-Raman spectrometer was also able to show the presence of slaked lime or limewash putty. Limewash putty is presumably present due to incomplete carbonation of the wet mortar, resulting in some of the slaked lime failing to react with carbon dioxide. Similar results have been reported in other Raman spectroscopy studies of wall paintings, including one conducted at the Maya site of Copán (Goodall *et al.*, 2007). Finally, a single spectrum recorded with the BRAVO shows the presence of an oxalate. Calcium oxalates are almost always interpreted as degradation products arising from microbial

metabolisms, although an alternative explanation is that they are produced by the breakdown of organic binders added to the paint (Pérez-Alonso, Castro and Madariaga, 2006, p. 125). Because this feature occurs only in the unsubtracted spectra of a single measurement, no further insight could be gained, and the identification is considered tentative. It is unclear why this material could be identified in the present work but not in 2005. Possible reasons are that the longer wavelength excitations used by the BRAVO produced less fluorescence allowing for the feature to appear in the spectra. However, calcium oxalate was identified at only a single location; since the exact locations tested in 2005 were not published, I cannot rule out the possibility that this position simply was not measured.

Several of the red and yellow samples could not be identified. The same result was observed in the 2005 study; however, Vandenabeele et al. noted that these samples showed large amounts of fluorescence. Photobleaching was used on some of the samples in an attempt to overcome this, but the elimination of the fluorescence revealed only the features of calcite. In the current study, fluorescence was present, but did not typically overwhelm the spectra. Nevertheless, no Raman features were observable besides those of calcite. Both Vandenabeele et al. and Alonso Olvera et al. suggested that organic dyes had been used to produce these colors. The data recorded here support this determination.

Finally, an important determination of the original paper was that a yellow colorant had been produced using the same components as Maya blue. Unfortunately, these results could not be confirmed in the present work because yellow frequently occurred only in small spots or stripes and often occurred along with blue or green colorants known to be made with Maya blue. This highlights an important drawback of both instruments. For the BRAVO, the main problem is the spot size, which was too large to measure small areas of yellow paint without also capturing the spectra of the surrounding colorants. The i-Raman failed to capture identifiable spectra of the Maya blue, meaning it was also unusable for this purpose.

5.1 Answers to research questions

In the first chapter, three primary research questions were set forth. Here, I will answer them succinctly.

Can the new mobile instrumentation be used to identify the same materials as the benchtop and the older mobile spectrometers?

The BRAVO spectrometer showed considerable success at identifying the same materials in the original study. Carbon black occasionally presented an interpretive problem, as the automated subtraction procedure sometimes obscured or eliminated the two diagnostic broad features. In addition, substances with strong vibrations that occur at wavenumbers below 300 cm^{-1} were more

difficult to identify with the BRAVO in two cases. Nonetheless, all of the original components of the paint and plaster were identifiable. In one case, the BRAVO data may also have shown the presence of an oxalate, although this is considered tentative.

The i-Raman was successful at identifying all of the original substances with the exception of Maya blue, which produced only one recognizable feature—a small band at 1571 cm^{-1}. It is uncertain whether the failure to produce a usable Maya blue spectrum arose primarily from the same combination of low concentrations of indigo, background interference from palygorskite and/or the plaster substrate, and NIR excitation that was observed in Wiedemann et al. (2007), or whether the poor result is due to brief exposure times, low laser power, and/or low accumulations which were meant to avoid flooding the detector. Identification of haematite, cinnabar, calcite, and carbon black was possible, however, and was often more straightforward than in the BRAVO data. In addition, the i-Raman showed the presence of slaked lime, which is not possible at lower excitation wavelengths.

How effective are the new spectrometers at eliminating fluorescence?

With the automated subtraction feature, the BRAVO produces spectra with little evidence of fluorescence. However, this can be misleading, as it sometimes resolves noise or fluorescence into peaks where there are no features in reality, or eliminates or obscures certain diagnostic features, such as those for carbon black and some of the low intensity features of Maya blue. In one case, very severe fluorescence was seen for a purple sample. However, the severe fluorescence that Vandenabeele et al. noted on yellow and red samples in 2005 was not observed, perhaps indicating the overall success of this spectrometer. Regardless, the yellow and red colorants could not be identified, as no Raman features other than those of calcite were observable.

The i-Raman spectrometer showed fluorescence despite its high wavelength excitation source. Nonetheless, the fluorescence generally did not overwhelm the Raman signal. As with the BRAVO, i-Raman spectra recorded on the red and yellow samples were not overwhelmed by fluorescence, but merely showed no evidence of the colorant.

What benefits and drawbacks does each new instrument present, and in general, are they viable alternatives to the earlier methodologies?

Benefits and drawbacks of each instrument are summarized in the following table:

Table 2 Comparison of the benefits and drawbacks observed for each instrument.

	i-Raman-EX		*BRAVO*	
	Benefits	**Drawbacks**	**Benefits**	**Drawbacks**
Setup	-Portable -Optic fiber allows for easy positioning of the laser -Spot size is relatively small -Continuous acquisition feature allows for focus and adjustment of settings -Laser power, acquisition time, and number of accumulations can be adjusted	-Requires connection to a power source and laptop -No objective lens to ensure that the laser is focused in the correct location -Trial and error are necessary to find the correct settings, meaning that acquiring spectra can be time-consuming -Gaining a focus and setting the correct parameters can be difficult if the user is unfamiliar with Raman spectroscopy	-Setup is extremely simple -Rapid acquisition of spectra -Extremely portable with few moving parts	-No user control over laser power -Exposure time and number of accumulations can only be controlled if the instrument is connected to the docking station and laptop -Fixed optical head makes positioning difficult -Spot size is large
Interpretation	- 1064-nm excitation decreases fluorescence -Spectral range includes the fingerprint region, 2500-100 cm^{-1}	-Raman intensity is reduced at long wavelength excitation -Detector frequently floods	-Software automatically subtracts fluorescence -Extended spectral range includes the CH stretching region	-Fluorescence subtraction can sometimes eliminate Raman features or add artifact peaks -Spectral range does not include wavenumbers below 300 cm^{-1}, which can make identification of oxides and sulfides difficult

In general, whether these new spectrometers should be considered viable alternatives to traditional benchtop instrumentation greatly depends upon the goals of research. If the goal is merely to identify pigments, the results of this research indicate that the new spectrometers are adequate in most circumstances. In the event that sampling is considered especially dangerous or generally undesirable for a cultural heritage object, these two spectrometers could likely be employed for *in situ* analysis with favorable results and minimal risks. *In situ* analyses could present additional challenges that were not explored in this study, including positioning of the instruments, access to a power source, and control of light and other ambient conditions, but previous *in situ* studies with these instruments have been able to overcome these issues (Germinario *et al.*, 2018; Saelens, 2018; Rousaki *et al.*, 2019).

If, however, the goal of research requires more precision than merely identifying materials, these spectrometers may fall short of traditional benchtop instrumentation. Certain factors, including spectral resolution, focusing capabilities, and control of parameters are considerably diminished compared to traditional methodologies. One of the most striking examples of this is spectral resolution. For the BRAVO, spectral resolution is 10-12 cm^{-1}, while it is less than 10 cm^{-1} for the i-Raman. In contrast, the RenishawSystem-1000—the benchtop instrument used in the original publication—has a resolution of only 1 cm^{-1}. This allows for considerably more precision in measurements recorded with the traditional instrumentation. Thus, if the research goal is based upon analytical chemistry or physics-oriented goals, such as identifying molecular vibrations, crystallinity, or a substance's response to temperature change, the new instrumentation is not likely to be precise enough. In terms of cultural heritage applications, neither instrument is ideal for focusing on small areas, which can make it difficult to identify spots of pigments, inclusions in the plaster, or small areas that could show degradation phenomena. The quality of the spectra produced by the new methodologies also varied considerably depending on the substance and was not always comparable to the benchtop instrumentation, which seems to have produced spectra with a much more favorable signal to noise ratio in the 2005 publication.

The original publication employed an interesting symbiotic relationship between mobile and benchtop instrumentation, as Vandenabeele et al. used the rapid acquisition of the mobile instrument at low spectral resolutions to determine the best parameters to set for measurements acquired with the benchtop spectrometer. In this way, spectra collected with the mobile instrument served not as an end in themselves but as tools to produce better quality spectra (2005a, p. 2350). Perhaps future studies could use the BRAVO or i-Raman instruments in a similar manner, as a preliminary step to obtaining higher quality spectra with a more precise instrument. For example, one can foresee a circumstance in which a cultural heritage object can only be sampled extremely

sparingly; in this case, perhaps the BRAVO or i-Raman instruments could be used to determine where certain substances were located so that sampling could occur more effectively.

In sum, the new instrumentation allows for rapid *in situ* identification of many substances, and is generally adequate for this purpose. If benchtop instrumentation cannot be applied because sampling is forbidden or extremely undesirable, the present work implies that the BRAVO and i-Raman spectrometers would generally be sufficient to identify the components of pigments and plaster, and possibly degradation products. Their built-in systems for limiting fluorescence proved somewhat useful as well, although in the case of the BRAVO instrument, problems with interpretation occasionally arose. While they did not outperform the benchtop instruments in several major facets—including spectral resolution, focusing capabilities, and signal to noise ratio—they allowed for the same conclusions to be reached as in the previous study, ultimately implying their applicability in cultural heritage studies.

5.2 Potential Directions for Future Research

Interesting directions for future research could include *in situ* pigment analysis. While a great deal of archaeometric analysis has already been conducted throughout Mesoamerica, new archaeological sites are constantly being uncovered. As discussed above, the movement of valuable mineral pigments such as cinnabar as well as the production of Maya blue is of great archaeological interest, and mobile Raman spectrometers could provide further data on these topics, particularly at the numerous remote archaeological sites. *In situ* Raman studies could also occur in museum contexts, which would be an ideal setting for the i-Raman spectrometer as it would afford the necessary access to a power source.

As stated above, deciding which analytical techniques to employ requires a calculation of information gained vs. risk of damage to the object. Mobile instruments can eliminate risks of damage associated with sampling but potentially provide less information than laboratory analyses. To mitigate this problem, multiple *in situ* techniques could be employed to increase the information gained. For example, a study conducted by Rousaki et al. successfully combined mobile Raman spectroscopy—including measurements taken with the BRAVO and i-Raman—with handheld XRF to analyze a Roman mosaic; the different techniques provided vital complementary data (Saelens, 2018; Rousaki *et al.*, 2019).

Regardless of the exact nature of future studies, one of the primary goals of this thesis is to help cultural heritage scientists make informed decisions when considering which archaeometric methodologies to employ. Assessments of this nature are crucial because cultural heritage is invaluable and utterly irreplaceable. The present thesis thus offers a concise assessment of the new instruments, both compared to each other and compared to benchtop Raman spectroscopy.

Bibliography

Alonso, A. *et al.* (2014) 'Comparative spectroscopic analysis of Maya wall paintings from Ek'Balam, Mexico', in *Materials Research Society Symposium Proceedings*. Materials Research Society, pp. 63–72. doi: 10.1557/opl.2014.455.

Alonso Olvera, A. *et al.* (2005) 'Resultados preliminares sobre la caracterización de materiales constitutivos y tecnología de la pintura mural de la Acrópolis de la Zona Arqueológica de Ek´Balam, Yucatán', *La ciencia de materiales y su impacto en la arqueología*, 2, pp. 84–126.

Alonso Olvera, A. (2013) 'Agregados de morteros y conglomerados de cal', in Barba Pingarron, L. and Villasenor Alonso, I. (eds) *La Cal: historia, propiedades y usos*. Mexico City: Universidad Nacional Autonoma de Mexico, pp. 73–93.

Aminzadeh, A. (1997) 'Fluorescence bands in the FT-Raman spectra of some calcium minerals', *Spectrochimica Acta - Part A: Molecular and Biomolecular Spectroscopy*, 53(5), pp. 693–697. doi: 10.1016/S1386-1425(96)01848-3.

Andrews, G. F. (1975) *Maya Cities: Placemaking and Urbanization*. Norman: University of Oklahoma Press.

Arnold, D. E. *et al.* (2012) 'The first direct evidence of pre-columbian sources of palygorskite for Maya Blue', *Journal of Archaeological Science*. Elsevier Ltd, 39(7), pp. 2252–2260. doi: 10.1016/j.jas.2012.02.036.

Baraldi, P. *et al.* (2007) 'A micro-Raman archaeometric approach to Roman wall paintings', *Vibrational Spectroscopy*, 43, pp. 420–426. doi: 10.1016/j.vibspec.2006.04.029.

Bell, I. M., Clark, R. J. H. and Gibbs, P. J. (1997) 'Raman spectroscopic library of natural and synthetic pigments (pre- ~1850 AD)', *Spectrochimica Acta - Part A: Molecular and Biomolecular Spectroscopy*, 53, pp. 2159–2179. doi: 10.1016/S1386-1425(97)00140-6.

Bellot-Gurlet, L., Pages-Camagna, S. and Coupry, C. (2006) 'Raman spectroscopy in art and archaeology', *Journal of Raman Spectroscopy*, 37, pp. 962–965. doi: 10.1002/jrs.

Bersani, D. *et al.* (2016) 'Methodological evolutions of Raman spectroscopy in art and archaeology', *Analytical Methods*. Royal Society of Chemistry, 8(48), pp. 8395–8409. doi: 10.1039/c6ay02327d.

Bersani, D. and Lottici, P. P. (2016) 'Raman spectroscopy of minerals and mineral pigments in archaeometry', *Journal of Raman Spectroscopy*, 47, pp. 499–530. doi: 10.1002/jrs.4914.

Bey, G. J. *et al.* (1998) 'The ceramic chronology of Ek Balam, Yucatan, Mexico', *Ancient Mesoamerica*,

9(1), pp. 101–120. doi: 10.1017/S0956536100001887.

Brindley, G. W. (1957) *Index to the X-ray Powder Data File*. Philadelphia: Minerals, American Society for Testing.

Burgio, L. and Clark, R. J. H. (2001) 'Library of FT-Raman spectra of pigments, minerals, pigment media and varnishes, and supplement to existing library of Raman spectra of pigments with visible excitation', *Spectrochimica Acta - Part A: Molecular and Biomolecular Spectroscopy*, 57(7), pp. 1491–1521. doi: 10.1016/S1386-1425(00)00495-9.

Buzatu, A. and Buzgar, N. (2010) 'The Raman Study of Single-Chain Silicates', *Analele Stiintifice de Universitatii AI Cuza din Iasi. Sect. 2, Geologie*, LVI(1), pp. 107–125.

Casadio, F., Daher, C. and Bellot-Gurlet, L. (2016) 'Raman spectroscopy of Cultural Heritage materials: overview of applications and new frontiers in instrumentation, sampling modalities, and data processing', *Topics in Current Chemistry*, 374, pp. 42–48. doi: 10.1007/s41061-016-0061-z.

Charnay, D. (1888) *Viaje a Yucatan a Fines de 1886: Relacion escrita con el titulo 'Ma derniere expedition au Yucatan'*. Merida, Mexico: Imp. de la Revista de Mérida. Available at: https://archive.org/details/viajeyucatanfines00chariala/page/110/mode/2up?q=balam.

Chiriu, D. *et al.* (2014) 'Raman Study on Pompeii Potteries : The Role of Calcium Hydroxide on the Surface Treatment', *Journal of Spectroscopy*, pp. 1–10.

Chiriu, D., Ricci, P. C. and Cappellini, G. (2017) 'Raman characterization of XIV – XVI centuries Sardinian documents : Inks , papers and parchments', *Vibrational Spectroscopy*, 92, pp. 70–81. doi: 10.1016/j.vibspec.2017.05.007.

Clark, R. J. H. (1995) 'Raman microscopy: application to the identification of pigments on medieval manuscripts', *Chemical Society Reviews*, 24(3), pp. 187–196. doi: 10.1039/cs9952400187.

Coe, M. D. (2000) *The Maya*. 6th edn. London: Thames & Hudson Ltd.

Conti, C. *et al.* (2016) 'Portable Sequentially Shifted Excitation Raman spectroscopy as an innovative tool for in situ chemical interrogation of painted surfaces', *Analyst*. Royal Society of Chemistry, 141, pp. 4599–4607. doi: 10.1039/c6an00753h.

Cotte, M. *et al.* (2006) 'Blackening of Pompeian cinnabar paintings: X-ray microspectroscopy analysis', *Analytical Chemistry*, 78(21), pp. 7484–7492. doi: 10.1021/ac0612224.

Coupry, C. (2000) 'Application of Raman microspectrometry to art objects', *Analusis*, 28(1), pp. 39–46. doi: 10.1051/analusis:2000280039.

Culka, A. and Jehlička, J. (2018) 'Sequentially shifted excitation: A tool for suppression of laser-induced fluorescence in mineralogical applications using portable Raman spectrometers', *Journal of Raman Spectroscopy*. John Wiley and Sons Ltd, 49(3), pp. 526–537. doi: 10.1002/jrs.5320.

Defrance, S. D. and Hanson, C. A. (2008) 'Labor, Population Movement, and Food in Sixteenth-Century', *Latin American Antiquity*, 19(3), pp. 299–316. Available at: https://www.jstor.org/stable/25478232.

Doménech, A. *et al.* (2012) 'Insights into the Maya Blue technology: Greenish pellets from the ancient City of La Blanca', *Angewandte Chemie - International Edition*, 51(3), pp. 700–703. doi: 10.1002/anie.201106562.

Doménech, A., Doménech-Carbó, M. T. and De Agredos Pascual, M. L. V. (2006) 'Dehydroindigo: A new piece into the Maya Blue puzzle from the voltammetry of microparticles approach', *Journal of Physical Chemistry B*. American Chemical Society, 110(12), pp. 6027–6039. doi: 10.1021/jp057301l.

Doménech, A., Doménech-Carbó, M. T. and Edwards, H. G. M. (2011) 'On the interpretation of the Raman spectra of Maya Blue: A review on the literature data', *Journal of Raman Spectroscopy*, 42(1), pp. 86–96. doi: 10.1002/jrs.2642.

Doménech, A., Doménech-Carbó, M. T. and Pascual, M. L. V. de A. (2009) 'Correlation between spectral, SEM/EDX and electrochemical properties of Maya Blue: A chemometric study', *Archaeometry*, 51(6), pp. 1015–1034. doi: 10.1111/j.1475-4754.2009.00453.x.

Doménech, A., Doménech-Carbõ, M. T. and Vázquez De Agredos-Pascual, M. L. (2011) 'From Maya Blue to "Maya Yellow": A connection between ancient nanostructured materials from the voltammetry of microparticles', *Angewandte Chemie - International Edition*, 50(25), pp. 5741–5744. doi: 10.1002/anie.201100921.

Edwards, H. G. M. *et al.* (2005) 'FT-Raman spectroscopic study of calcium-rich and magnesium-rich carbonate minerals', *Spectrochimica Acta - Part A: Molecular and Biomolecular Spectroscopy*, 61(10), pp. 2273–2280. doi: 10.1016/j.saa.2005.02.026.

Edwards, H. G. M. *et al.* (2008) 'A Raman spectroscopic and combined analytical approach to the restoration of severely damaged frescoes: the Palomino project', *Journal of Raman Spectroscopy*, 39(4), pp. 444–452. doi: 10.1002/jrs.1854.

Edwards, H. G. M. and Farwell, D. W. (2008) 'The conservational heritage of wall paintings and buildings : an FT-Raman spectroscopic study of prehistoric, Roman, mediaeval and Renaissance lime substrates and mortars', *Journal of Raman Spectroscopy*, 39(8), pp. 985–992. doi: 10.1002/jrs.1917.

De Faria, D. L. A., Venâncio Silva, S. and De Oliveira, M. T. (1997) 'Raman microspectroscopy of some iron oxides and oxyhydroxides', *Journal of Raman Spectroscopy*, 28(11), pp. 873–878. doi: 10.1002/(sici)1097-4555(199711)28:11<873::aid-jrs177>3.0.co;2-b.

Fernandes, R. F. *et al.* (2017) 'Raman spectroscopic analysis of a belltower commemorative wall decoration', *Applied Physics A: Materials Science and Processing*. Springer Berlin Heidelberg, 123, pp. 1–8. doi: 10.1007/s00339-017-0761-4.

Ferraro, J. R., Nakamoto, K. and Brown, C. W. (2003) *Introductory Raman Spectroscopy: Second Edition*. 2nd edn, *Introductory Raman Spectroscopy: Second Edition*. 2nd edn. Boston: Academic Press. doi: 10.1016/B978-0-12-254105-6.X5000-8.

Fiedler, A., Baranska, M. and Schulz, H. (2011) 'FT-Raman spectroscopy - A rapid and reliable quantification protocol for the determination of natural indigo dye in Polygonum tinctorium', *Journal of Raman Spectroscopy*, 42(3), pp. 551–557. doi: 10.1002/jrs.2726.

Froment, F., Tournié, A. and Colomban, P. (2008) 'Raman identification of natural red to yellow pigments: Ochre and iron-containing ores', *Journal of Raman Spectroscopy*, 39(5), pp. 560–568. doi: 10.1002/jrs.1858.

Frost, R. L. (2004) 'Raman spectroscopy of natural oxalates', *Analytica Chimica Acta*, 517(1–2), pp. 207–214. doi: 10.1016/j.aca.2004.04.036.

Frost, R. L., Martens, W. N. and Kloprogge, J. T. (2002) 'Raman spectroscopic study of cinnabar (HgS), 77K', *Neues Jahrbuch für Mineralogie-Monatshefte*, 2002(10), pp. 469–480. doi: 10.1127/0028-3649/.

Garcia Moreno, R. *et al.* (2008) 'Discovery and characterization of an unknown blue-green maya pigment: Veszelyite', *Archaeometry*, 50(4), pp. 658–667. doi: 10.1111/j.1475-4754.2007.00370.x.

Garcia Moreno, R., Strivay, D. and Gilbert, B. (2008) 'Maya blue-green pigments found in Calakmul, Mexico: a study by Raman and UV-visible spectroscopy', *Journal of Raman Spectroscopy*, 39(8), pp. 1050–1056. doi: 10.1002/jrs.1972.

De Gelder, J. *et al.* (2007) 'Reference database of Raman spectra of biological molecules', *Journal of Raman Spectroscopy*, 38, pp. 1133–1147. doi: 10.1002/jrs.

Germinario, C. *et al.* (2018) 'Multi-analytical and non-invasive characterization of the polychromy of wall paintings at the Domus of Octavius Quartio in Pompeii', *European Physical Journal Plus*, 133(9), pp. 1–12. doi: 10.1140/epjp/i2018-12224-6.

Gettens, R. J. (1962) ‘Maya Blue : An Unsolved Problem in Ancient Pigments’, *American Antiquity*, 27(4), pp. 557–564.

Gettens, R. J. and Stout, G. L. (1946) *Paint materials: a short encyclopedia*. New York: Van Nostrand.

Gilbert, A. S. (2016) *Vibrational, rotational and raman spectroscopy, historical perspective*. 3rd edn, *Encyclopedia of Spectroscopy and Spectrometry*. 3rd edn. Elsevier Ltd. doi: 10.1016/B978-0-12-803224-4.00308-3.

Giustetto, R. *et al.* (2011) ‘Chemical stability and dehydration behavior of a sepiolite / indigo Maya Blue pigment’, *Applied Clay Science*. Elsevier B.V., 52(1–2), pp. 41–50. doi: 10.1016/j.clay.2011.01.027.

Goodall, R. A. *et al.* (2007) ‘Raman microprobe analysis of stucco samples from the buildings of Maya Classic Copan’, *Journal of Archaeological Science*, 34(4), pp. 666–673. doi: 10.1016/j.jas.2006.07.008.

Goodall, R. A. (2007) *Spectroscopic Studies of Maya Pigments*. Queensland University of Technology.

Goodall, R. A. *et al.* (2008) ‘Micro-Attenuated Total Reflection Spectral Imaging in Archaeology: Application to Maya Paint and Plaster Wall Decorations’, *Applied Spectroscopy*, 62(1), pp. 10–16. doi: 10.1366/000370208783412627.

Grube, N. and Krochock, R. (2007) ‘Reading Between the Lines: Hieroglyphic Texts from Chichen Itza and Its Neighbors’, in Kowalski, J. K. and Kristan-Graham, C. (eds) *Twin Tollas. Chichén Itzá, Tula and the Epiclassic to Early Postclassic Mesoamerican World*. Washington, D.C.: Dumbarton Oaks Research library and Collection, pp. 205–249.

Gunasekaran, S., Anbalagan, G. and Pandi, S. (2006) ‘Raman and infrared spectra of carbonates of calcite structure’, *Journal of Raman Spectroscopy*, 37(9), pp. 892–899. doi: 10.1002/jrs.1518.

Haude, M. E. (1998) ‘Identification of colorants on maps from the early colonial period of New Spain (Mexico)’, *Journal of the American Institute for Conservation*, 37(3), pp. 240–270. doi: 10.1179/019713698806082822.

Houck, C. W. (2004) *The Rural Survey of Ek Balam, Yucatan, Mexico*. Tulane University.

Houston, S. *et al.* (2009) *Veiled Brightness: A History of Ancient Maya Color*. Austin: University of Texas Press.

Jehlička, J. *et al.* (2017) ‘Comparison of seven portable Raman spectrometers: beryl as a case study’, *Journal of Raman Spectroscopy*. John Wiley and Sons Ltd, 48(10), pp. 1289–1299. doi: 10.1002/jrs.5214.

Jubb, A. M. and Allen, H. C. (2010) 'Vibrational spectroscopic characterization of hematite, maghemite, and magnetite thin films produced by vapor deposition', *ACS Applied Materials and Interfaces*, 2(10), pp. 2804–2812. doi: 10.1021/am1004943.

Karapanayiotis, T. *et al.* (2004) 'Raman spectroscopic and structural studies of indigo and its four 6,6'-dihalogeno analogues', *Analyst*. Royal Society of Chemistry, 129(7), pp. 613–618. doi: 10.1039/b401798f.

Kaszowska, Z. *et al.* (2016) 'Raman scattering or fluorescence emission? Raman spectroscopy study on lime-based building and conservation materials', *Spectrochimica Acta - Part A: Molecular and Biomolecular Spectroscopy*, 169, pp. 7–15. doi: 10.1016/j.saa.2016.06.012.

Keune, K. and Boon, J. J. (2005) 'Analytical Imaging Studies Clarifying the Process of the Darkening of Vermilion in Paintings', *Analytical Chemistry*, 77(15), pp. 4742–4750. doi: 10.1021/ac048158f.

Kleber, R., Masschelein-Kleiner, L. and Thissen, J. (1967) 'Etude et Identification du "Bleu Maya"', *Studies in Conservation*, 12(2), pp. 41–56.

Košařová, V. *et al.* (2013) 'Microanalysis of clay-based pigments in painted artworks by the means of Raman spectroscopy', *Journal of Raman Spectroscopy*, 44(11), pp. 1570–1577. doi: 10.1002/jrs.4381.

Lacadena Garcia-Gallo, A. (2004) *The Glyphic Corpus from Ek' Balam, Yucatán, México*. Available at: http://www.famsi.org/reports/01057/01057LacadenaGarciaGallo01.pdf.

Lauwers, D. *et al.* (2014) 'Characterisation of a portable Raman spectrometer for in situ analysis of art objects', *Spectrochimica Acta - Part A: Molecular and Biomolecular Spectroscopy*. Elsevier B.V., 118, pp. 294–301. doi: 10.1016/j.saa.2013.08.088.

Lauwers, D. *et al.* (2016) 'Evaluation of portable Raman spectroscopy and handheld X-ray fluorescence analysis (hXRF) for the direct analysis of glyptics', *Spectrochimica Acta - Part A: Molecular and Biomolecular Spectroscopy*. Elsevier B.V., 157, pp. 146–152. doi: 10.1016/j.saa.2015.12.013.

Lesser, J. M. and Weidie, A. E. (1988) 'Region 25, Yucatan Peninsula', in Back, W., Rosenshein, J. S., and Seaber, P. R. (eds) *Hydrogeology*. Boulder, CO, USA: Geological Society of America, pp. 237–241. doi: 10.1130/dnag-gna-o2.237.

Littmann, E. R. (1960) 'Ancient Mesoamerican Mortars, Plasters, and Stuccos: The Use of Bark Extracts in Lime Plasters', *American Antiquity*, 25(4), pp. 593–597. doi: 10.2307/276642.

Lundy, H. D. (2016) *Architecture and Placemaking at a Northern Maya City: Ek'Balam and the*

Question of Style. Florida State University. Available at: https://diginole.lib.fsu.edu/islandora/object/fsu%3A366089/.

Macdonald, A. M. and Wyeth, P. (2006) 'On the use of photobleaching to reduce fluorescence background in Raman spectroscopy to improve the reliability of pigment identification on painted textiles', *Journal of Raman Spectroscopy*, 37(8), pp. 830–835. doi: 10.1002/jrs.1510.

Magaloni Kerpel, D. (2001) 'Materiales y técnicas de la pintura mural Maya', in De la Fuente, B. and Staines Cicero, L. (eds) *La Pintura Mural Prehispanica, Vol. II: Area Maya, Tomo III Estudios*. Mexico City: Universidad Nacional Autonoma de Mexico, Instituto de Investigaciones Esteticas, pp. 155–198.

Manciu, F. S. *et al.* (2007) 'Raman and infrared studies of synthetic Maya pigments as a function of heating time and dye concentration', *Journal of Raman Spectroscopy*, 38(9), pp. 1193–1198. doi: 10.1002/jrs.1751.

Marcus, J. (1976) *Emblem and State in the Classic Maya Lowlands: An Epigraphic Approach to Territorial Organization*. Washington, D.C.: Dumbarton Oaks, Trustees for Harvard University.

Martínez-Hernández, A. *et al.* (2018) 'Analysis of heritage stones and model wall paintings by pulsed laser excitation of Raman, laser-induced fluorescence and laser-induced breakdown spectroscopy signals with a hybrid system', *Journal of Cultural Heritage*. Elsevier Masson SAS, 32, pp. 1–8. doi: 10.1016/j.culher.2018.02.004.

Marucci, G. *et al.* (2018) 'Raman spectroscopic library of medieval pigments collected with five different wavelengths for investigation of illuminated manuscripts', *Analytical Methods*. Royal Society of Chemistry, 10, pp. 1219–1236. doi: 10.1039/c8ay00016f.

Mennella, V. *et al.* (1995) 'Raman spectra of carbon-based materials excited at 1064 nm', *Carbon*, 33(2), pp. 115–121. doi: 10.1016/0008-6223(94)00113-E.

Merwin, H. E. (1931) 'Chemical analysis of pigments', in Morris, E. H., Charlot, J., and Morris, A. A. (eds) *Temple of the warriors at Chichen-Itza, Yucatán*. Washington, D.C.: Carnegie Institution of Washington, pp. 355–356.

Morley, S. G. (1928) 'Report of S.G. Morley on the Ekbalam Expedition', in *Year Book No. 27*. Washington, D.C.: Carnegie Institute of Washington, pp. 317–318.

Morley, S. G., Brainer, G. W. and Sharer, R. J. (1983) *The Ancient Maya*. Stanford: Stanford University Press.

Neiman, M. K., Balonis, M. and Kakoulli, I. (2015) 'Cinnabar alteration in archaeological wall

paintings: an experimental and theoretical approach', *Applied Physics A: Materials Science and Processing*. Springer Berlin Heidelberg, 121(3), pp. 915–938. doi: 10.1007/s00339-015-9456-x.

van Olphen, H. (1966) 'Maya Blue : A Clay-Organic Pigment?', *Science*, 154(3749), pp. 645–646.

Osticioli, I., Zoppi, A. and Castellucci, E. M. (2006) 'Fluorescence and Raman spectra on painting materials: reconstruction of spectra with mathematical methods', *Journal of Raman Spectroscopy*, 37(10), pp. 974–980. doi: 10.1002/jrs.1587.

Pérez-Alonso, M., Castro, K. and Madariaga, J. M. (2006) 'Investigation of degradation mechanisms by portable Raman spectroscopy and thermodynamic speciation: The wall painting of Santa María de Lemoniz (Basque Country, North of Spain)', *Analytica Chimica Acta*, 571, pp. 121–128. doi: 10.1016/j.aca.2006.04.049.

Pozzi, F. *et al.* (2019) 'Evaluation and optimization of the potential of a handheld Raman spectrometer: in situ, noninvasive materials characterization in artworks', *Journal of Raman Spectroscopy*. John Wiley and Sons Ltd, 50(6), pp. 861–872. doi: 10.1002/jrs.5585.

Quintana, P. *et al.* (2015) 'Spectrochemical Characterization of Red Pigments Used in Classic Period Maya Funerary Practices', *Archaeometry*. Blackwell Publishing Ltd, 57(6), pp. 1045–1059. doi: 10.1111/arcm.12144.

Radepont, M. *et al.* (2011) 'The use of microscopic X-ray diffraction for the study of HgS and its degradation products corderoite , kenhsuite and calomel in historical paintings The use of microscopic X-ray diffraction for the study of HgS and its degradation products corderoite (α', *Journal of Analytical Atomic Spectrometry*, 26(5), pp. 959–968. doi: 10.1039/C0JA00260G.

Reinen, D., Köhl, P. and Müller, C. (2004) 'The Nature of the Colour Centres in "Maya Blue" - The Incorporation of Organic Pigment Molecules into the Palygorskite Lattice', *Zeitschrift fur Anorganische und Allgemeine Chemie*, 630(1), pp. 97–103. doi: 10.1002/zaac.200300251.

Rousaki, A. *et al.* (2017) 'The first use of portable Raman instrumentation for the in situ study of prehistoric rock paintings in Patagonian sites', *Journal of Raman Spectroscopy*, 48(11), pp. 1459–1467. doi: 10.1002/jrs.5107.

Rousaki, A. *et al.* (2018) 'On-field Raman spectroscopy of Patagonian prehistoric rock art: Pigments, alteration products and substrata', *Trends in Analytical Chemistry*, 105, pp. 338–351. doi: 10.1016/j.trac.2018.05.011.

Rousaki, A. *et al.* (2019) 'A comparative mobile Raman study for the on field analysis of the Mosaico de los Amores of the Cástulo Archaeological Site (Linares, Spain)', *Journal of Raman Spectroscopy*,

pp. 1–11. doi: 10.1002/jrs.5624.

Rousaki, A., Moens, L. and Vandenabeele, P. (2018) 'Archaeological investigations (archaeometry)', *Physical Sciences Reviews*, pp. 1–9. doi: 10.1515/psr-2017-0048.

Saelens, D. (2018) *In-Situ Analysis of Roman Mosaics at Cástulo , Linares (Jaén , Spain): a Comparative and Non-Destructive Study*. University of Evora.

Sánchez del Río, M. *et al.* (2006) 'On the Raman spectrum of Maya blue', *Journal of Raman Spectroscopy*, 37(10), pp. 1046–1053. doi: 10.1002/jrs.1607.

Sánchez Del Río, M. *et al.* (2011) 'The Maya Blue Pigment', *Developments in Clay Science*, 3(1962), pp. 453–481. doi: 10.1016/B978-0-444-53607-5.00018-9.

Scheuermann, W. and Ritter, G. J. (1969) 'Raman Spectra of Cinnabar (HgS), Realgar (As4S4) and Orpiment (As2S3)', *Zeitschrift fur Naturforschung - Section A Journal of Physical Sciences*, 24(3), pp. 408–411. doi: 10.1515/zna-1969-0317.

Sharer, R. J. and Traxler, L. P. (2006) *The Ancient Maya*. 6th edn. Stanford: Stanford University Press.

Shepard, A. O. and Gottlieb, H. B. (1962) 'Maya Blue: Alternative Hypothesis', in *Notes from a Ceramic Laboratory*. Washington, D.C.: Carnegie Institution of Washington, pp. 45–66.

Siesler, H. W. (2016) 'Vibrational Spectroscopy', in *Reference Module in Materials Science and Materials Engineering*. Elsevier, pp. 1–51. doi: 10.1016/B978-0-12-803581-8.01318-7.

Smith, D. C. (2000) 'Pigments rouges et bleus sur cinq œuvres d'Amérique: analyse non destructive par MRM (Microscopie Raman Mobile)', *Techne*, 11, pp. 69–83.

Smith, G. D. and Clark, R. J. H. (2004) 'Raman microscopy in archaeological science', *Journal of Archaeological Science*, 31, pp. 1137–1160. doi: 10.1016/j.jas.2004.02.008.

Tagle, A. A. *et al.* (1990) 'Maya Blue : Its Presence in Cuban Colonial Wall Paintings', *Studies in Conservation*, 35(3), pp. 156–159. Available at: https://www.jstor.org/stable/1506168.

Tomasini, E. P. *et al.* (2012) 'Micro-Raman spectroscopy of carbon-based black pigments', *Journal of Raman Spectroscopy*, 43, pp. 1671–1675. doi: 10.1002/jrs.4159.

Tozzer, A. M. (1941) 'Landa's Relación de las Cosas de Yucatán', *Papers of the Peabody Museum of American Archaeology and Ethnology*, 18.

Vagnini, M. *et al.* (2017) 'Handheld new technology Raman and portable FT-IR spectrometers as complementary tools for the in situ identification of organic materials in modern art', *Spectrochimica*

Acta - Part A: Molecular and Biomolecular Spectroscopy. Elsevier B.V., 176, pp. 174–182. doi: 10.1016/j.saa.2017.01.006.

Vandenabeele, P. *et al.* (2004) 'A new instrument adapted to in situ Raman analysis of objects of art', *Analytical and Bioanalytical Chemistry*, 379(1), pp. 137–142. doi: 10.1007/s00216-004-2551-z.

Vandenabeele, P. (2004) 'Raman spectroscopy in art and archaeology', *Journal of Raman Spectroscopy*, 35(8–9), pp. 607–609. doi: 10.1002/jrs.1217.

Vandenabeele, P. *et al.* (2005a) 'Raman spectroscopic analysis of the Maya wall paintings in Ek'Balam, Mexico', *Spectrochimica Acta Part A: Molecular and Biomolecular Spectroscopy*, 61(10), pp. 2349–2356. doi: 10.1016/j.saa.2005.02.034.

Vandenabeele, P., *et al.* (2005b) 'In situ analysis of mediaeval wall paintings: A challenge for mobile Raman spectroscopy', *Analytical and Bioanalytical Chemistry*, 383(4), pp. 707–712. doi: 10.1007/s00216-005-0045-2.

Vandenabeele, P. *et al.* (2007) 'Comparative study of mobile Raman instrumentation for art analysis', *Analytica Chimica Acta*, 588, pp. 108–116. doi: 10.1016/j.aca.2007.01.082.

Vandenabeele, P. (2013) *Practical Raman Spectroscopy - An Introduction*. West Sussex: Wiley & Sons, Ltd.

Vandenabeele, P. and Donais, M. K. (2016) 'Mobile spectroscopic instrumentation in archaeometry research', *Applied Spectroscopy*, 70(1), pp. 27–41. doi: 10.1177/0003702815611063.

Vandenabeele, P., Edwards, H. G. M. and Jehlička, J. (2014) 'The role of mobile instrumentation in novel applications of Raman spectroscopy: archaeometry, geosciences, and forensics', *Chemical Society Reviews*, 43, pp. 2628–2649. doi: 10.1039/c3cs60263j.

Vandenabeele, P., Edwards, H. G. M. and Moens, L. (2007) 'A decade of Raman spectroscopy in art and archeology', *Chemical Reviews*, 107(3), pp. 675–686. doi: 10.1021/cr068036i.

Vandenabeele, P. and Moens, L. (2003) 'Micro-Raman spectroscopy of natural and synthetic indigo samples', *Analyst*, 128(2), pp. 187–193. doi: 10.1039/b209630g.

Vandenabeele, P., Verpoort, F. and Moens, L. (2001) 'Non-destructive analysis of paintings using fourier transform Raman spectroscopy with fibre optics', *Journal of Raman Spectroscopy*, 32(4), pp. 263–269. doi: 10.1002/jrs.691.

Vargas de la Pena, L. and Castillo Borges, V. R. (1999) 'Ek' Balam: Ciudad que empieza a reveler sus secretos', *Arqueologia Mexicana*, pp. 24–31.

Vargas de la Pena, L. and Castillo Borges, V. R. (2001) 'La Pintura Mural Prehispanica en Ek'Balam, Yucatan', in Staines Cicero, L. (ed.) *La Pintura Mural Prehispanica, Vol. II: Area Maya, Tomo IV Estudios*. Mexico City: Universidad Nacional Autonoma de Mexico, Instituto de Investigaciones Esteticas, pp. 403–418.

Vazquez de Agredos-Pascual, M. L. (2010) *La pintura mural maya. Materiales y técnicas artísticas*. Merida: Universidad Nacional Autonoma de Mexico.

Vázquez de Ágredos-Pascual, M. L. *et al.* (2019) 'Multianalytical characterization of pigments from funerary artefacts belongs to the Chupicuaro Culture (Western Mexico): Oldest Maya blue and cinnabar identified in Pre-Columbian Mesoamerica', *Microchemical Journal*. Elsevier, 150, pp. 1–8. doi: 10.1016/j.microc.2019.104101.

Vazquez de Ágredos-Pascual, M. L. and Munoz Cosme, G. (2014) 'The new technology in the study of Maya mural painting: over a century of progress', in Vidal Lorenzo, C. and Munoz Cosme, G. (eds) *Artistic Expressions in Maya Architecture: Analysis and Documentation Techniques: Expresiones artísticas en la arquitectura maya: Técnicas de análisis y documentación*. Oxford: Archaeopress, pp. 165–178. doi: 10.30861/9781407313405.

Vázquez de Ágredos Pascual, M. L. (2007) 'Los colores y las técnicas de la pintura mural maya', *Anales del Museo de América*, 15, pp. 55–66.

Vázquez de Agredos Pascual, M. L., Batista dos Santos, A. F. and Yusa Marco, D. J. (2010) 'Annatto in America and Europe. Tradition, treatises and elaboration of an ancient colour', *Arché*, (4–5), pp. 97–102.

Vázquez de Ágredos Pascual, M. L., Lorenzo, C. V. and Cosme, G. M. (2014) 'Archaeometrical Studies of Classic Mayan Mural Painting at Peten: La Blanca and Chilonche', *MRS Proceedings*, 1618, pp. 45–62. doi: 10.1557/opl.2014.454.

Voß, A. and Eberl, M. (1999) 'A New Emblem Glyph from the Northeastern Yucatan', *Mexicon*, 21(6), pp. 124–131.

Wiedemann, H. G. *et al.* (2007) 'Thermal and Raman-spectroscopic analysis of Maya Blue carrying artefacts, especially fragment IV of the Codex Huamantla', *Thermochimica Acta*, 456(1), pp. 56–63. doi: 10.1016/j.tca.2007.02.002.

Witke, K., Brzezinka, K. W. and Lamprecht, I. (2003) 'Is the indigo molecule perturbed in planarity by matrices?', *Journal of Molecular Structure*, 661–662(1–3), pp. 235–238. doi: 10.1016/S0022-2860(03)00511-8.

Yucatan Times (2020) ‘Chichén Itzá became the most visited archaeological site in the country overtaking Teotihuacán’. Available at: https://www.theyucatantimes.com/2020/03/chichen-itza-became-the-most-visited-archaeological-site-in-the-country-overtaking-teotihuacan/.